Final Report

THE ROLE OF POLYETHYLENE DUCT CRACKING IN FAILURE OF POST TENSIONING CABLES IN FLORIDA SEGMENTED BRIDGES (BD220)

submitted to:

Florida Department of Transportation Research Center
605 Suwannee Street, MS 30
Tallahassee, Florida 32399

submitted by:
Florida Atlantic University
Boca Raton, Florida 33431

William H. Hartt, Jorge Suarez, and Florent David,
Center for Marine Materials
Department of Ocean Engineering
Florida Atlantic University

Grace Hsuan and Jingyu Zhang
Department of Civil, Architectural and Environmental Engineering
Drexel University

January 20, 2005

Disclaimer

The opinions, findings, and conclusions expressed in this publication are those of the authors and not necessarily those of the State of Florida Department of Transportation.

Technical Report Documentation Page

1. Report No.	2. Government Accession No.	3. Recipient's Catalog No.

4. Title and Subtitle	5. Report Date
The Role of polyethylene Duct Cracking in Failure of Port Tensioning Cables in Florida Segmented bridges	January 20, 2005
	6. Performing Organization Code
7. Author(s)	8. Performing Organization Report No.
William H. Hartt, Jorge Suarez, Florent David, Grace Hsuan, Jingyu Zhang	FAU-CMM-05.01
9. Performing Organization Name and Address	10. Work Unit No. (TRAIS)
Florida Atlantic University 777 Glades Road Boca Raton, Florida 33431	11. Contract or Grant No. BD 220
12. Sponsoring Agency Name and Address	13. Type of Report and Period Covered
Florida Department of Transportation Research Center MS 30 Florida Department of Transportation 605 Suwannee Street Tallahassee, FL 32399	Research Nov. 14, 2001 – Nov. 30, 2004
	14. Sponsoring Agency Code

15. Supplementary Notes

16. Abstract

During the past 20-plus years, designs based on the post-tension segmental box concept have evolved to become a predominant form of bridge construction; however, during the past five years, instances of tendon deterioration and failure have been disclosed on several Florida bridges. The underlying mechanism has been diagnosed as strand corrosion at grout voids in which bleed water accumulated. Cracking of high-density polyethylene (HDPE) ducts within which the grouted strands reside has also been disclosed. The purpose of the present research was to 1) assess the cause(s) and mechanism(s) of this HDPE duct cracking, 2) develop performance based assessment tests, and 3) propose a standard for HDPE ducts employed in Florida bridges. Testing of simulated tendon specimens and results of finite element modeling indicated that grout voids facilitate, but are not necessary requisites for, duct cracking. Duct material properties that were determined via standardized tests, both for samples acquired from seven Florida bridges and samples representing the present technology limit, included density (ASTM D 792), melt index (ASTM D 1238), carbon black (ASTM D 4218), flexural modulus (ASTM D 790), tensile yield strength (ASTM D 638), environmental stress cracking resistance (ESCR, ASTM D 1693), oxidative induction time (ASTM D 3895), single point notched constant tensile load (SP-NCTL, ASTM D 5397-Appendix) test, fatigue tests, three-point bend tests, and positron annihilation lifetime spectroscopy (PALS). In some cases, methods were modified to be performance based. The results indicate that duct samples from the Mid Bay (MB) and Sunshine Skyway (SSK) Bridges, both of which have exhibited cracking in service, were of relatively poor quality such that cracking is projected to have commenced within several years of construction. Results for samples from the Long Key and Seven Mile Bridges indicated that these ducts are intermediate in quality and performance with times-to-cracking in excess of 50 years in service being projected. The PE-3408 material (the duct material employed in the SSK rehabilitation), on the other hand, performed best and should serve maintenance free in tendon duct applications for the design life of bridges.

17. Key Word	18. Distribution Statement
Post-tensioning tendons, high-density-polyethylene, ducts, segmental bridges, corrosion	Unlimited

19. Security Classif. (of this report)	20. Security Classif. (of this page)	21. No. of Pages	22. Price
Unclassified	Unclassified	167	

EXECUTIVE SUMMARY

During the past 20-plus years, designs based on the post-tension segmental box concept have evolved to become a predominant form of bridge construction. Critical to safety and longevity of such structures is the integrity of post-tensioning tendons; however, during the past five years, instances of tendon deterioration and failure have been disclosed on several Florida bridges. The underlying mechanism has been diagnosed as strand corrosion at grout voids in which bleed water accumulated. Cracking of high-density polyethylene (HDPE) ducts within which the grouted strands reside has also been disclosed; and while none of the failures to-date has been related to this cracking, left unaddressed, access of moisture, chlorides, and oxygen to the strands will invariably result in corrosion in the long term. For the purpose of 1) assessing the cause(s) and mechanism(s) of this HDPE duct cracking, 2) developing performance based assessment tests, and 3) proposing a standard for HDPE ducts employed in Florida bridges, a research project commenced in 2002 that involved investigators at both Florida Atlantic and Drexel Universities. The project consisted of six tasks as:

I. Acquisition of New and In-Service Polyethylene (PE) Cable Duct Samples.
II. Evaluation of Material Properties of Retrieved and New Duct Samples.
III. Evaluation of Duct Cracking Mechanism.
IV. Evaluation of Pipe SCR Using Performance Tests.
V. Assessment of Current Material Specifications for Smooth PE Duct.
VI. Experimental and Analytical Modeling of Tendon Duct Cracking.

Testing of simulated tendon specimens and results of finite element modeling indicated that grout voids facilitate, but are not necessary requisites for, duct cracking. Duct material properties that were determined via standardized tests, both for samples acquired from seven Florida bridges and samples representing the present technology limit, included density (ASTM D 792), melt index (ASTM D 1238), carbon black (ASTM D 4218), flexural modulus (ASTM D 790), tensile yield strength (ASTM D 638), environmental stress cracking resistance (ESCR, ASTM D 1693),

oxidative induction time (ASTM D 3895), single point notched constant tensile load (SP-NCTL, ASTM D 5397-Appendix) test, fatigue tests, three-point bend tests, and positron annihilation lifetime spectroscopy (PALS). In some cases, methods were modified to be performance based. The results indicate that duct samples from the Mid Bay (MB) and Sunshine Skyway (SSK) Bridges, both of which have exhibited cracking in service, were of relatively poor quality such that cracking is projected to have commenced within several years of construction. Results for samples from the Long Key and Seven Mile Bridges indicated that these ducts are intermediate in quality and performance with times-to-cracking in excess of 50 years in service being projected. The PE-3408 material (the duct material employed in the SSK rehabilitation), on the other hand, performed best and should serve maintenance free in tendon duct applications for the design life of bridges.

CONCLUSIONS AND RECOMMENDATIONS

Conclusions

Material properties of high density polyethylene (HDPE) duct samples from seven Florida post-tensioned bridges and new PE3408 duct were evaluated for the purpose of 1) defining material properties, 2) projecting performance in segmental bridge applications, 3) understanding cracking mechanisms in cases where cracking has occurred, and 4) developing a performance based standard. Also, experiments and analyses were conducted that modeled duct stressing in service. The following conclusions were reached regarding quality and performance of high density polyethylene (HDPE) ducts in Florida post-tensioned bridges:

1. For the Mid Bay (MB) and Sunshine Skyway (SSK) Bridges, where extensive duct cracking has occurred, initiation generally occurred at defects (impurities and air voids) on the interior surface and from there propagated through thickness and longitudinally. This required that a tensile stress (either applied or residual or a combination of the two) be present at the internal duct surface. The predominant mechanism of crack propagation was slow crack growth and fatigue. Also, various material properties did not meet the specification requirements. In particular, stress crack resistance was poor and the remaining amount of antioxidant was low.

2. Duct samples acquired from the Garcon Point, Seven Mile, Long Key, Channel Five and Niles Channel Bridges generally conformed to the applicable specifications. This is consistent with the observation that little or no duct cracking has occurred on these bridges. At the same time, there were relatively large differences in stress cracking resistance and antioxidant content between the different samples.

3. The best material properties were determined for newly acquired duct samples that are based on the PE3408 resin. Such ducts should provide satisfactory service for the design life of major bridge structures.

4. Based upon results from fatigue tests, experiments involving strain-gage instrumented simulated tendons, and finite element analysis, it is projected that thermal cycle induced fatigue is a probably source of stressing and that this caused the cracking in the lower duct quality cases (see Conclusion 1). Stresses arising from thermal cycling are likely to be higher at locations where a grout void is

present. The analysis projected that cracking of the MB and SSK ducts probably commenced within the initial few years of construction, whereas ducts in the Garcon Point, Seven Mile, Long Key, Channel Five and Niles Channel Bridges should see 50-plus years of crack-free service provided material properties, antioxidant content in particular, do not degrade with time.

Recommendation

As a part of this project, a new performance based material properties specification for HDPE post-tensioning ducts was developed and has already been adapted by the FDOT as Section 462 of the Post-Tensioning specification document.

TABLE OF CONTENTS

TABLE OF CONTENTS (continued)

LIST OF TABLES

LIST OF FIGURES

LIST OF FIGURES (continued)

LIST OF FIGURES (continued)

LIST OF FIGURES (continued)

INTRODUCTION

During the past several decades, segmental construction using pre-cast concrete elements has evolved to become a preferred design and construction method for many bridges. By this, segments are pre-cast, placed in position according to design of the sub- or super-structure, and held together by post-tensioned cables that are either internal (contained within the concrete segments) or external to the concrete but within the segment interior. These cables consist of 1) multiple seven wire high strength steel cables that conform to ASTM A416 (typically with a 1,860 MPa (270 ksi) minimum ultimate strength), 2) a high density polyethylene (HDPE) duct within which the cables are strung, and 3) a cementiteous grout fill within the duct. For a superstructure, individual cables terminate relatively high within bulkheads at the end of a pre-cast section and traverse and hold together six or more sections by their passing through periodically spaced deviation blocks along the base. The nature of this method is such that tendon integrity is critical to the safe operation and structural integrity of the bridge.

In the summer of 1999, a failed tendon was disclosed within the Niles Channel Bridge in the Florida Keys. Subsequent analysis revealed severe corrosion near one of the termination blocks and anchor region. Instances of tendon corrosion on other cables within this bridge were also identified. Similar severe tendon corrosion and failed tendons were subsequently found on the Skyway and Mid Bay Bridges.

The tendon corrosion and cable failures are thought to have resulted from accumulation of bleed water in conjunction with grout subsidence or within grout voids (1,2); however, a compounding factor may be the nature of the HDPE duct, its response to environmental factors (temperature variations in particular), and the manner with which the duct interacts with the grout. In this regard, numerous longitudinal splits were apparent on the HDPE ducts of the Mid Bay Bridge (3). These have occurred to a lesser extent on ducts in the Skyway Bridge and hardly at all in the Niles Channel Bridge. Such splitting is likely to render tendons more exposed to the environment, and resultant strand corrosion may compromise the long-term integrity of the cables. Preliminary analyses have indicated that the relatively poor performance of the Mid Bay Bridge ducts resulted from 1) an inferior duct resin and 2) stresses arising from thermal expansion/contraction combined with compounding affects associated with grout voids (4). Comprehensive evaluation of this problem and future direction recommendations have been made (5).

PROJECT OBJECTIVES

The objectives of this research project were to 1) characterize the material properties of HDPE duct materials that have been employed in the past and are presently being specified for cable applications in Florida bridges, 2) perform experiments that reproduce the duct cracking that has occurred, 3) quantify construction and exposure factors that affect duct cracking, and 4) identify possible alternative duct materials, construction methods, and specifications and standards that provide improved resistance to cracking. These were accomplished in terms of six tasks, as:

I. Acquisition of New and In-Service Polyethylene (PE) Cable Duct Samples.
II. Evaluation of Material Properties of Retrieved and New Duct Samples.
III. Evaluation of Duct Cracking Mechanism.
IV. Evaluation of Pipe SCR Using Performance Tests.
V. Assessment of Current Material Specifications for Smooth PE Duct.
VI. Experimental and Analytical Modeling of Tendon Duct Cracking.

Efforts in each of these categories are described below.

TASK I: ACQUISITION OF NEW AND IN-SERVICE POLYETHYLENE (PE) CABLE DUCT SAMPLES

A total of 77 field duct samples were retrieved from seven bridges located in different regions of the State and which were constructed at different times, as indicated in Table 1. All samples were from the bridge roadway except for the Sunshine Skyway Bridge where both roadway and column samples were acquired. Each field duct sample was identified according to its position with respect to the bridge tendon layout. In some cases, material information was printed on the exterior duct wall surface.

Table 1: Details of the acquired field samples.

Bridge	County Location	Field Sample Age (yr.)	Total No. of Field Samples	No. of Cracked Samples
Mid Bay (MB)	Okaloosa	10	3	3
Garcon Point	Santa Rosa	4	1	0
Seven Mile	Monroe	21	1	0
Skyway (SSK)	Pinellas	17	32 column	4
			34 span	3
Channel Five	Monroe	21	1	0
Long Key	Monroe	22	3	0
Niles Channel	Monroe	20	2	0

Age of the field samples varied from 4 to 22 years. Samples from the four Monroe County bridges had been exposed to the ambient environment for approximately 20 years, and there was no sign of cracking. In contrast, samples from the Mid Bay Bridge (MB) were only 10 years old, and significant cracking was observed.

For comparison purposes, new, four inch diameter HDPE PE3408 pipe ducts were acquired from two sources and served as the basis for the studies described in Tasks II-V. One set of these (designated as FAU) was from a general source whereas the other, designation SSK, was replacement material that is being employed on the Sunshine Skyway Bridge.

TASK II: EVALUATION OF MATERIAL PROPERTIES OF RETRIEVED AND NEW DUCT SAMPLES

Introduction

Within this task, material properties of retrieved duct samples from the seven bridges and currently available new samples from two sources (see Table 1), including physical, mechanical properties, long-term behavior, and failure mechanisms, were evaluated. The results are summarized below with details being presented in Appendices A-D. In addition, supplemental testing including fatigue, three-point bend, positron annihilation lifetime spectroscopy (PALS), and Soxhlet extraction were also performed.

Material properties of all retrieved field duct samples were evaluated according to either the specification that applied during bridge construction or, if this was not available, the AASHTO specification. For cracked duct samples, the cracking mechanism was investigated. The detailed results of the evaluations are presented as four appendices of this report, as listed below:

- Mid Bay Bridge – Appendix A
- Garcon Point and Seven Miles Bridges – Appendix B
- Channel Five, Long Key, and Nile Channel Bridges – Appendix C
- Skyway Bridge – Appendix D

Retrieved Duct Samples

Summary of Material Properties

The material specifications for HDPE ducts in each of the seven bridges are listed in Table 2. With

the exception of the Sunshine Skyway (SSK) Bridge, for which no material specification was available and, thus, the AASHTO specification was used, properties of the HDPE duct samples were evaluated according to the indicated specification(s) for the individual bridges. In this regard, all polyethylene (PE) resins used in pipe applications are specified according to cell classes as defined in the ASTM D 3350 "Standard Specification for Polyethylene Plastics Pipe and Fittings Materials".

Table 2: Material specification for the HDPE ducts in each bridge.

Bridge	Source	Material Specification
Mid Bay	Construction specification	ASTM D3350 with a cell classification PE 345433C
Garcon Point	Printed on the exterior wall	PE 3408
Seven Miles	Supplied by duct manufacturer	ASTM D3350 with a cell classification PE 335433C
Skyway	No material specification available	AASHTO specification was used ASTM D3350 with a cell classification PE 345433C
Channel Five	Printed on the exterior wall	ASTM 3350 with a cell classification PE 335433C
Long Key	Printed on the exterior wall	PE 3406 and PE 3408
Niles Channel	Printed on the exterior wall	PE 3406

Table 3 lists the required test methods in ASTM D 3350 and the specified cell classes for the individual bridges. The differences among the three specifications reflected in Table 3 are the cell classes for melt index (MI) and flexural modulus. The specification for the Mid Bay (MB) Bridge is the same as the AASHTO specification which has been applied for the SSK Bridge in that both require cell class 4 (< 0.15 g/10 min) for the MI while the other bridges require cell class 3 (< 0.4 - 0.15 g/10 min). The MI value can be qualitatively related to the molecular weight of the polymer. Other factors being the same, a low MI indicates high molecular weight and vise versa. Thus, the MB and AASHTO specifications require a higher molecular weight polymer. PE 3406 and PE 3408 (see Garcon Point, Long Key, and Niles Channel bridge references in Table 3) specify a lower value for flexural modulus than for ducts in the other bridges. On the other hand, two methods are defined in ASTM D 3350 for measuring SCR; they are the ESCR and HDB tests. The latter was not performed in this study, since it requires a complete duct sample which was not available with the retrieved field samples. For the ESCR test, all four specifications list the same criterion: a maximum of 20 percent failure for 10 test specimens after 196 hours.

Table 3: Specified properties for PE duct according to the ASTM D 3350 cell classification.

Property	Test Method	MB and SSK Bridges	Required Value	Seven Mile and Channel 5 Bridges	Required Value	Long-Key and Garcon Point Bridges (PE 3408)	Nile Channel and Long-Key Bridge (PE 3406)	Required Value
Density (g/cc)	ASTM D 792	3	>0.940-0.955	3	>0.940-0.955	3	3	>0.940-0.955
Melt index (g/10 min.)	ASTM D 1238	4	< 0.15	3	<0.4-0.15	3	3	<0.4-0.15
Flexural Modulus (psi)	ASTM D 790	5	110,000 - <160,000	5	110,000 - <160,000	4	4	80,000 - <110,000
Tensile yield strength (psi)	ASTM D 638 Type IV	4	3000 - <3500	4	3000 - <3500	4	4	3000 - <3500
ESCR*	ASTM D 1693	3	F_{20} = 192 hr	3	F_{20} = 192 hr	3	3	F_{20} = 192 hr
SCGR** (hr)	ASTM F 1473	0	Not specified	0	Not specified	0	0	Not specified
HDB*** (psi)	ASTM D 2837	3	1250	3	1250	0	0	Not specified
Carbon black (%)	ASTM D 4218	C	> 2	C	> 2	C	C	> 2

* ESCR – environmental stress crack resistance.
** SCGR – slow crack growth resistance
*** HDB – hydrostatic design basis.

In this study, two additional tests, the single point-notched constant tensile load (SP-NCTL) test (ASTM D 5397-Appendix) and the oxidative induction time (OIT) test (ASTM D 3895), were included in the materials evaluation program. The first of these was recently adopted to replace the ESCR test (ASTM D1693) for corrugated polyethylene non-pressured pipe in the AASHTO M294 specification. The reason for this replacement was the large standard deviation of the test and its qualitative nature of the ESCR test. The SP-NCTL test provides quantitative test values to distinguish between different SCR grades of HDPE ducts. The OIT test is used for assessing the amount of antioxidants remaining in the duct. The role of antioxidants is to protect the HDPE from oxidation degradation throughout its service life.

Table 4 shows the test results for samples from each bridge with respect to the applicable material specification. All field samples conformed to the density, tensile strength, and flexural modulus requirements. However, some of the duct samples failed to meet the specified values for MI, ESCR, and carbon black. In this regard, samples from four of the seven bridges contain carbon black less than the required two percent. The function of carbon black is to protect the duct from ultraviolet (UV) light. Once the duct is installed inside the concrete segment box and shield from sunlight, UV protection is no longer required. Thus, a carbon black content of less than two percent would not affect duct longevity in service. The MI test results indicate that duct samples from the MB and SSK bridges have values higher than specified, suggesting that these ducts were made from polymers with a lower molecular weight.

The SP-NCTL test for SCR revealed relatively large variations among duct samples from the different bridges. In particular, samples from the MB and SSK bridges exhibited much shorter failure times than those from the others; which are consistent with the poor field performance of these ducts. However, large variations in SCR of ducts from the other five bridges were observed. Ducts from the Garcon Point Bridge and the PE 3408 coded duct from the Long-Key Bridge had failure times well over 100 hours, even at an applied stress of 25 percent of yield (σ_y). On the other hand, ducts from the Seven Mile and Channel Five Bridges and PE 3406 from the Long-Key Bridge had failure times of 10-20 hours at 25 percent σ_y.

In addition to SCR, long-term performance of ducts depends strongly on chemical stability of the polymer which, in turn, is governed by the depletion rate of antioxidants. The OIT test is used to assess the amount of antioxidants remaining in the duct sample. The measured OIT varied from 1 to 100 minutes, suggesting a large range of antioxidant content in these field samples. Ducts from the MB and

SSK bridges have the shortest OIT values, indicating that the amount of antioxidants in these samples is very limited or nil. Duct from the Garcon Point Bridge showed the longest OIT value; however, it should be recognized that this field sample was only 4 years old. The 20 year old ducts taken from the four Monroe County bridges all exhibited similar OIT values, in the range of 15 minutes. Unfortunately, it is not possible to estimate antioxidant depletion rate since the original OIT value is unknown.

Table 4: Summary of test results with respect to the applicable material specification.

Test Method	Result						
	MB	Garcon Point	Seven Mile	SSK	Channel-5	Long-Key	Niles Channel
Density	Passed	Passed	Passed	Passed	Passed	Passed	Passed
Melt index	Higher	Passed	Passed	Majority Higher	Passed	Passed	Passed
Flexural Modulus	Passed	Passed	Passed	Passed	Passed	Passed	Passed
Tensile strength	Passed	Passed	Passed	Passed	Passed	Passed	Passed
ESCR	Failed	Passed	Passed	na	na	na	na
Carbon black	Lower	Passed	Passed	Lower	Some lower	Some lower	Some lower
SP-NCTL (hr) at 15% σ_y	3 to 4	> 1000	80	3 to 11			
SP-NCTL (hr) at 25% σ_y		524	19		13	16 (PE 3406) 243 (PE 3408)	50 - 70
OIT (min)	1.3	110	14.2	2 to 8	16.5	15-18	13-16

Note: ESCR – environmental stress crack resistance.
SP-NCTL – Single point notched constant tensile load.
OIT – oxidative induction time.
na – non-available

Discussion of Material Properties

It is well known that the SCR of HDPE is related to molecular weight and crystallinity of the material as well as to other factors such as polymerization techniques and type of catalysts and co-monomers. In this study, the molecular weight of the polymer was assessed using the MI test. Density, on the other hand, is an indicator of crystallinity and the SP-NCTL test of SCR. It should be noted that higher MI and density values, both of which have a negative impact on the SCR of the material, were obtained from the cracked compared to non-cracked ducts.

The correlations between, first, SCR and MI and, second, SCR and density were evaluated using data obtained from SSK Bridge samples. In this regard, the graph in Figure 1 plots MI value against failure time for specimens in the SP-NCTL test and indicates an inverse relationship between these two parameters.

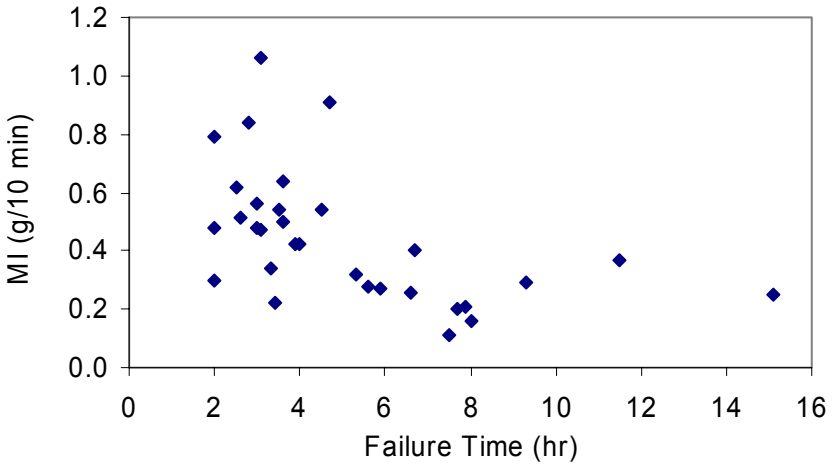

Figure 1. Failure time versus MI of field duct samples from the SSK Bridge.

Correspondingly, Figure 2 shows a plot of density versus failure time. The correlation in this case is relatively poor, although the general trend is one where samples with high density values tend to have shorter failure times than those with low density.

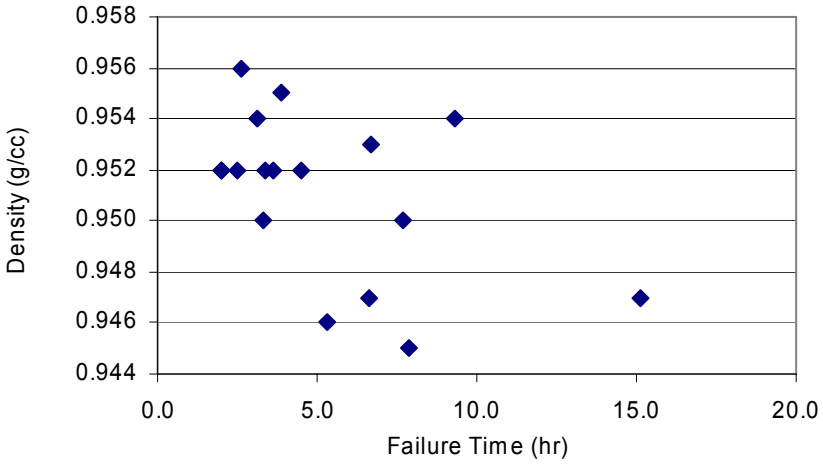

Figure 2. Density versus failure time of field duct samples from the SSK Bridge.

In summary, molecular weight, as reflected by MI, and crystallinity, as reflected by density, can have effects on the SCR; but they cannot confidently predict the SCR of the material. Samples with low MI and density, in general, exhibit higher SCR, as reflected by their relatively long failure times in the SP-NCTL test. Of the two tests, the MI correlated slightly better with SCR than did density.

Currently Available New Duct Samples

Test Materials

Two groups of ducts were acquired and evaluated. The first consisted of four internal corrugated ducts (three polypropylene (PP) ducts and one HDPE duct) with the focus being upon antioxidant content. The second group consisted of two new HDPE external ducts, one of which was acquired by FAU and the other of samples of replacement material for the SSK Bridge columns (see Table 1). A description of the six new ducts is provided in Table 5. Properties of these currently available new duct materials were assessed according to a specification that was adapted by the FDOT in April, 2003.

Table 5: Description of the new ducts.

Name	Color	Polymer	Corrugation Style
Freyssinet	Black	HDPE	Helical
General Technology	Opaque	PP	Annular
General Technology	Opaque	PP	Annular with longitudinal channel
DSL	Black	PP	Annular
HDPE-FAU	Black	HDPE	Smooth
HDPE-SSK	Black	HDPE	Smooth

Evaluation of Internal Corrugated Ducts (Group 1)

The oxidative induction time (OIT) test (ASTM D3895) was used to assess the amount of antioxidant in the duct material as an indicator of durability. Table 6 shows the OIT values for the four duct materials and indicates that these ranged from 15 to 51 minutes from specimen to specimen within the same duct sample. For the HDPE corrugated duct sample, the average OIT value was 10 minutes which is lower than obtained from the PP ducts.

Discussion

The purpose of the OIT test is to assess the level of antioxidants in various internal duct samples. The function of antioxidants is to protect duct samples from oxidation degradation which can be in the

Table 6: OIT values of samples from the different ducts.

Name	Polymer Type	Corrugation Style	OIT (min)		Average OIT (min)
Freyssinet	HDPE	Helical	12.2	9.4	10.8
General Technology	PP	Annular	21.0	15.4	18.2
General Technology	PP	Annular with longitudinal channel	18.5	26.1	22.3
DSL	PP	Annular	27.8	51.1	39.5

form of either thermoxidation or photoxidation. Once an internal duct is surrounded by cement grout, the available oxygen that can react with the polymer is extremely small. However, before the ducts are installed and grouted, they are often exposed to sunlight at the construction site for an uncertain period of the time. An antioxidant together with carbon black can protect the duct from photoxidation during this pre-installation exposure period. Furthermore, antioxidant can also protect the duct from potential thermal oxidation induced by the grout hydration heat. Thus, a certain amount of antioxidant should be present to ensure adequate resistance to this form of degradation. The OIT values of these corrugated pipes were used in the development of a new material specification which is discussed in a later section of this report.

Evaluation of External Smooth Ducts

As noted above, the material properties of the two new HDPE smooth ducts were evaluated according to the specification that was adapted by FDOT in April, 2003. Table 7 shows the test values for these two ducts together with the FDOT specified values. Both ducts were made from PE 3408 resin and have very similar properties. Although a direct comparison of the SP-NCLS test results is not applicable due to differences in applied stresses, the failure times fall within the range of samples from the PE 3408 ducts that were taken from the Long-Key and Garcon Point Bridges.

Other Tests

General

Three additional, non-standardized test, 3-point bend, positron annihilation lifetime spectroscopy (PALS), and Soxhlet extraction, were investigated, as potential assessment methods for HDPE duct.

Table 7: Comparison of material properties of two new HDPE ducts to those required by the FDOT specification

Property	Test Method	FDOT Specification	Required Value	Test Result	
				FAU Duct	SSK Duct
Density (g/cc)	ASTM D 792	3	>0.940-0.955	0.938	0.941
Melt index (g/10 min.)	ASTM D 1238	4	< 0.15	0.09	0.1
Flexural Modulus (psi)	ASTM D 790	4	80,000 - <110,000	108,000	101,000
Tensile yield strength (psi)	ASTM D 638 Type IV	4	3000 - <3500	3380	3044
ESCR	ASTM D 1693	0	Not specified	na	na
HDB (psi)	ASTM D 2837	4	1600	na	na
Carbon black (%)	ASTM D 4218	C	> 2	2.5	2.3
SP-NCLS test (hour)	ASTM D 5397	na	500	> 1000 hr (at 15% σ_y)	332 (at 25% σ_y)
OIT (min)	ASTM D3895	na	40	52	51

Note: ESCR – Environmental stress crack resistance.
HDB – Hydrostatic design basis.
SP-NCTL – Single point notched constant tensile load.
OIT – Oxidative induction time.
na – Non-available

Each of these is described below.

Three-Point Bend Tests

In addition to the above, 3-point bend tests upon various HDPE types were performed. The parameters measured were strain and load as a function of time. Figure 3 is a photograph of the three-point bend experimental set-up that was employed. For this, load was applied through a motor driven bolt and was measured using a load cell between the bolt and specimen. Tests ware performed using a bolt displacement rate of five mm per minute. Strain, on the other hand, was measured via strain gages attached to the specimen and connected to a strain indicator.

Figure 4 schematically illustrates the geometry of the three-point bend specimens. Figure 5 shows results for a preliminary experiment where outputs from two gauges, USG (upper strain gauge on the

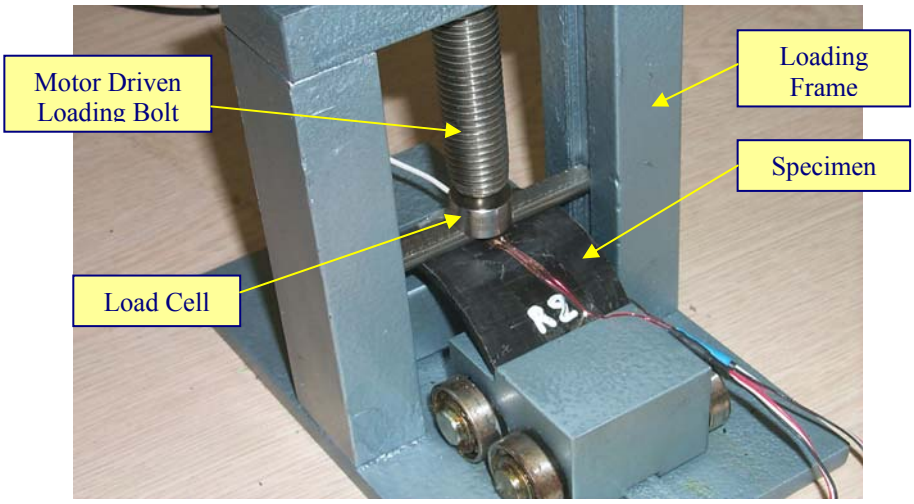

Figure 3: Photograph of the three-point bending loading system and a test specimen.

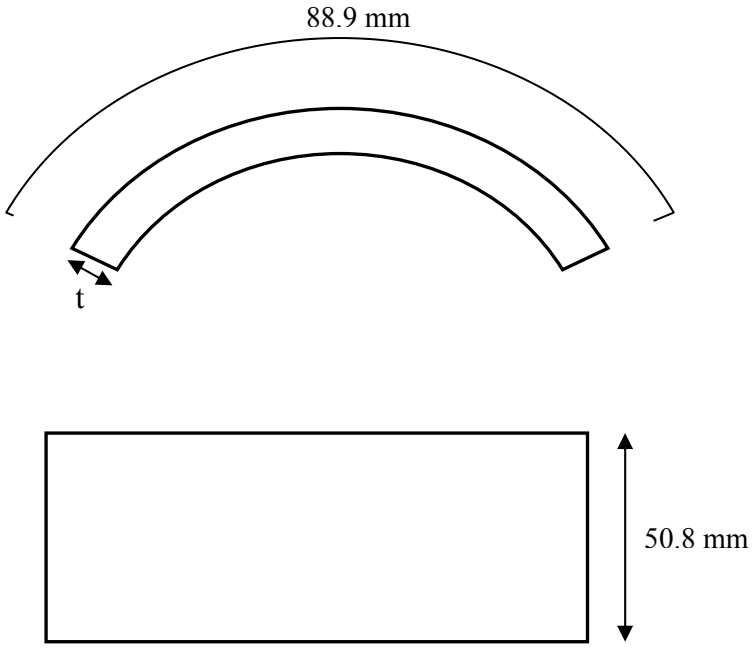

Figure 4: Schematic illustration of the three-point bend specimen.

compression face) and LSG (lower strain gauge on the tensile face) are indicated. This reveals generally linear behavior until strain was relatively large at which point the gauges disbonded. Likewise, Figure 6 plots USG strain versus LSG strain and shows good correlation between the two.

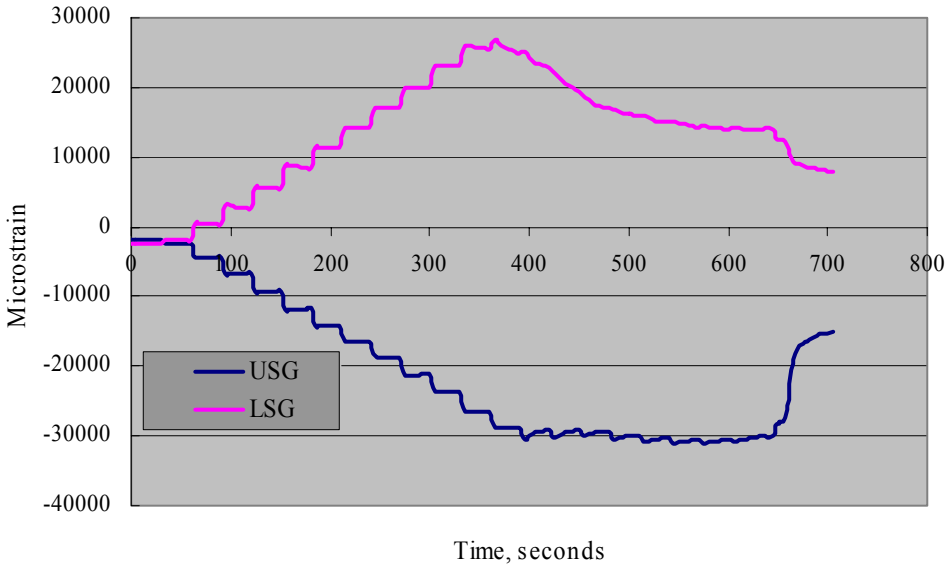

Figure 5: Strain versus time record for gauges mounted on the tension (LSG) and compression (USG) faces of a three point bend specimen (loading was incremental rather than continuous).

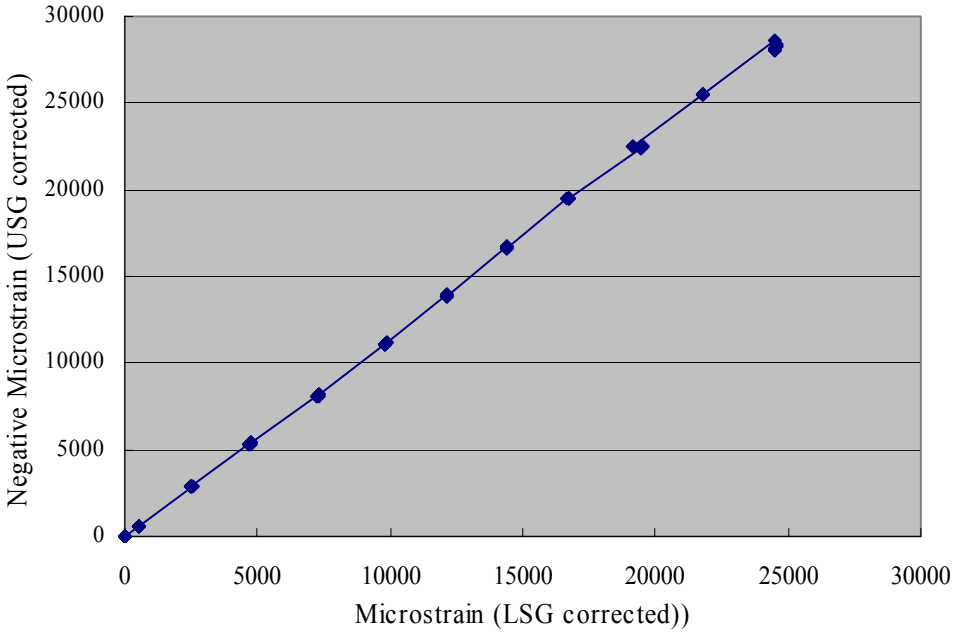

Figure 6: Plot of strain recorded from gauge USG versus that for gauge LSG during a three-point bending test.

Figure 7 plots stress versus microstrain for three-point bend specimens of the FAU-3408 HDPE along with that for samples from the MB, SSK, Niles Channel, and Long Key Bridges. For all materials, the modulus is approximately the same; however, specimens from the MB and SSK exhibit reduced

ultimate stress and strain-to-fracture (specimens of the FAU-3408 HDPE did not fracture but strained to the limit of the three-point bend test fixture). Response of the other materials was generally similar with differences probably falling within the range of experimental scatter.

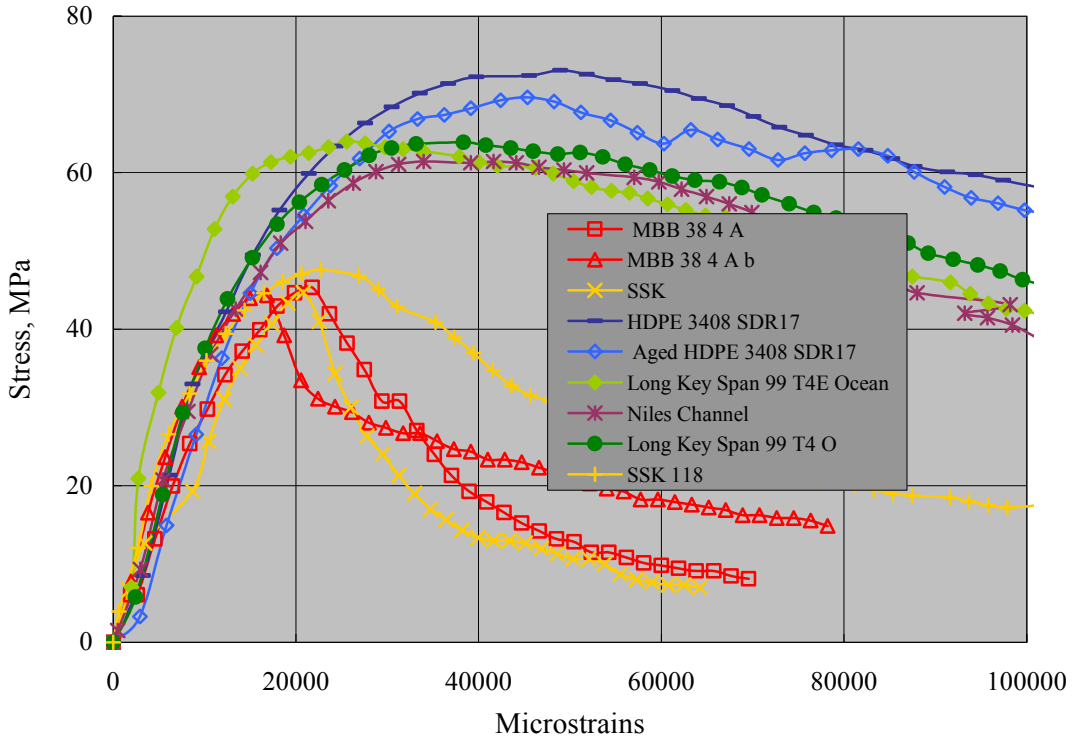

Figure 7: Plot of stress versus microstrain for three-point bend tests on various HDPE specimens.

Positron Annihilation Lifetime Spectroscopy (PALS) (contributed by Dr. Richard Granata)

The size and distribution of local free volume (unoccupied molecular spaces) in polymer structures plays an important role in determining physical properties. Positron Annihilation Lifetime Spectroscopy (PALS) is a tool employed by polymer scientists to characterize this void space. It was reasoned that HDPE properties and service performance could be affected by this void space; and with this in mind, initial experiments were performed to evaluate this.

Figure 8 shows a schematic illustration of the crystalline PE structure with a unit cell identified. Correspondingly, Figure 9 provides a more general representation of how crystals and amorphous regions make up the structure. It can be reasoned from this that void space develops at chain ends, side groups, and within the amorphous structure.

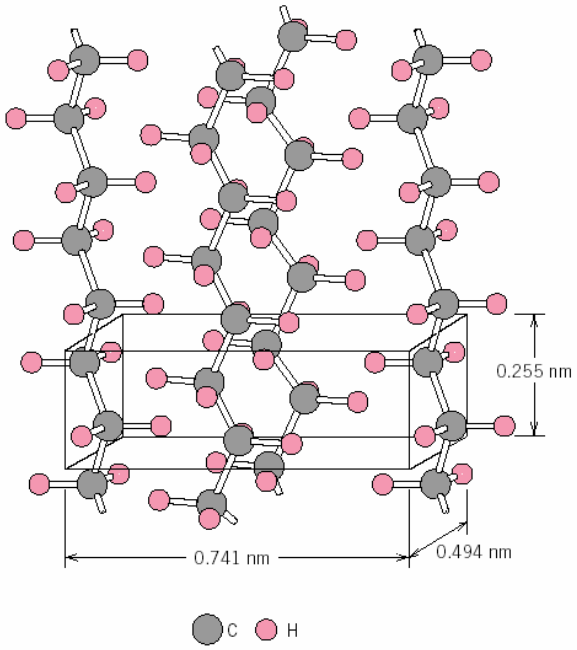

Figure 8: Schematic illustration of the crystalline PE structure (from C.W. Bunn, *Chemical Crystallography*, Oxford University Press, Oxford, 1945, p. 233).

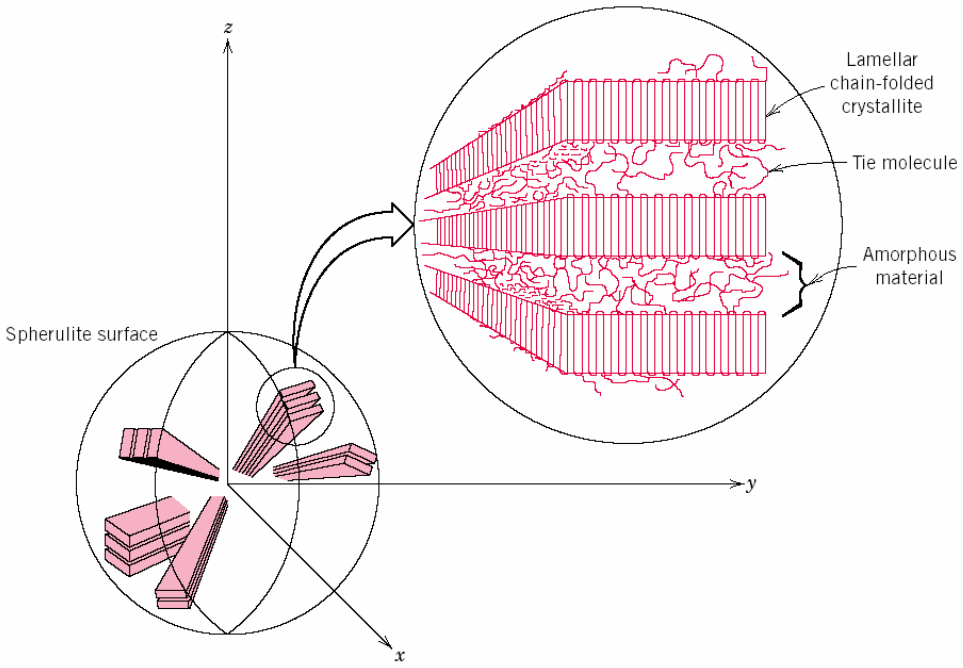

Figure 9: General representation of the PE structure (J.C. Coburn, "Dielectric Relaxation Processes in Poly(ethylene terephthalate)," PhD Dissertation, Univ. of Utah, 1984.

The PALS method utilizes a Na^{22} source that decays by emitting a gamma ray and positron (positively charged electron). The positron enters the sample; and once its energy has decreased

sufficiently, resides in a void where it captures an electron, annihilates, and emits a gamma ray of wavelength different from the initial one. The operating principle of PALS is based upon measurement of the time lag between emission of the two gamma rays with longer times indicating larger voids. PALS spectra are analyzed with a program called POSITRONFIT. Mathematically, a sum of the several decay times is convoluted with the resolution function of the system (a Gaussian-type function). The output consists of several lifetimes that are dependent on the positron annihilation in the sample with corresponding intensities as well as statistical standard deviation and variance. The second and third lifetimes exceed 0.5 ns and are dependent on the size of the free volume in the sample.

Several of the duct samples employed in the 3-point bend tests (see Figure 7) have been analyzed using PALS. Figure 10 shows the results of this as a plot of the PALS void size sensitive parameter versus area under the stress-strain curve from the 3-point bend tests (Figure 7). A general correlation is seen between the two parameters with large void size corresponding to less stress-strain curve area. Since generation of a PALS spectra is relatively straightforward and requires only about one day to complete, the method has the potential for providing a relatively quick, inexpensive technique for assessing duct quality and performance properties.

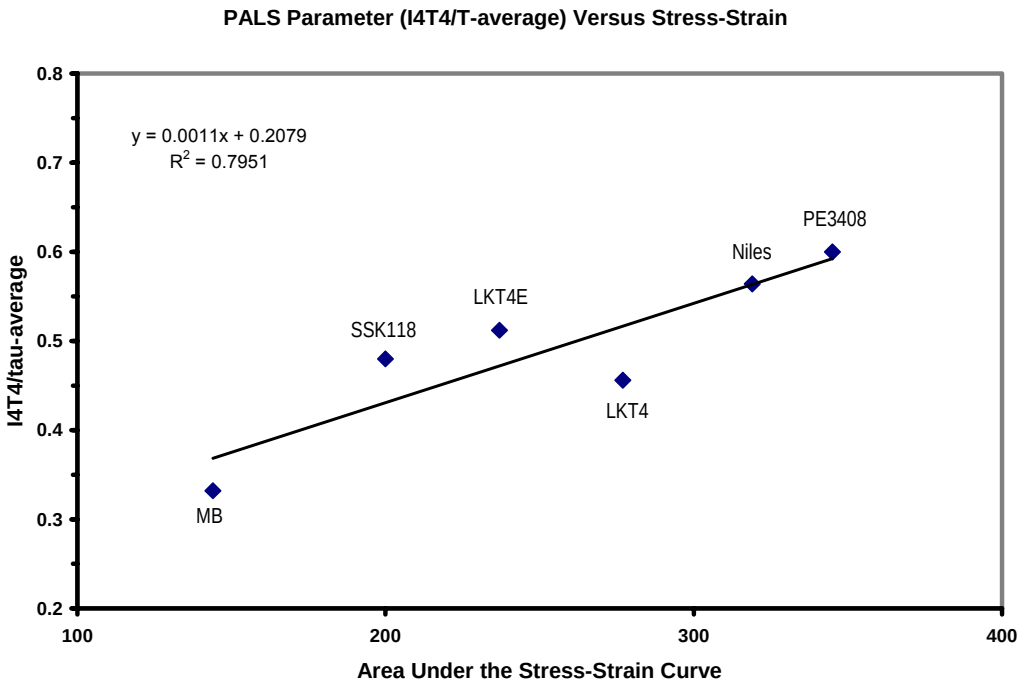

Figure 10: Plot of the void size indicating PALS parameter versus area under the stress-strain curve for different duct samples.

Soxhlet Extraction

The purpose of these experiments was to identify a method for determining the degree of cure of resins in the different polyethylenes. The procedure involved measurement of weight loss for thin HDPE shavings exposed to Methyl Ethyl Ketone (MEK) for one week. Two sets of specimens, one from the Mid Bay Bridge (MB) and the second from the FAU-3408 duct, were employed. Table 8 provides the results from these tests.

Table 8: SP-NCTL test results in air and in 10% Igepal.

Average Yield Stress = 4317 psi; Applied Stress = 15%* 4317 psi = 648 psi					
Applied Stress (psi)	Average Thickness (inches)	Ligament Thickness (inches)	Applied Load (grams)	Failure Time in Air (hours)	Failure Time in 10% Igepal (hours)
648	0.071	0.057	524	17.3	2.4
	0.071	0.057	524	15.8	2.3
	0.071	0.057	524	14.5	2.6
	0.074	0.060	551	22.7	2.5
	0.074	0.060	551	25.9	2.5
Average Failure Time				19.3	2.5
Standard Deviation				4.8	0.1

Based upon the close correspondence for the average of the two materials (1.27 percent weight loss for the FAU-3408 samples and 1.31 for MB), it was concluded that Soxhlet extraction did not reveal any difference between the two materials. Consequently, these tests were not pursued further.

TASK III. EVALUATION OF DUCT CRACKING MECHANISM

As noted above, cracking was observed in ducts from the Mid-Bay and Skyway Bridges. This section provides a summary of the cracking mechanism, as discerned from fractographic analysis, with details being provide in Appendices A (Mid Bay) and D (Skyway). The retrieved cracked duct samples were investigated for their cracking mechanism by examining the microstructure of the fracture surfaces. In all cases, cracking initiated from the inner surface of duct wall and propagated through the wall thickness. The direction of the crack growth suggests that the inner duct surface was subjected to a tensile stress.

Many of the cracks initiated, in conjunction with a tensile stress, at points at impurities or air bubble voids. The multiple small cracks that were generated at various initiations grew with time and eventually joined together to form a single long crack. The impurities were observed in all cracked ducts and seemed to be the dominant cause of crack initiations. It was not possible to determine the chemical composition of the impurities; however, the fracture morphology of these features was different from that of the polyethylene duct material itself, as shown in Figure 11.

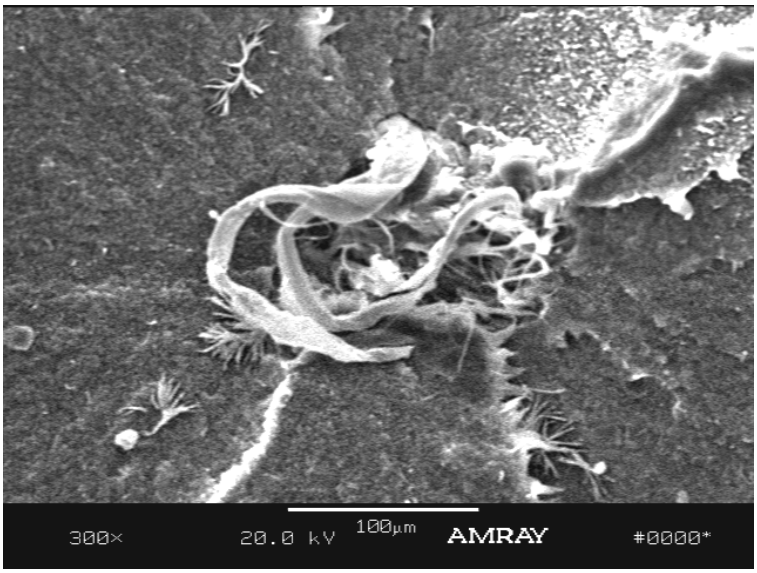

Figure 11: An example of an impurity in a duct sample from which a crack initiated.

The fracture surface of all examined specimens was dominant by a fibril structure, as shown in Figure 12, and resulted from a slow crack growth mechanism. The appearance of fibril structure was not the same on the different fracture surfaces, however, since the appearance of fibril structures is stress dependent where a high stress tends to yield long fibers. Also, these structures can be damaged by abrasion between two opposite fracture surfaces subsequent to cracking. In addition, fatigue lines running parallel to the longitudinal axis of the duct were observed on some of the fracture surfaces. The occurrence of fibril structure with fatigue lines indicates that some portion of the cracks had undergone a combination of steady slow and fatigue crack growth.

Identification of the cracking mechanism (slow crack growth) was essential for selecting proper tests in the material property evaluation portion of this study. The two stress crack resistance tests, environmental stress crack resistance (ESCR) and single point tensile load (SP-NCTL), are specifically designed to assess susceptibility to steady slow crack growth.

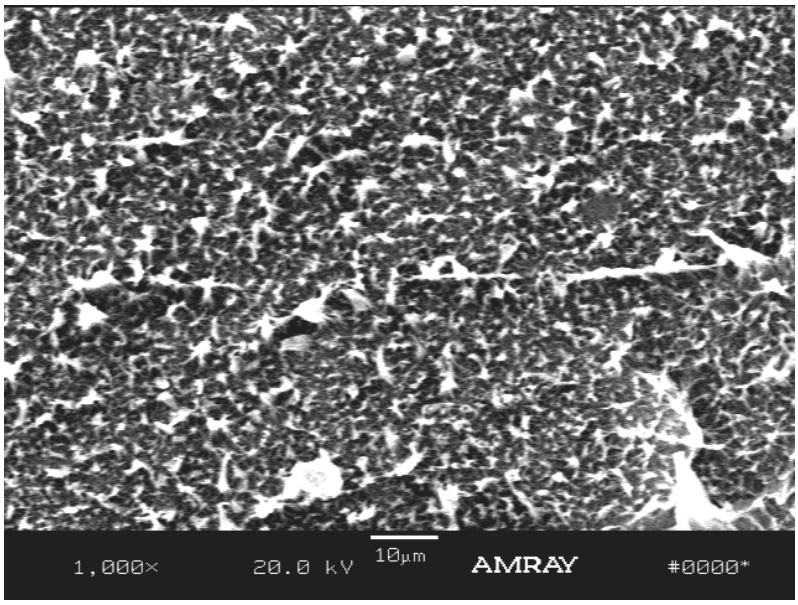

Figure 12: An example of a fibril structure on the fracture surface of a cracked duct sample.

TASK IV: EVALUATION OF PIPE SCR USING PERFORMANCE TESTS

Introduction

The SCR behavior of the HDPE ducts was evaluated using two additional tests other than that of SP-NCTL. The latter test is designed to distinguish SCR of different HDPE materials under an accelerated test condition that can be completed in a relatively short period of time. However, the test results under the acceleration environment may not correlate with field performance. In particular, the 10 percent Igepal solution used in the SP-NCTL test does not simulate field situations where HDPE ducts are exposed to ambient air inside segmental boxes. For performance types of test, the design should simulate the field situation to the maximum extent possible. Two different methods were used in an attempt to provide results more relevant to actual service: the SP-NCTL method in air and fatigue tests at ambient temperature.

SP-NCTL Tests in Air

It is known that slow crack growth proceeds much slower in air than in an Igepal solution. To overcome this, test temperature for the air SP-NCTL tests was selected as 50^{o}C. Table 9 shows the results

for tests performed in each of the two environments. The acceleration factor induced by the 10 percent Igepal solution was by a factor of approximately 8.0.

Table 9: Specified properties for PE ducts.

Property	Test Method	AASHTO	FDOT	Required Value
Density (g/cc)	ASTM D 1505 or D 792	3	3	>0.940-0.955
Melt index (g/10 min)	ASTM D 1238	4	4	< 0.15
Flexural Modulus (psi)	ASTM D 790	5		110,000 - < 160,000
			4	80,000 - <110,000
Tensile yield strength (psi)	ASTM D 638 Type IV	4	4	3000 - <3500
SCGR*	ASTM D 1693 (ESCR test)	3		F_{20} = 192 hr
	ASTM F 1473 (PENN Test)		6	100 hr
HDB** (psi)	ASTM D 2837	3		1250
			4	1600
Carbon black	ASTM D 1603	C	C	> 2%
Additional Tests				
OIT (min)	ASTM D3895	-	40	

* SCGR – slow crack growth resistance
** HDB – hydrostatic design basis
+ OIT – oxidative induction time

Evaluation of Fatigue Properties of Retrieved and New Duct Samples

A possible source of stress that may cause longitudinal cracking in a duct is from thermal cycling in conjunction with diurnal, seasonal, and weather-front temperature changes. Such stressing is cyclic or time variable and may be most severe when a channel type grout void is present, as discussed subsequently. For this reason, fatigue properties of the different duct materials were assessed, as described below.

Fatigue Test Procedure

Fatigue resistance of the materials was evaluated based on load control tests performed on compression molded specimens. Specimen preparation involved cutting duct samples into small pieces

and compression molding these into plaque with thickness of 0.25 in. The molding procedure was according to ASTM D1928 Procedure C at a cooling rate of 15 ± 5°C. Four inch long by one inch wide specimens were cut from the plaque using a die. A 20 percent notch depth (0.05 inch) was introduced at the center of the specimens at a notching rate of 0.02 inch/min.

The fatigue tests were performed based on a three point bending configuration with a two inch span. Figure 13 shows a general view of the fatigue test system and Figure 14 of the mounting device and specimen.

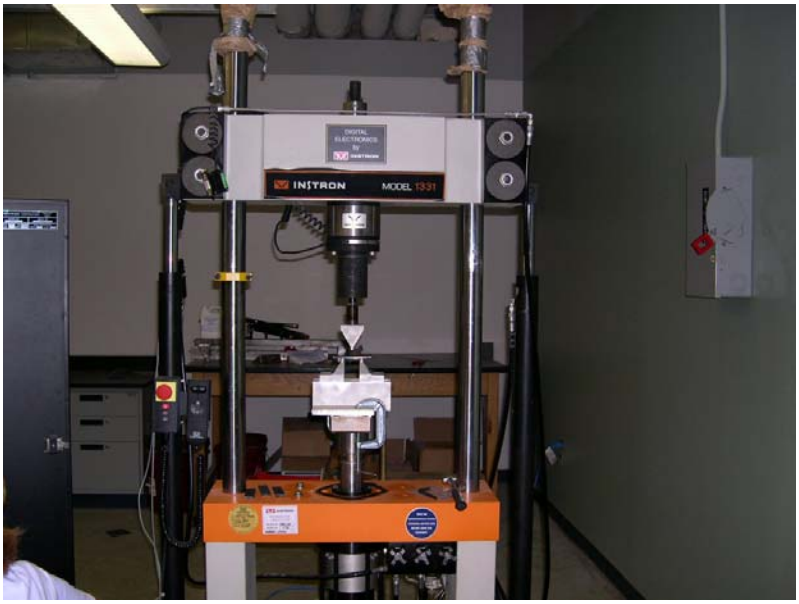

Figure 13: General view of the fatigue test machine and specimen.

The fatigue loading profile was a half-sine wave with a 10 pound initial load. Specimens were subjected to a constant amplitude cyclic loading until failure, at which point the machine automatically stopped with the number of cycles being recorded. Failure was defined as the number of cycles at which a vertical deformation of one inch occurred. The loading frequency was 3 Hz. Maximum applied loads 20 to 110 lb (load ranges from 10 lb to 100 lb) were used, and the corresponding stress (σ) was calculated using Equation 1:

$$\sigma = \frac{3PL}{2bd^2} \qquad (1$$

where: P = applied load (lb),

L = span length (2 inches),
b = width of specimen cross section (1 inch), and
d = depth of specimen cross section (0.25 inch).

Figure 14: Close-up view of the three point bending device with test specimen.

Fatigue Test Results and Discussion

A total of six duct materials were evaluated by fatigue testing. These included samples from the Mid-Bay (MB), Sunshine Skyway (SSK), Seven-Mile, and Long-Key (PE 3406) Bridges. The other two samples were new duct materials, which are designated as FAU-3408 and SSK-3408 (see Tables 1 and 5).

The results of the fatigue tests are presented as a plot of maximum stress versus cycles-to-failure (S-N plot), as shown in Figure 15. These conform to a Power Law relationship according to the expression,

$$\sigma = AN^{b} \qquad (2$$

where: σ = stress,
N = cycles-to-failure, and
A and b are material constants,

and can be divided into three groups. The MB and SSK specimens exhibited similar fatigue behavior and have the lowest fatigue resistance of the six materials. The two new PE 3408 duct specimens behaved

similarly and exhibit the highest resistance. Results for the Seven Mile and Long Key Bridge duct specimens are intermediate. It should be noted that the order of the fatigue resistance of these six ducts is identical to that of the SCR measured by the SP-NCTL test. Also, while the 3-point bend results indicated poorest performance by the MB and SSK specimens, it did not distinguish between the PE, Seven Mile, and Long Key Bridge specimens (Figure 7).

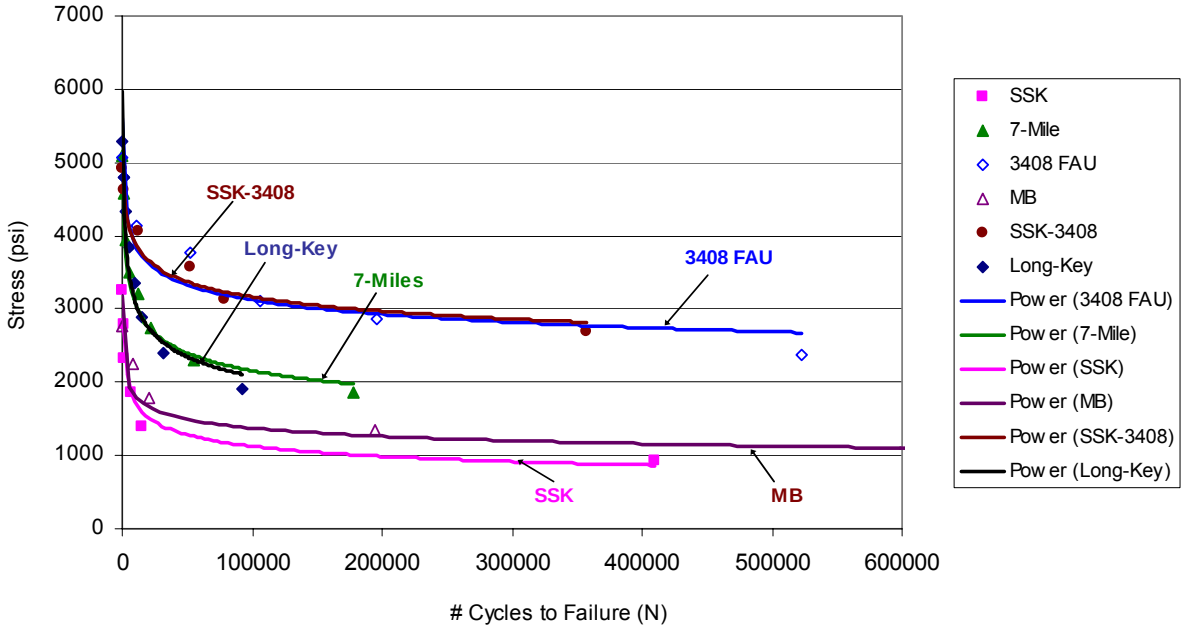

Figure 15: Fatigue S-N curves for the six tested duct materials.

TASK V: ASSESSMENT OF CURRENT MATERIAL SPECIFICATIONS FOR SMOOTH PE DUCT

As part of this study, a proposed revision of the material specification for smooth PE ducts was developed. This was adopted by the FDOT in April, 2003 and is presented as Section 462 of the Post-Tensioning specification document.

Table 10 compares the recently adopted FDOT specification, which is based on the cell class in ASTM D 3350, with the AASHTO specification. Major changes pertain to the SCR requirement and the additional of the OIT test.

The new FDOT specification basically requires that PE ducts to be made from the pressure rated resins. In the gas pipe industry, the PENN (ASTM F 1473) test is commonly used as the quality control

and quality assurance test in additional to the HDB test, which is performance based. Since the manufacturers do not use the SP-NCTL test for product evaluation, implementing such test in the specification would not be practical. Thus, the PENN test is used to assess the slow crack growth of PE ducts instead of the SP- NCTL test. Ducts that are made from PE 3408 resins (duct from the Garcon Point Bridge) showed a failure time of 110 hours in the PENN test.

Table 10: Soxhlet extraction results.

Sample Number	Sample Source*	Initial Weight, g	Final Weight, g	Weight Loss, percent
S1	New 3408 Pipe	0.50456	0.49736	1.43
S2	New 3408 Pipe	0.51899	0.51326	1.10
S3	MBB 67-5A*	0.50181	0.48153	4.04
S4	MBB 67-5A*	0.50596	0.50075	1.03
S5	MBB 38-4A*	0.50616	0.49763	0.02
S6	MBB 38-4A*	0.51239	0.50657	1.14
S7	MBB 38-4A*	0.50381	0.49822	1.11
S8	MBB 67-5A*	0.50715	0.50342	0.74
S9	MBB 67-5A*	0.56444	0.55803	1.14

TASK VI: EXPERIMENTAL AND ANALYTICAL MODELING OF TENDON DUCT CRACKING

Simulated Tendon Experiments

Background

The purpose of these tests was to experimentally determine the strain that can arise in a partially grouted duct as it is subjected to thermal cycling. Figure 16 schematically illustrates the basis for this, where bending stresses are projected to occur in a duct opposite a void channel during periods of thermal contraction. It has previously been opined that this contributed in part to tendon duct cracking at the Mid-Bay Bridge (4).

Experimental Procedure

The experimental approach involved fabrication and exposure to thermal cycling of reduced length,

instrumented simulated tendon specimens. Figure 17 shows the component parts for these prior to assembly, and Figure 18 is a photograph of a completed simulation tendon, including a restraining frame. These assemblies were 54.5 cm (21.5 in) long and were comprised of 102 mm (4 in) nominal diameter HDPE 3408 pipe. Figure 19 illustrates the locations of strain gages and thermocouples upon these tendons. The strain gauges at the 12 o'clock orientation were intended to provide information regarding the stress state that arose in the duct from thermally induced dimensional changes and presence of a grout void. The fabrication and experiments consisted of the following steps:

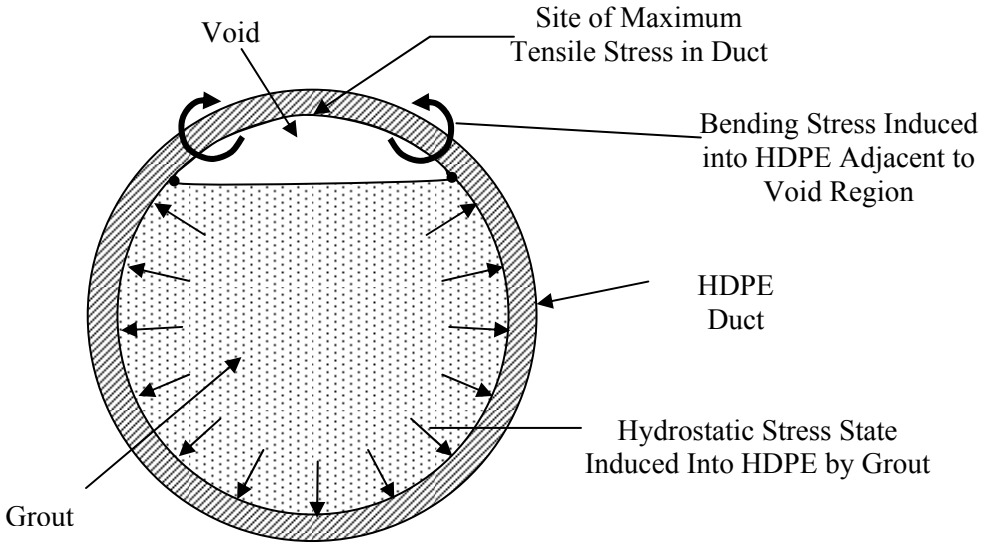

Figure 16: Schematic illustration of the bending stresses in duct above a grout void.

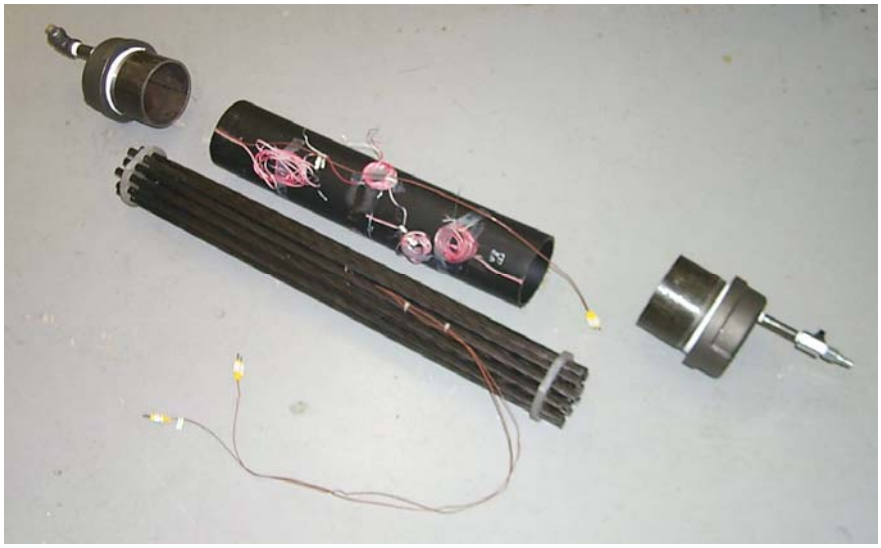

Figure 17: Photograph of simulated tendon components prior to assembly (couplers between end caps and duct not shown).

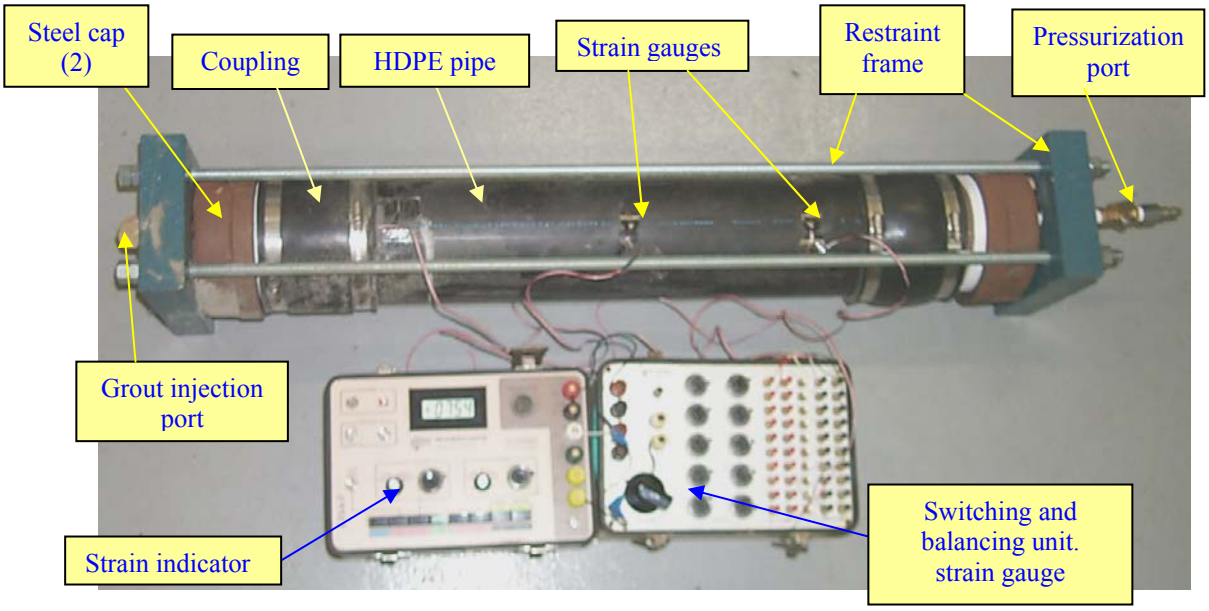

Figure 18: Photograph of an instrumented tendon duct specimen.

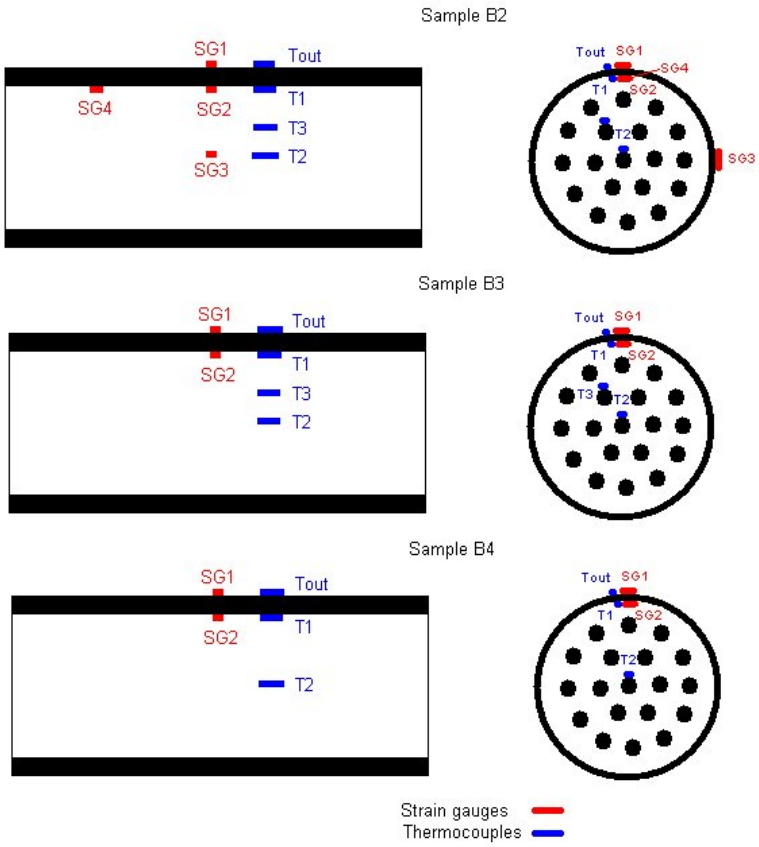

Figure 19: Schematic illustration of tendon segment specimens with locations of strain gauges and thermocouples,

1. Grout injection under pressure to a prescribed fraction of the pipe cross section such that a void channel resulted along the upper duct interior,

2. Grout setting under pressure,

3. Pressure release, and

4. Cyclic exposure to different temperatures.

Table 11 provides the pressurization levels and times for step 2. Subsequent to setting, strain gauge outputs and temperature were monitored during the thermal cycling.

Table 11: Pressurization levels and times for simulated tendon specimens during grouting and grout setting.

Specimen Number	B2	B3	B4
Pipe SDR	21	26	17
Pressure during Setting, MPa (psi)	0.414 (60)		
Time of Pressure Application, hrs	22	2	21.5

Specimens B2 and B4 were subjected to a 14 day thermal cycle which consisted of, for the first 98 days, seven days in a freezer at -39°C ± 2°C followed by seven days outdoors (temperature between 20 and 35°C at the time of measurement). Subsequently, a more severe temperature cycle of four days in a heated chamber at 45±2°C followed by three days at -39±2°C was employed. Specimen B3 was maintained outdoors for the entire exposure (temperature between 15 and 35°C at the time of measurement). For a ventilated, sheltered outdoor Florida exposure, an extreme temperature range should vary from about 36^{o}C (2 to 38^{o}C) in the Keys and 50^{o}C (-9 to 41^{o}C) in the northern region. These are less than for the simulated tendon exposures where the ranges for specimens B2 and B4 were 59-74^{o}C initially and 84^{o}C subsequently). However, it can be reasoned that since the simulated tendons were prepared and pressurized indoors (22-24^{o}C), duct strain gage outputs that occurred during exposure at higher temperatures reflected thermal expansion of the duct only and not mechanical strains, since the coefficient of thermal expansion of the duct exceeded that of the grout. On this basis, the thermal cycling was from -39 to 22-24^{o}C such that the range was 61-63^{o}C, which is about 20 percent greater than what should occur in service (see above). The specimens were under test for 220 days.

Results and Discussion

Experiments: Figure 20 shows temperature as recorded via the outer side surface mounted thermocouple

(T_{out}) and corresponding inner surface mounted one (T_1) versus time for Specimen B2. Here, close time interval temperatures are indicated during the transition periods for several cycles; but otherwise only steady-state values are reported. The data indicate that, while temperature distinctions occurred during the transition periods, the steady state values were essentially the same on both pipe walls. Temperatures for Specimen B4 were essentially the same as for B2, as the two specimens underwent the same thermal cycling. Likewise, Figure 21 shows the corresponding temperature data for Specimen B3. These temperatures are not necessarily maximum and minimum values but for the time the measurements were made. Variations between the inside and outside surface temperatures are magnified here compared to those in Figure 20 because of scale difference.

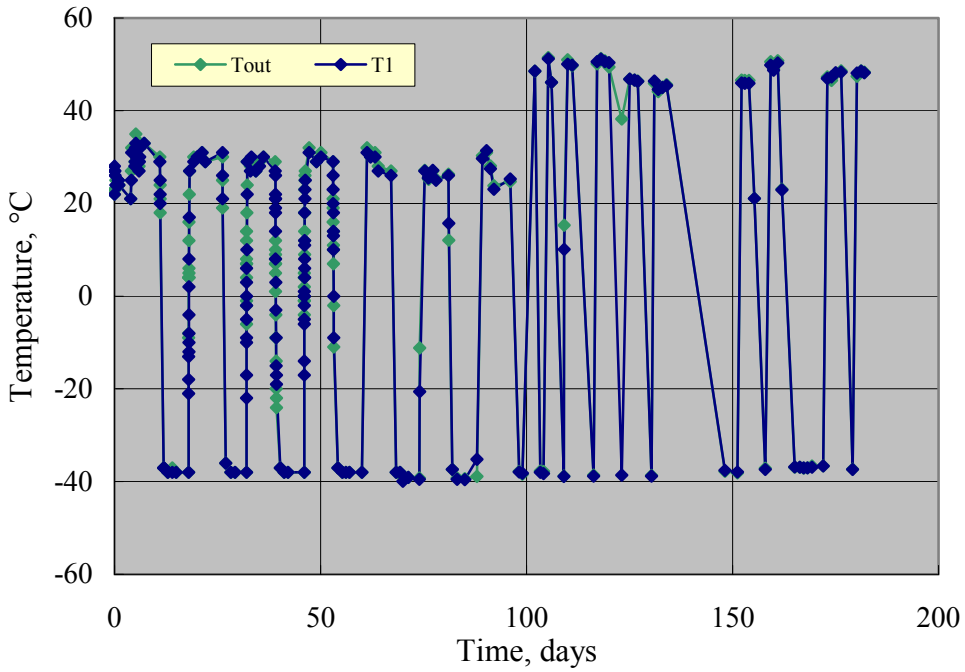

Figure 20: Temperature versus time data for Specimen B2.

Figure 22 shows an expanded time scale view of a warming cycle for Specimen B2. This indicates that temperature differentials across the HDPE wall in the void region were as high as 15°C, whereas between the outside wall and tendon interior this difference reached 40°C. Of course, this degree of thermal shock and, hence, gradient, is not expected in service where temperature changes should be more gradual.

Figure 23 shows a plot of micro-strain versus time for Specimen B2 at the four gauge locations in

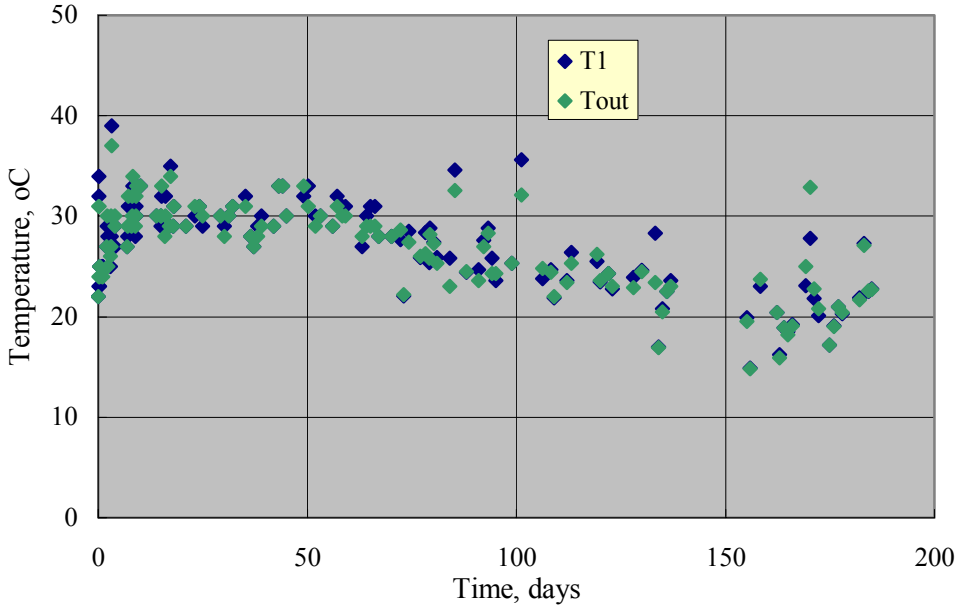

Figure 21: Temperature history for Specimen B3.

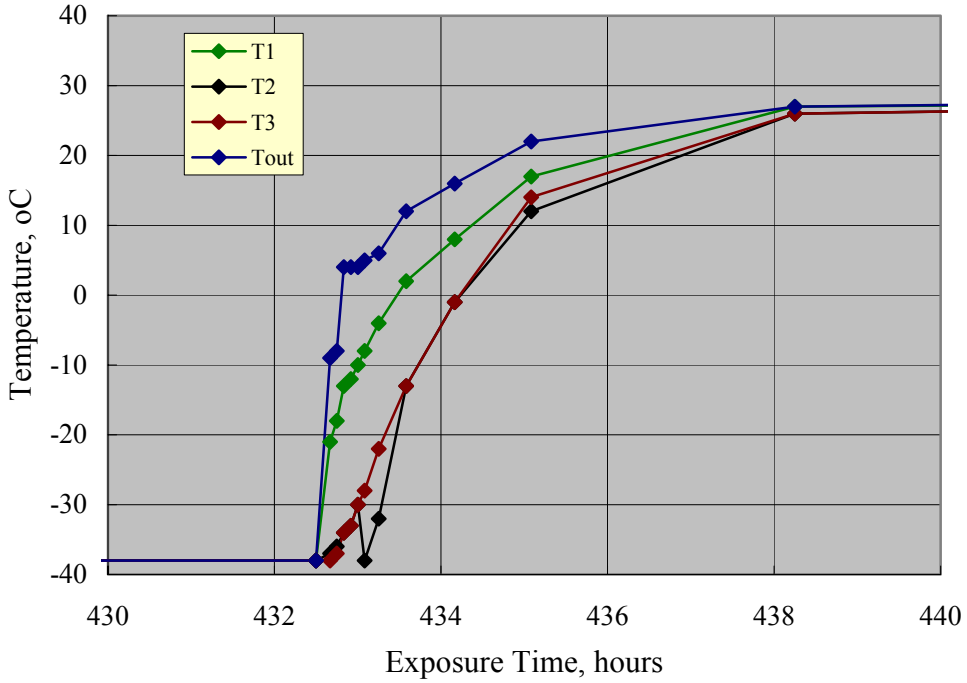

Figure 22: Expanded time scale view of temperature change for different locations within Specimen B2 during the warming portion of a cycle.

Figure 18. The initially high positive (tensile) strain for all gauges reflects the pressurization that was maintained initially (Table 11). Output from all four gages dropped about 20-25 percent upon pressure release, followed by a further strain decrease with time for SG1-SG3. For specimen B3 this decrease was

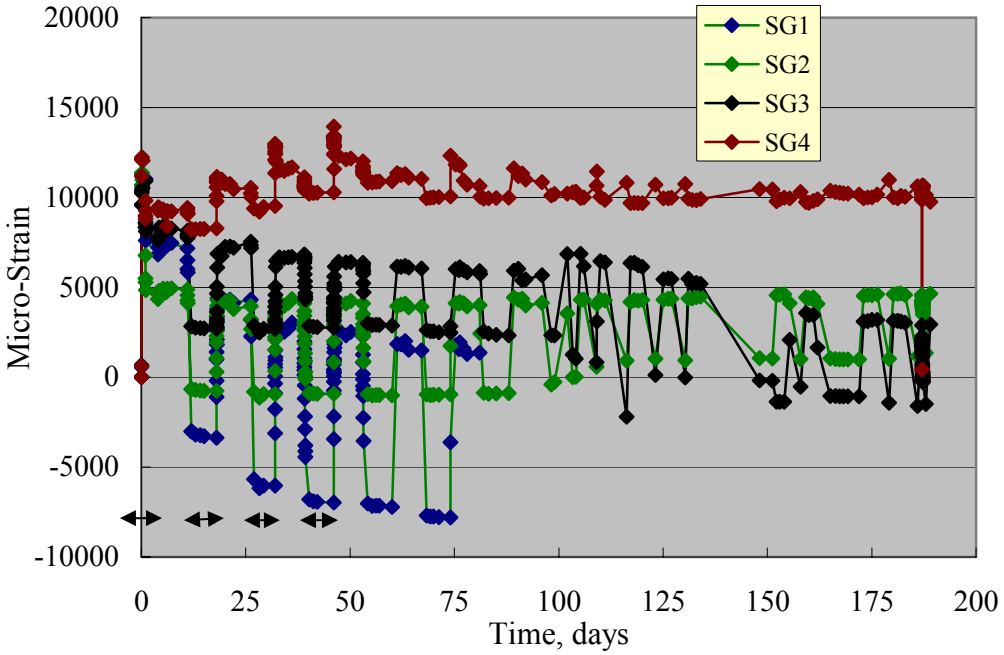

Figure 23: Strain versus time history as determined by gauges on Specimen B2 (arrow ranges indicate periods at ambient temperature).

by 60-70 percent and about 33 percent for B4. The greater strain decrease for B3 is consistent with the shorter time that this specimen was pressurized (see Table 11) such that the duct was probably able to contract upon pressure release to a greater extent than for B2 and B4 by deforming the partially set grout. The cyclic variation that is apparent during periods when strain was measured at close time intervals coincides with the thermal cycling shown in Figure 20. The magnitude of these strain changes was greatest for SG1, followed by those for SG 2 and SG3. This ordering is consistent with variations for SG3 reflecting hydrostatic and thermal expansion/contraction effects only, whereas bending stresses may also have been a factor for SG1 and SG2 (see Figure 16). The strain variations with time were generally reproducible from one cycle to the next, although an overall downward trend is apparent in some cases. Figure 24 provides a combined temperature/micro-strain versus time plot for gauges SG1 and SG2 during the cooling portion of a cycle.

Figure 25 plots micro-strain versus temperature for Specimen B2 and indicates that the former parameter generally increased in proportion to the latter, albeit with relatively large scatter. Four different thermal cycles are represented here. At any given temperature, the tensile strain recorded by SG3 was highest and for SG1 lowest.

Figure 26 reproduces the data from Figure 25 such that the periods of heating and cooling are

distinguished. This shows that much of the data variation in Figure 25 can be accounted for by considering the two thermal components (heating versus cooling) separately. While a hysteresis with higher strain during heating is indicated by SG2 (see arrows), the trend was opposite for SG3. In the case of SG1, no trend with time is apparent.

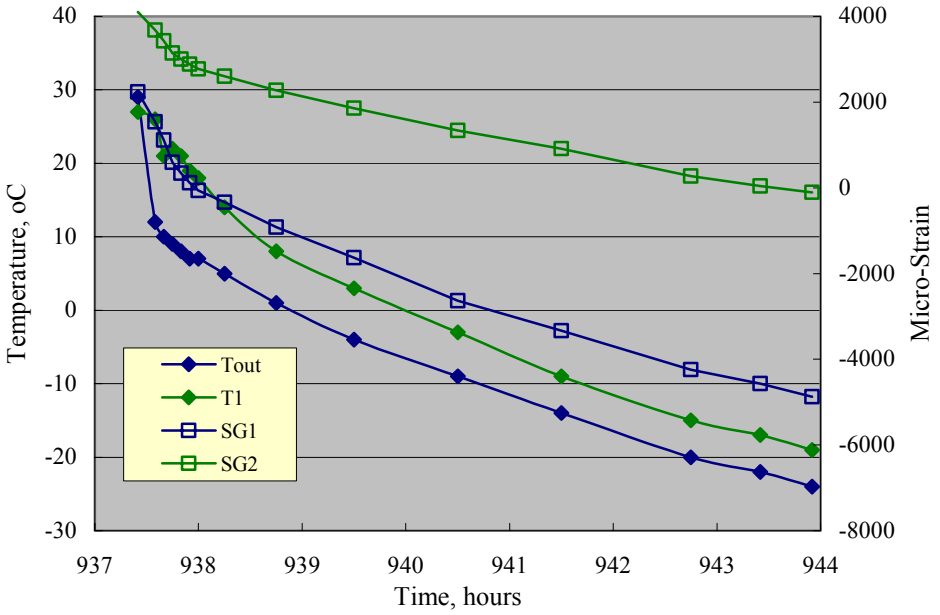

Figure 24: Temperature and micro-strain variations during the cooling transition period of a thermal cycle for Specimen B2.

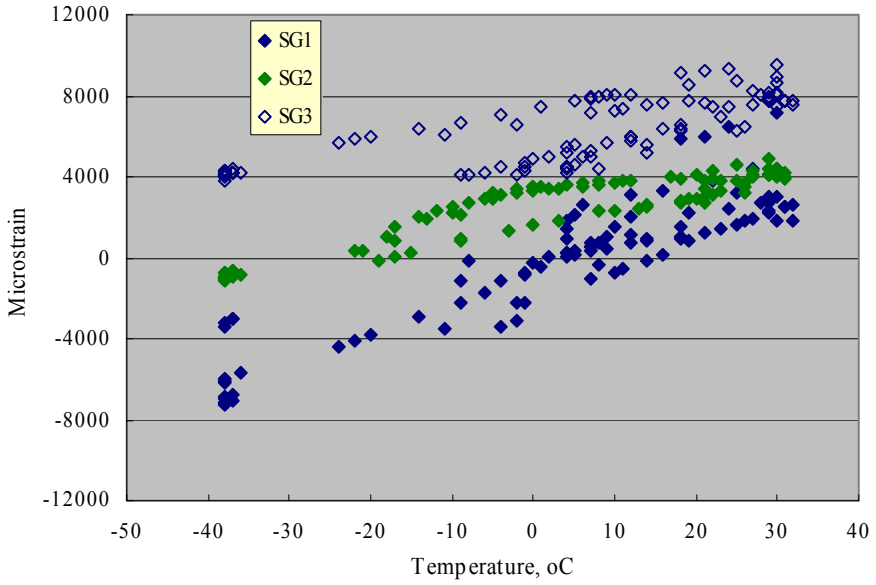

Figure 25: Plot of micro-strain as measured by SG1and SG2 as a function of temperature for Specimen B2.

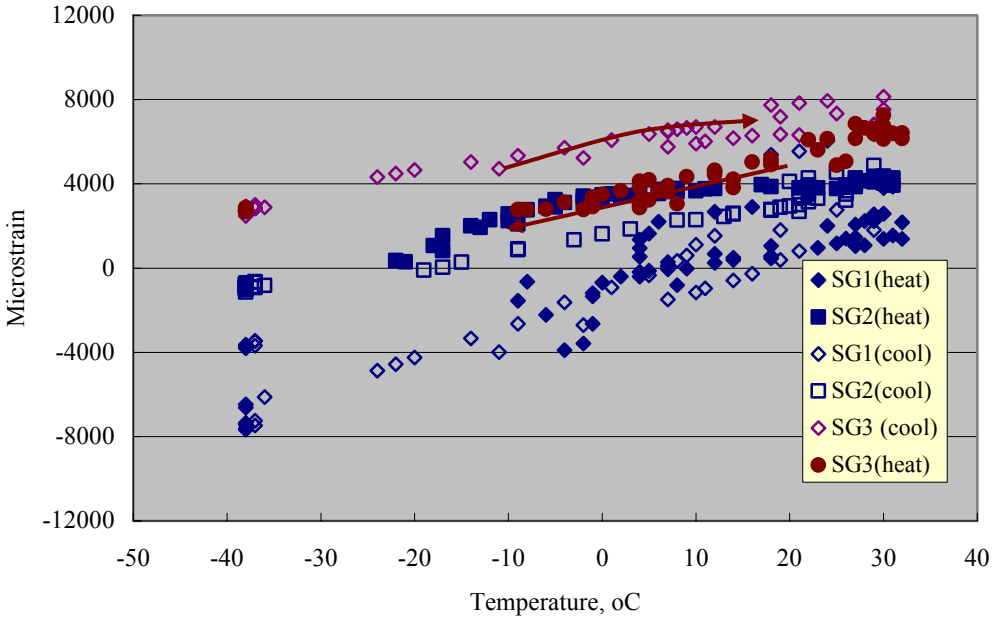

Figure 26: Plot of micro-strain versus temperature for Specimen B2 with periods of heating and cooling distinguished.

Correspondingly, Figure 27 shows strain versus temperature results for Specimen B4. Here, hysteresis is more clearly defined for both gauges than in the case of Specimen B2, particularly at intermediate temperatures. The arrows reflect the temperature-microstrain trend for SG2. No gages were

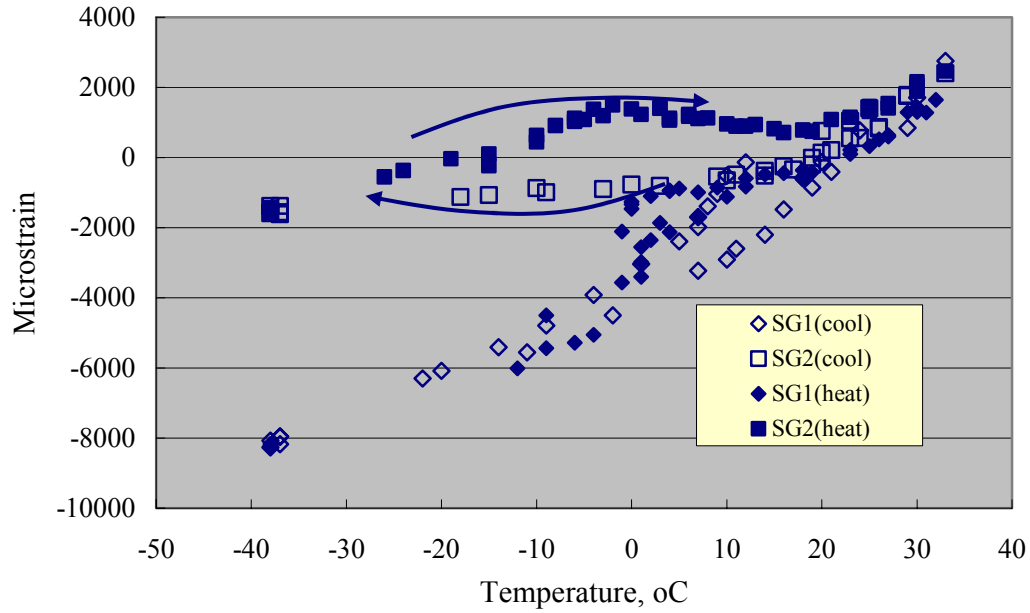

Figure 27: Plot of micro-strain versus temperature for Specimen B4 with periods of heating and cooling distinguished.

employed at the SG3 and SG4 positions for this specimen. Also, while SG1 exhibited a greater temperature dependence than SG2 for Specimen B2, this distinction is more apparent for Specimen B4.

Figure 28 shows corresponding data for Specimen B3 (ambient outdoor exposure). Here, the temperature at the interior and exterior surfaces tended to track one another. Also, temperature and micro-strain variations mutually correlate, the effect being more apparent for SG1. Strain variations with time were more moderate than for Specimens B2 and B4, as should be expected. Nonetheless, a tensile strain on the interior pipe surface near 4,000 micro-units and a strain differential by as much as this same magnitude resulted. Figure 29 plots microstrain versus temperature for Specimen B3 and shows that the strain gage output for SG2 was relatively temperature insensitive over the range covered by the data. Strain gage outputs for Specimens B2 and B4 were also relatively temperature insensitive over this same temperature range (20-35^{o}C), however. Temperature sensitivity for SG1 (Specimen B3) was generally the same as for Specimens B2 and B4. The outdoor exposure of this specimen took place in south Florida and was initiated during the summer when temperature variations were relatively modest. The progressive temperature drop with increasing exposure time (Figure 28) reflects the change in season. The specimen was normally sheltered from direct sunlight; however, the highest temperatures and strains occurred during brief periods when the specimen was placed directly in sunlight.

The data in Figures 23 and 25-29 indicate that decreasing temperature resulted in a strain gage output of decreasing tension in some cases and increasing compression in others (SG1-SG3). This is counter-

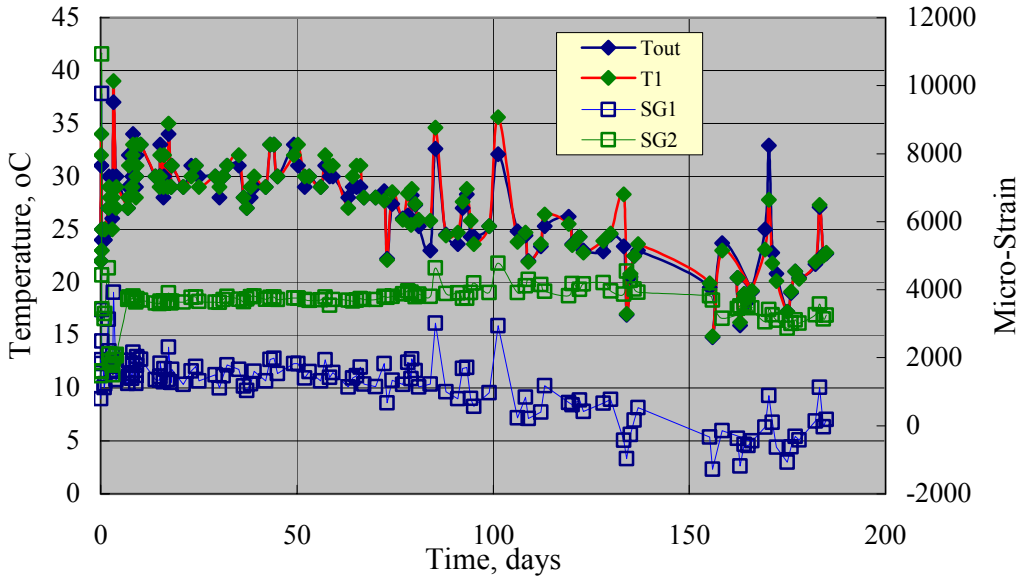

Figure 28: Temperature and strain history for Specimen B3.

intuitive since deceasing temperature should cause the duct, which is expected to have a higher coefficient of thermal expansion than the grout (see below), to contract about the grout. This should result in a progressively greater tensile stress state in the duct with decreasing temperature.

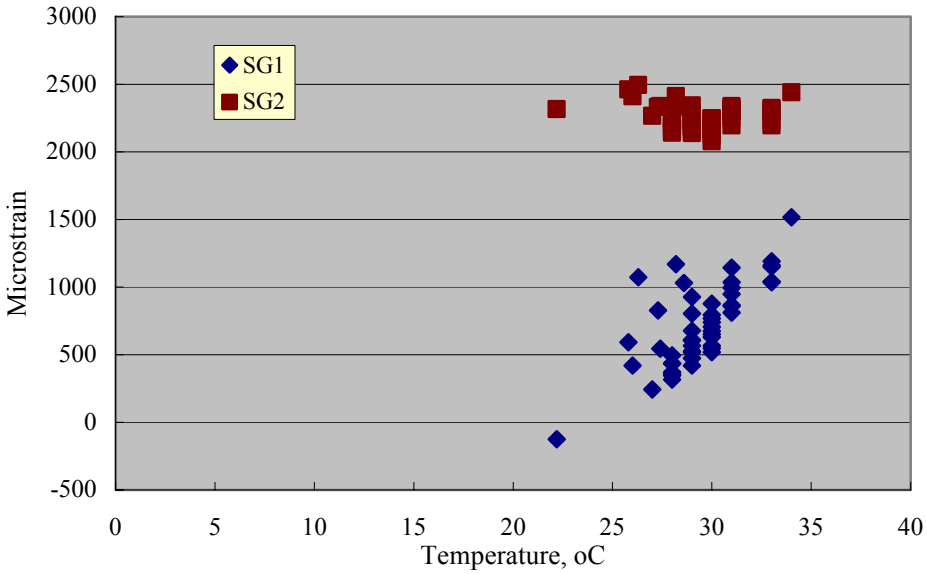

Figure 29: Plot of micro-strain versus temperature for Specimen B3.

With the above in mind, the strain gage output versus temperature data were processed in order to address the above issue. This was accomplished by subtracting the thermally induced dimensional change from the measured strain value. As an initial step, independent experiments were performed to measure the thermal expansion coefficient of both the PE3408 duct and what was assumed to be a representative grout (sample for the Sunshine Skyway Bridge). The procedure and results are provided in Appendix E. Based upon these, a strain versus temperature expression of the form (see Figure 2 Appendix E),

$$\varepsilon = 117 \cdot T + 2340\,, \qquad (3$$

was determined. The strain indicated by this was then subtracted from the measured strain, subject to adjustment of the intercept coefficient to the specific data sets.

Figure 30 shows a corrected strain versus exposure time plot for Specimen B2 for the time span during which SG1 functioned. This reveals that all three gages exhibited a cyclic variation in corrected strain where strain was highest at low temperature and lowest at high. Also, the maximum calculated

strain and strain range were approximately the same for SG2 and SG3, whereas these parameters were lower for SG1.

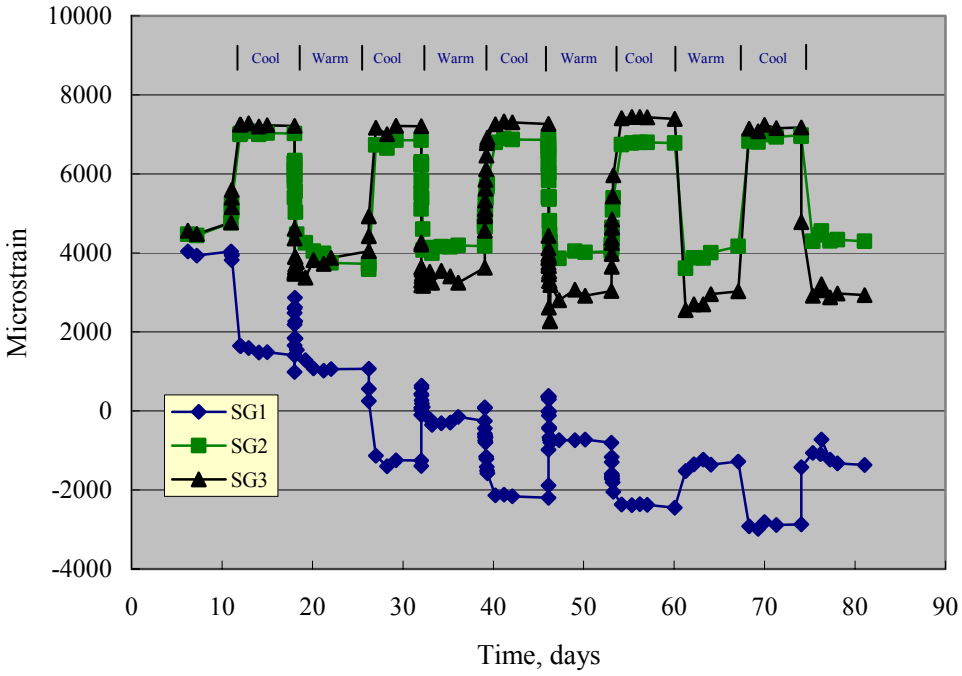

Figure 30: Plot of corrected strain versus time for Specimen B2.

Correspondingly, Figure 31 presents these same data in a strain-temperature format. Here, the data for SG2 and SG3 indicate increasing tensile strain with decreasing temperature, which is consistent with Figure 30, while those for SG1 show an opposite trend. The indicated straight lines are based upon the strain data at the temperature extremes and disregard the intermediate.

Figure 32 shows a corrected strain versus temperature plot for the Specimen B3 data. The general trend here is the same as for Specimen B2 (Figure 31) with regard to temperature dependence; however, in this case the SG1 data occur at a higher strain than those for SG2. No corrected strain-time plot was generated because of the random nature of the temperature variations compared to those of the controlled experiments for Specimens B2 and B4.

Figures 33 and 34 present plots of corrected strain versus time and temperature, respectively, for Specimen B4. The general trend here is the same as for Specimen B2 and B3 in that the highest strains occurred on the interior duct surface during the cool periods and on the exterior during the warm. Also,

while the corrected maximum strain at SG2 on Specimen B2 was approximately 7,000 micro-units, for B4 it was 3,000 micro-units; however, strain range for this same site on B4 exceeded that on B2 (approximately 5,000 compared to 3,000 micro-units). The corrected strain-temperature behavior of SG1 and SG2 on Specimen B4 was intermediate to that for the other two specimens in that at high temperatures the strain at SG1 exceeded that at SG2, but this trend was reversed at low temperature.

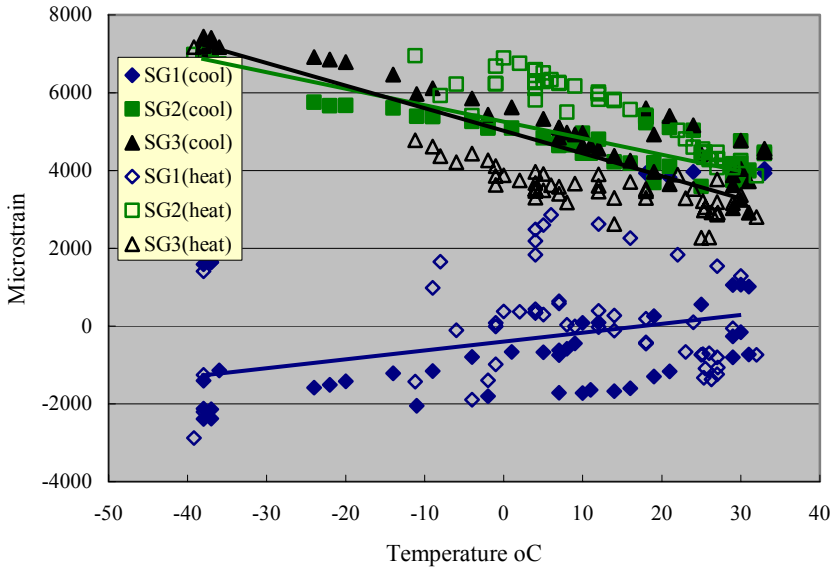

Figure 31: Plot of corrected strain versus temperature for Specimen B2 (best fit lines in each case are based upon the extreme temperature values).

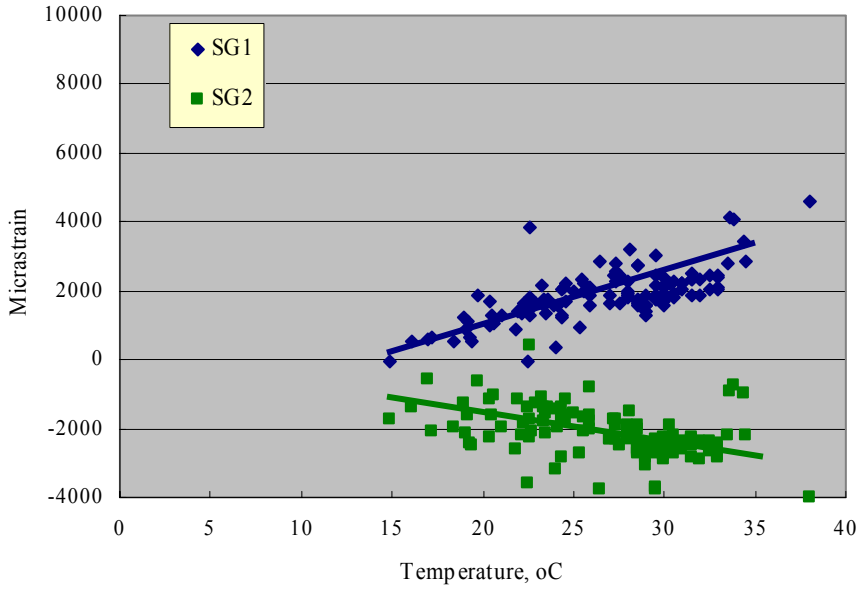

Figure 32: Plot of corrected strain versus time for Specimen B3 showing the best fit line through the respective data.

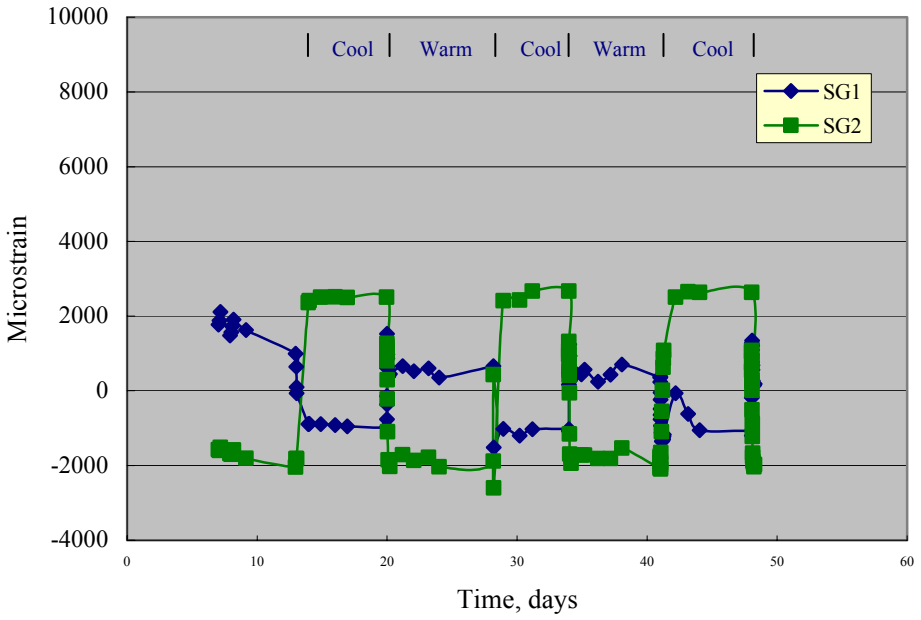

Figure 33: Plot of corrected strain versus time for Specimen B4.

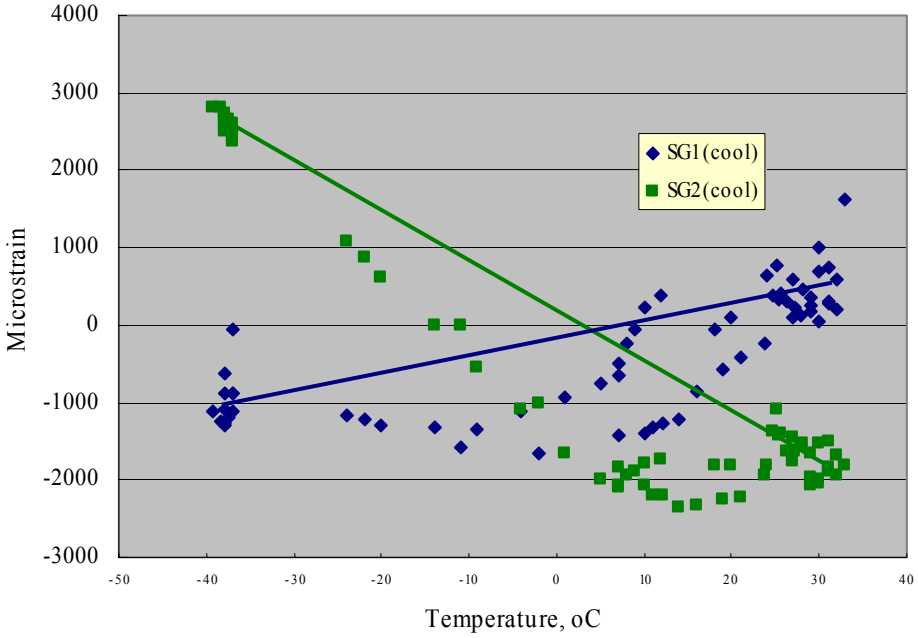

Figure 34: Plot of corrected strain versus time for Specimen B4 showing the best fit line between the extreme temperature data.

It can be reasoned that temperature increases above that at the time of grouting, while serving to increase strain gage output due to duct expansion, did not contribute to an actual mechanical strain, as discussed above. Instead, these tended to relieve strains that developed in conjunction with the pressure

release. On this basis, the extreme of temperature induced mechanical duct strains should result in cases where grouting is performed at times of high ambient temperature. Also, the heat of grout hydration should heat the tendon assembly further.

Each of the three specimens was dissected for the purpose of assessing the size of the grout void channel along the top of the tendon interior. Figures 35-37 provide general views of specimens B2, B3, and B4, respectively, and indicate that in each case the void channel tapered such that it was smaller at the exit grout port end and larger at the entrance end. Figures 38-40 show close up views of each void

Figure 35: View of Specimen B2 subsequent to testing and removal of the HDPE duct so that void channel is apparent.

Figure 36: View of Specimen B3 subsequent to testing and removal of the HDPE duct so that void channel is apparent.

Figure 37: View of Specimen B4 subsequent to testing and removal of the HDPE duct so that void channel is apparent.

Figure 38: Close-up view of the void channel in Specimen B2 at the location of strain gauges SG1, SG2, and SG3 in perspective to a section of duct.

channel at the mid-specimen length (location of gauges SG1-SG3) with a section of duct positioned about the grout to provide a visualization of the void size. These photographs indicate that the void channel of Specimen B2 was largest at the center location and of Specimen B3 the smallest. These dimensional variations may have been responsible for the difference in strain gauge behavior discussed above. The

fact that SDR differed for the specimens (Table 11) may also have been a factor in that a higher bending stress is expected the thicker the duct, all other factors being the same. Thus, Specimen B4 had the smallest SDR; and this may have contributed to the relatively high cyclic stress for SG2.

Figure 39: Close-up view of the void channel in Specimen B3 at the location of strain gauges SG1 and SG2 in perspective to a section of duct.

Figure 40: Close-up view of the void channel in Specimen B4 at the location of strain gauges SG1 and SG2 in perspective to a section of duct.

Finite Element Analysis (FEA): For the purpose of better understanding the results of the tendon simulation experiments and relating the fatigue data (Figure 15) to tendon cracking, a finite element tendon model was developed using ANSYS. The model was a two dimensional representation of the cross-section of a SDR 21 HDPE duct with an interior grout void that comprised either 3, 8, or 10 percent of the interior. Triangular, six node elements were used with a general illustration of the mesh being shown in Figure 41. An expanded view of the modeled duct section above the grout void is shown in Figure 42. Stress-strain response of both materials was considered to be linearly elastic with modulus $1.01 \cdot 10^3$ MPa (146 ksi) for the HDPE and 2.80 10^3 MPa (406 ksi) for the grout. A probable source of fatigue stressing is thermal cycling, as noted above.

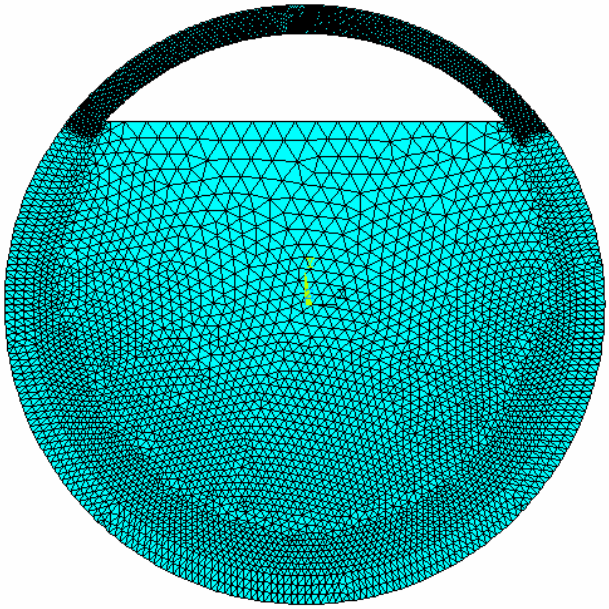

Figure 41: General illustration of the FEA mesh.

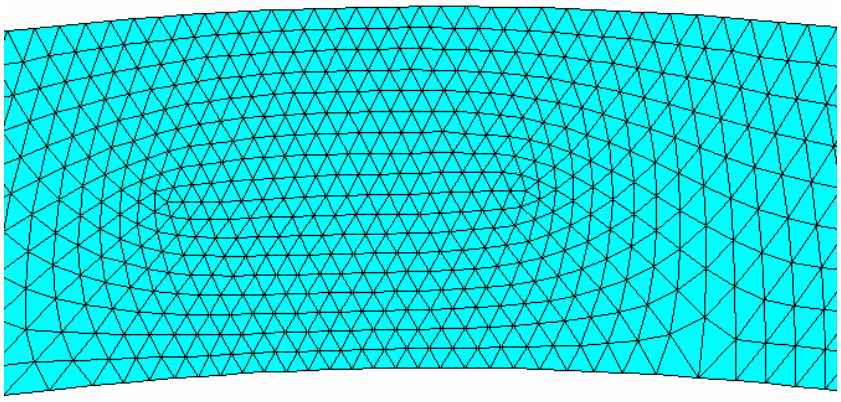

Figure 42: Expanded view of the FEA mesh in the region above a void..

The simulation assumed pressurization of the duct while the grout was plastic, followed by a 30°C temperature drop subsequent to the grout setting. The first step (pressurization) was modeled as a temperature drop of either 33.3°C, which was determined to be equivalent to a 0.414 MPa (60 psi) internal pressure or 41.6°C which corresponds to 0.518 MPa (75 psi). The duct coefficient of thermal expansion was taken as $117 \cdot 10^{-6}$ °C^{-1} and for the grout $10 \cdot 10^{-6}$ °C^{-1} (see Appendix E). Poisson's ratio for the duct and grout were taken as 0.28 and 0.21, respectively.

Results of the analyses are shown in Figures 43-48 as color contoured plots of the first principal (hoop) stress. Of these, Figures 43 and 44 pertain to a ten percent grout void volume, Figures 45 and 46 to eight percent, and Figures 47 and 48 to three percent. Also, the first example in each pair models a grouting pressure of 0.414 MPa (60 psi) and the second 0.518 MPa (75 psi). From these results, it is apparent that tensile stress was high at three specific locations on the simulated ducts. These include the locations of strain gauges SG2 and SG3 from the tendon simulation experiments (see Figure 19), while the third is at the outer duct surface opposite the grout void corner (one on each side). Table 12 lists the FEM computed stress at each of these three locations for the two grouting pressurizations and three void volumes. Correspondingly, Figure 49 summarizes these as a plot of stress range at each of these three

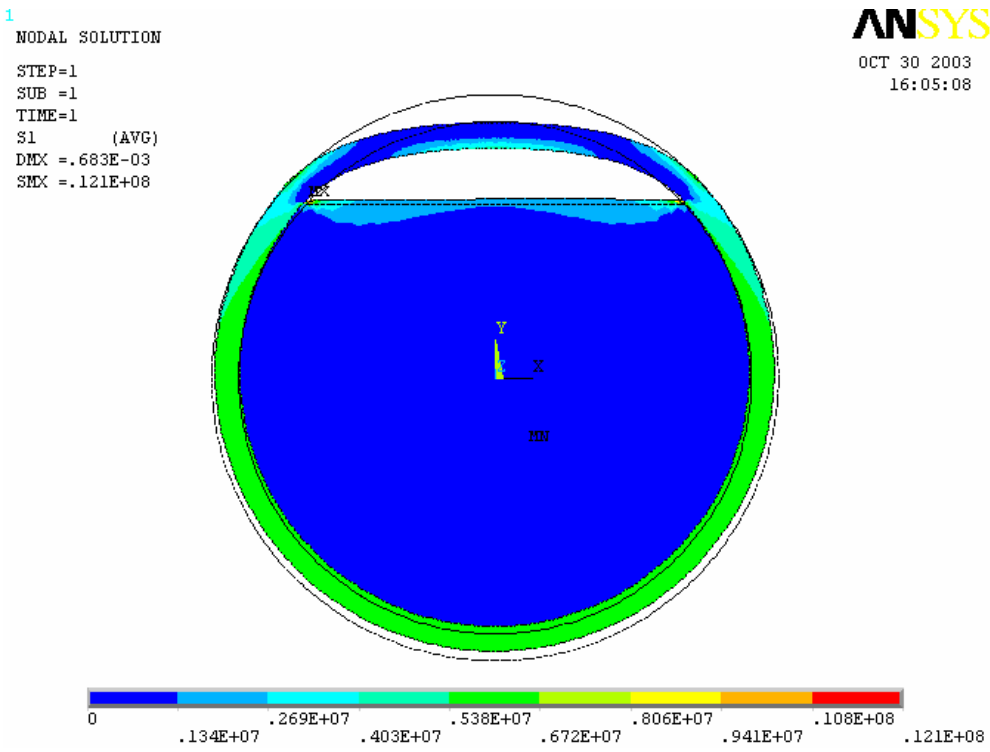

Figure 43: FEA result showing principal stress (hoop) in cylindrical coordinates for a duct with 10 percent grout void and grouting pressure 0.414 MPa. (60 psi) (color-coded units on graph in Pa).

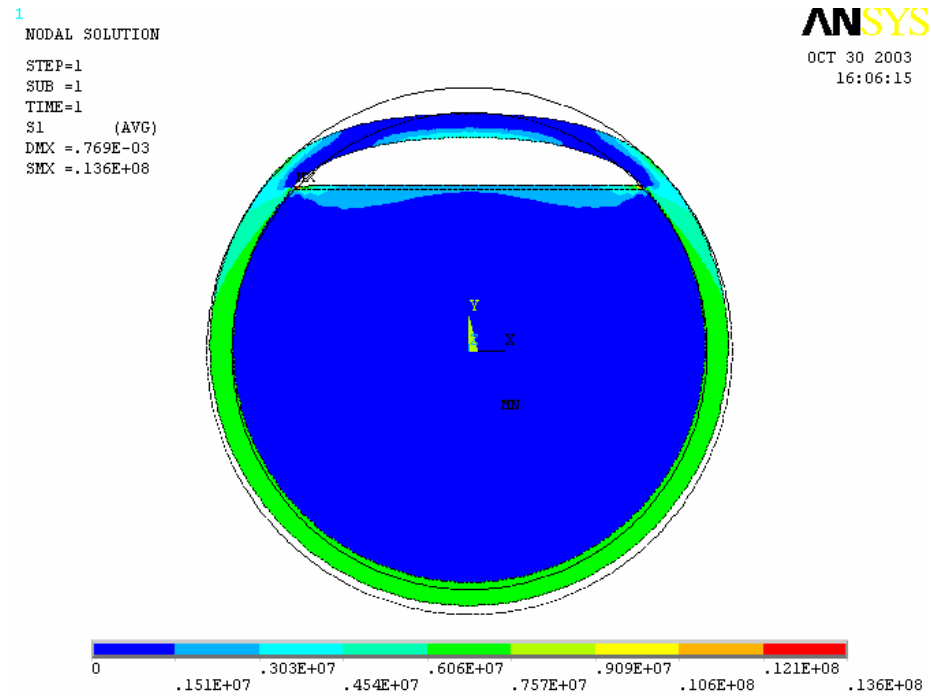

Figure 44: FEA result showing principal stress (hoop) in cylindrical coordinates for a duct with 10 percent grout void and grouting pressure 0.518 MPa. (75 psi) (60 psi) (color-coded units on graph in Pa).

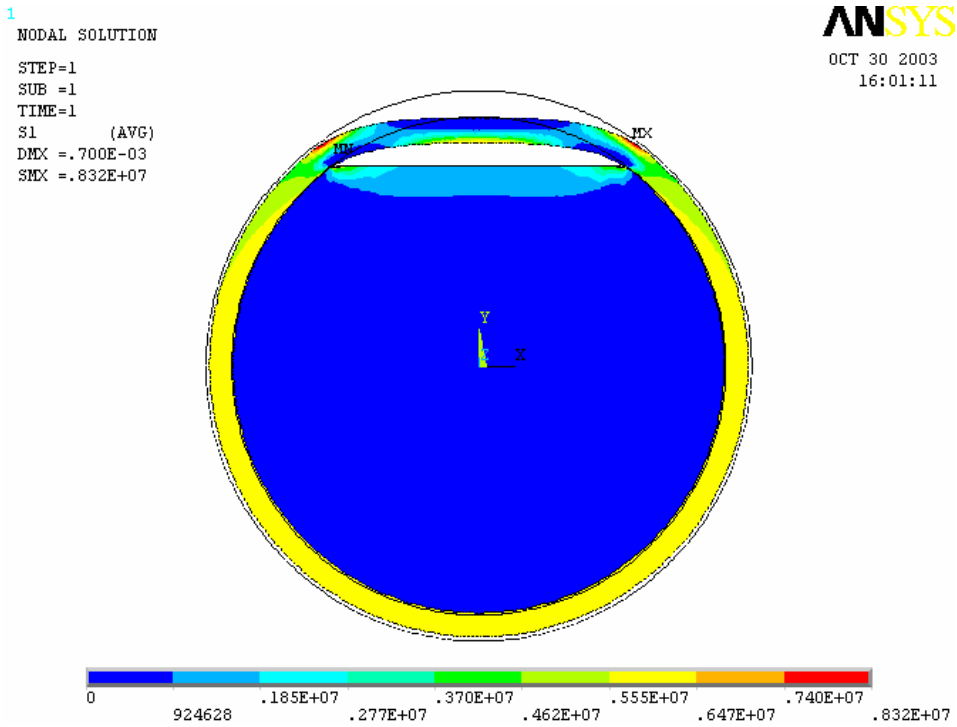

Figure 45: FEA result showing principal stress (hoop) in cylindrical coordinates for a duct with 8 percent grout void and grouting pressure 0.414 MPa. (0.60 ksi) (60 psi) (color-coded units on graph in Pa).

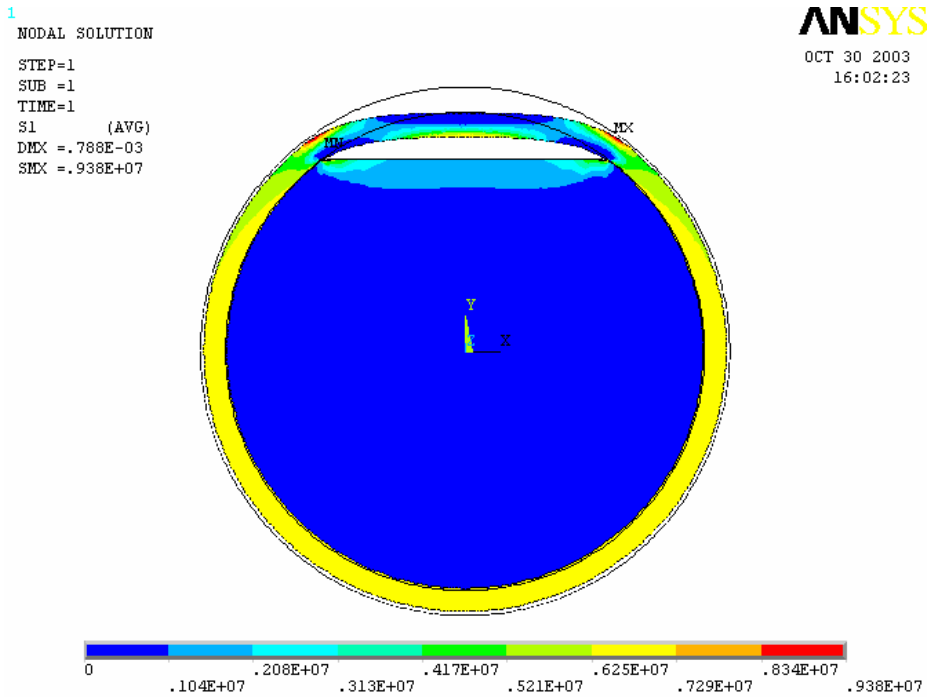

Figure 46: FEA result showing principal stress (hoop) in cylindrical coordinates for a duct with 8 percent grout void and grouting pressure 0.518 MPa. (75 psi) (60 psi) (color-coded units on graph in Pa).

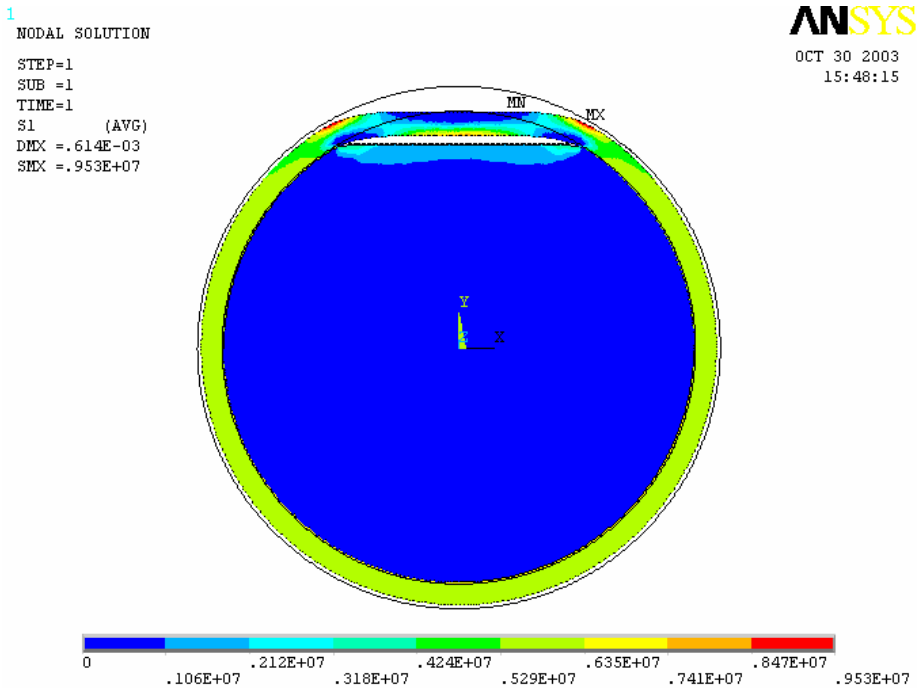

Figure 47: FEA result showing principal stress (hoop) in cylindrical coordinates for a duct with 3 percent grout void and grouting pressure 0.414 MPa. (0.60 ksi) (60 psi) (color-coded units on graph in Pa).

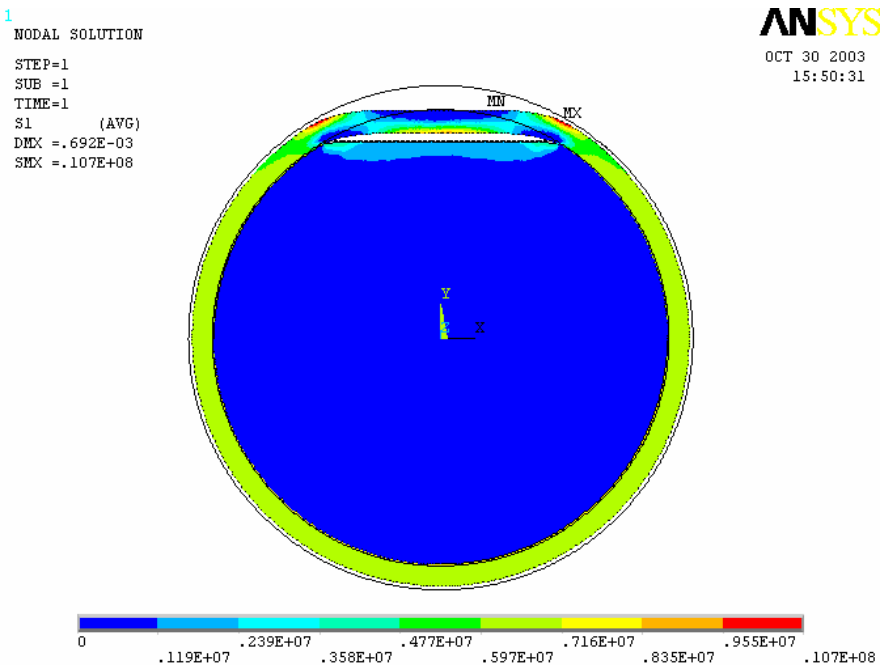

Figure 48: FEA result showing principal stress (hoop) in cylindrical coordinates for a duct with 3 percent grout void and grouting pressure 0.518 MPa. (75 psi) (60 psi) (color-coded units on graph in Pa).

Table 12: Localized duct stress as a function of grouting pressure and void volume.

		Stress, MPa (ksi)		
Pressure, MPa (psi)	Void Volume, percent	SG2	SG3	Corner
0.414 (60)	10	5.38 (0.78)	6.72 (0.97)	6.72 (0.97)
0.518 (75)		6.06 (0.88)	7.57 (1.10)	7.57 (1.10)
0.414 (60)	8	6.47 (0.94)	6.47 (0.94)	8.32 (1.21)
0.518 (75)		7.29 (1.06)	6.25 (0.91)	9.38 (1.36)
0.414 (60)	3	8.47 (1.23)	6.35 (0.92)	9.53 (1.38)
0.518 (75)		9.55 (1.38)	7.16 (1.04)	10.7 (1.55)

locations (stress range is taken as from zero, as should occur at the grouting temperature, to the respective value in Figures 43-48) as a function of void size and grouting pressure. For the smallest model void size (three percent), stress was greatest at the corner locations followed by at the SG2 site. These stresses decrease with increasing void size and merge with measured values from the simulated tendon specimens B2 and B4 (Figures 30 and 33, respectively) for which void volumes at the strain gauge locations were measured as 16 and 10 percent, respectively. This may seem fortuitous in view of the fact that the experimental simulated tendon data were for a 60°C temperature range, whereas the MEA model is based

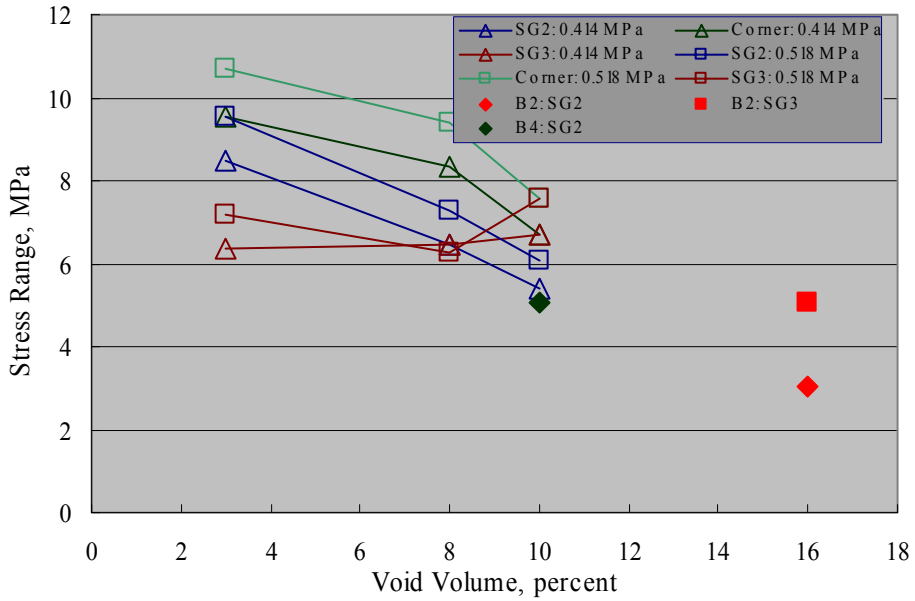

Figure 49: Local duct stress as a function of position, level of pressurization during grouting setting, and void volume.

on a 30°C range; however, the grout heat of hydration should reduce this difference. In all cases, stress was greater for the higher grouting pressure. The correlation between the experimental and analytical results is good. Also shown is the stress range projected for SG3 of specimen B4, which is about 50 percent of the maximum bending, void apex stress (three percent void area). Stress at the B3 location should be independent of void size. The same duct elastic modulus as for the FEM models ($1.01 \cdot 10^3$ MPa) was assumed in converting from strain to stress.

Analysis of Fatigue Data Using FEA: An attempt was made to evaluate the fatigue data (Figure 15) using results of the FEA (Figure 49). As an initial step, consideration was given to the fact that the actual ducts probably contained residual stresses, whereas the fatigue test specimens, which were prepared from molded plaque, did not. For the purpose of taking this into account, a determination was made of residual stresses in the FAU-3408 material (such determinations could not be made upon field acquired samples because in-tact circumferential sections were not available). Two techniques were employed, as described in Appendix F, with results being as shown in Table 13. This indicates that the average residual stresses measured by method 2 was 6.6 MPa which is about 60 percent higher than by method 1. Considering such a residual stress, the highest absolute stress (thermally plus residual) was at the interior void apex position (SG2 in the simulated tendon tests, see Figure 17), since the residual stress on the exterior duct surface was compressive. If then the thermally induced stress on the duct interior is taken as 10.0 MPa (Figure 49) and a residual stress of 6.6 MPa is added to this, a new absolute tensile stress of

(16.6 MPa) results. Both the FEA and simulated tendon experiments indicated that cyclic stressing as a consequence of temperature changes can occur also in the absence of grout voids (Figure 49); however, the stress range is of lower magnitude in this case.

Table 13: Results of residual stress determinations.

Material/ Specimen No.	Strain Change, micro-units (Method 1)	Stress, MPa (Method 1)	Stress, MPa (Method 2)
SDR 17	5249	4.92	6.89
SDR 21	3540	3.32	5.42
SDR 26	3530	3.31	5.89
Specimen B2	5510	5.19	8.23

Figure 50 replots the Figure 15 data in terms of stress range and on log-log coordinates and shows that a stress range of 16.6 MPa corresponds approximately to failure of the MB and SSK specimens at less than 10^3 cycles. Considering that the in-service ducts experienced one thermally induced stress cycle per day, then cracking is projected to have occurred for ducts in these two bridges several years after construction. For the Seven Mile and Long Key Bridges, the cycles-to-failure corresponding to the above fatigue strength (16.6 MPa) is approximately $2*10^4$ or 50-plus years. For ducts utilizing the PE-3408

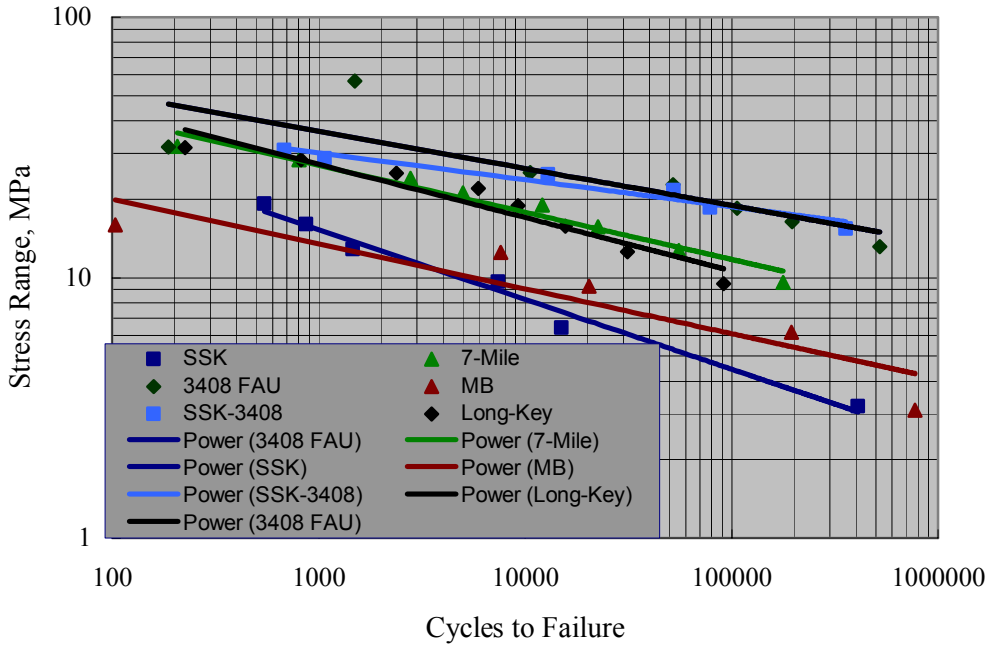

Figure 50: Fatigue data for various duct samples.

resin, this time is beyond 100 years. This, of course, assumes that there are no significant long term detrimental reactions, such as antioxidant depletion, that compromise mechanical properties.

BIBLIOGRAPHY

1. A. Ghorbanpoor and S.C. Madathanapalli, "Performance of Grouts for Post-Tensioned Bridge Structures," Report No. FHWA-RD-92-095, Federal Highway Administration, Washington, DC, Dec., 1993.

2. H. Tabatabai, A.T. Ciolko, and T.J. Dickson, "Implications of Test Results from Full-Scale Fatigue Tests of Stay Cables Composed of Seven-Wire Prestressing Strand," Proceedings Fourth International Bridge Engineering Conference, Vol. 1, Transportation Research Board, National Research Council, Washington, DC, 2000.

3. "Mid-Bay Bridge Post-Tensioning Evaluation," Final Report submitted to Florida Department of Transportation District 3 by Corven Engineering, October 10, 2001.

4. W.H. Hartt and S. Venugopalan, "Corrosion Evaluation of Post-Tensioned Tendons on the Mid Bay Bridge in Destin, Florida," Final Report submitted to Florida Department of Transportation by Florida Atlantic University, January 2, 2002.

5. "New Directions for Florida Post-Tensioned Bridges," Final Report submitted to Florida Department of Transportation by Corven Engineering, February 15, 2002.

APPENDIX A

EVALUATION OF THE HIGH DENSITY POLYETHYLENE DUCTS IN THE MID-BAY BRIDGE

INTRODUCTION

The objective of this study is to determine the material properties of retrieved field high-density polyethylene (HDPE) duct samples that contained cracks. The material properties included in this test program were largely limited to the specification that was applied at the time of construction of the bridge. However, four new tests have been added, and one of the specified tests has been omitted from the test program. An explanation for these changes will be presented in a later section of this study.

TEST MATERIALS

Three duct samples were provided for this study by the Florida Department of Transportation (FDOT). It is assumed that all HDPE ducts used in the bridge were manufactured from a single resin by a single pipe company. Therefore, three duct samples are sufficient to characterize the duct material with reasonable statistical confidence.

The three duct samples were coded as MBB 67-5-A, MBB 38-4-C and MBB 126-4-A. The length of the samples was 48 inches. The samples were taken from three different locations of the bridge as described by the sampling description sheets provided by FDOT. Additionally, photos of the tendon were taken before and after the sampling. Photos 1 to 3 show the tendon from which Sample 67-5-A was taken. The position of the crack in Sample 67-5-A was found to be at 8 o'clock. Photos 4 to 6 show the tendon from which Sample 38-4-C was taken. The position of the crack in Sample 38-4-C was found to be at 12 o'clock. Photos 7 to 9 show the tendon from which Sample 126-4-A was taken. The position of the crack in Sample 126-4-A was found to be at 11 o'clock.

All cracks observed in the three duct samples were longitudinal and propagated almost along a straight line. The direction of the cracks indicates that a circumferential stress was acting on the duct wall. The cracked section of the pipe was carefully cut from the sample for microscopic investigation. The remaining pipe material was used for material evaluation. Figure 1 shows a schematic drawing of the cracked area in Sample MBB 67-5-A. A small crack was observed at the center of the duct sample. The crack length on the inside duct surface (5-inch) was measured to be half inch longer than that on the outer surface (4.5-inch). In Sample MBB 38-4-A, cracking has propagated through the entire 48 inches sample length. The sample contained two separate cracks, Cracks B1 and B2, as shown in Figure 2. Two cracks were also observed in Sample MBB 126-4-A: Cracks C1 and C2, as shown in Figure 3. In all three samples, there were no small hairline cracks observed in the inner surface of the ducts.

Photo 1 – The middle of the three tendons was the location of Sample 67-5-A

Position of Crack

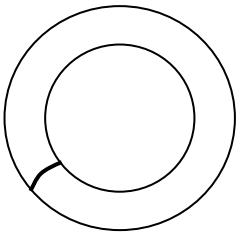

Photo 2 – A close view of the tendon from which Sample 67-5-A was taken. The position of crack was found to be at 8 o'clock

Photo 3 – A view of the tendon after the Sample 67-5-A was removed, thereby exposing the grout material

Photo 4 – The lowest of the three tendons was the location of Sample 38-4-A

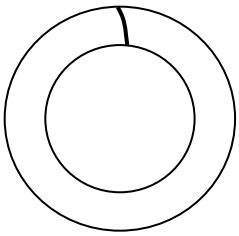

Photo 5 – A close view of the tendon from which Sample 38-4-A was taken. The position of crack was found to be at 12 o'clock

Photo 6 – A view of the tendon after the Sample 38-4-A was removed, thereby exposing the grout material

Photo 7 – The lowest of the three tendons was the location of Sample 126-4-A

Position of Crack

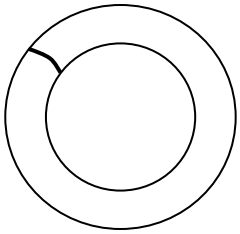

Photo 8 – A close view of the tendon from which Sample 126-4-A was taken.
The position of crack was found to at 10 o'clock

Photo 9 – A view of the tendon after the Sample 127-3-A was removed,
Thereby exposing the grout material

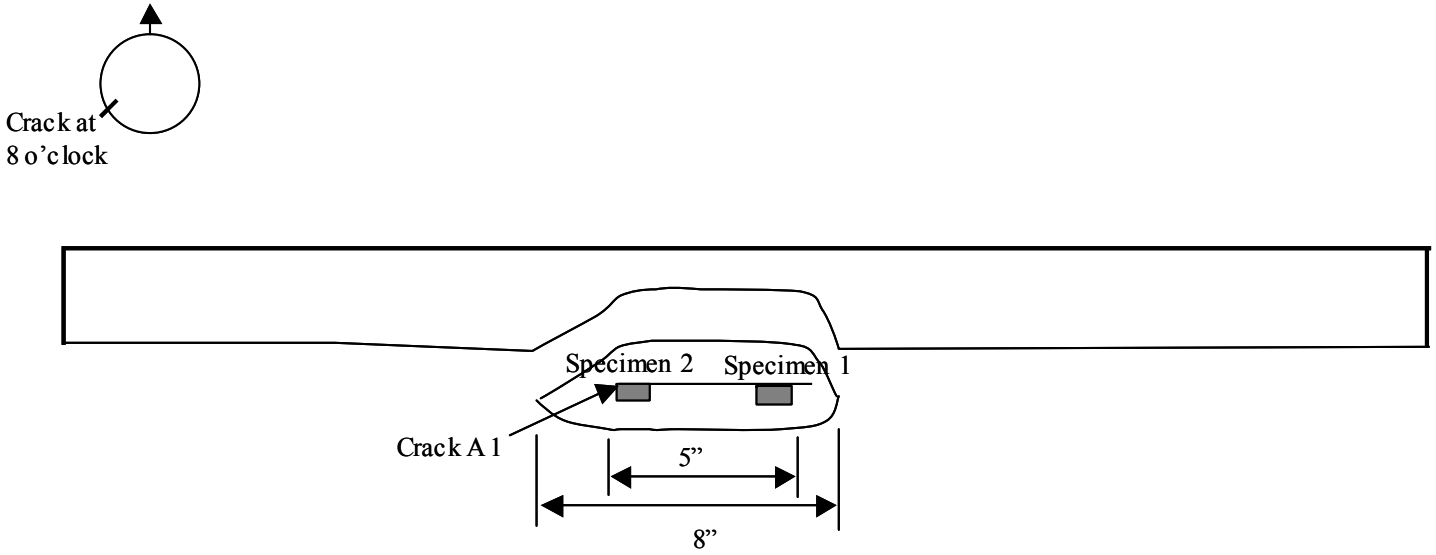

Descriptions:

There is only one crack (A1) on the middle of the pipe. The inside surface crack is about 5 inch long, and the outside is 4.5 inch.

Figure 1 – Schematic drawing of Sample MBB 67-5-A, which contains a small crack

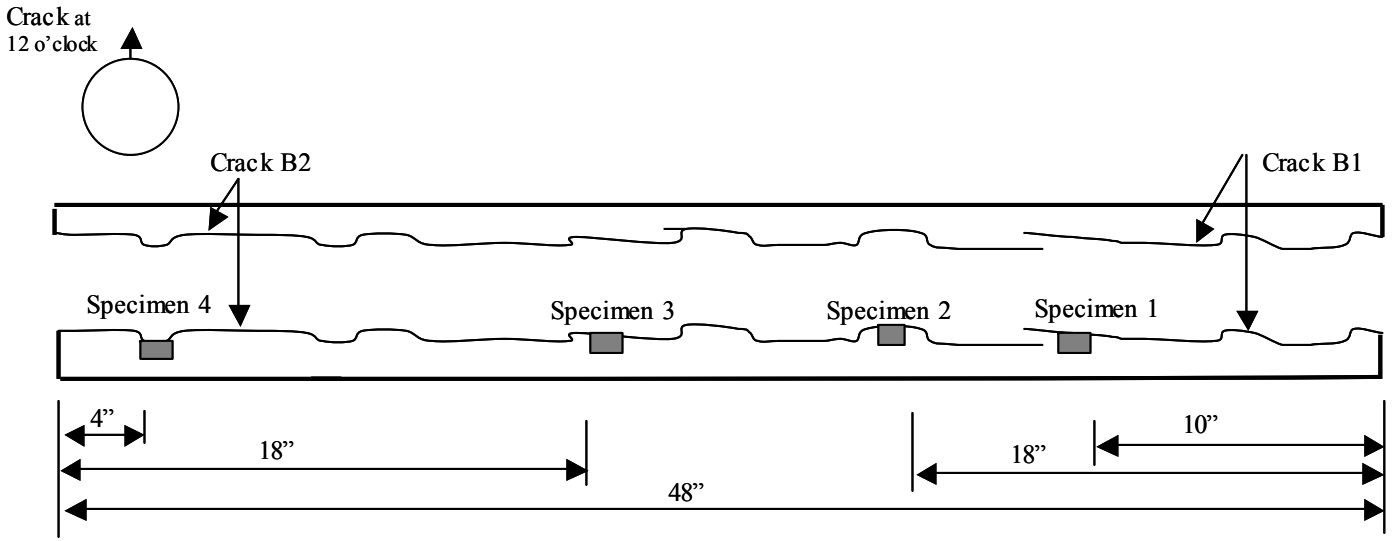

Description:

There are two cracks in this pipe. The two cracks propagate and overlap each other by 1 inch long without connecting.

Crack-B1 is 13 in. on the inside surface, and 13in on the outside surface;

Crack-B2 is 34 inch on the inside, and 34 inch on outside.

Figure 2 – Schematic drawing of a section of Sample MMB 38-4-A which contains two cracks

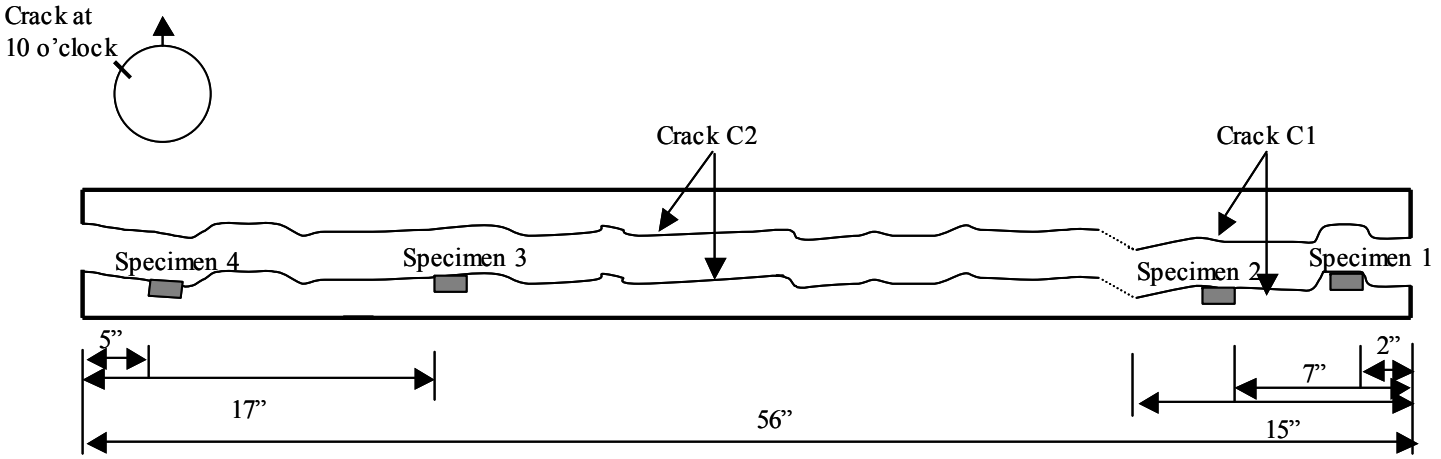

Description: There are two cracks in this pipe. The two cracks are one inch apart from each other measured on the inside surface.

Crack-C1 is 14 inch on the inside surface, and 13 in on the outside surface;

Crack-C2 is 40 inch on the inside, and 38 inch on outside.

Figure 3 – Schematic drawing of a section of Sample MMB 126-4-A which contains two cracks

EVALUATION OF RETRIEVED DUCT SAMPLES

The retrieved field duct samples were evaluated for the cracking mechanism and material properties. The results of these two evaluation are described in the following sections and represent the major portion of this analysis.

Task A – Cracking Mechanism

The microstructure of the fracture surface was examined using a scanning electron microscope (SEM) to identify the crack initiation site(s) and propagation direction. In addition, the cracking mechanism can be indicated by the fracture morphology.

The microstructure of the fracture surfaces was examined by taking representative specimens at various locations across the crack. A description of the microstructure is presented below:

- Sample MBB 67-5-A – Two specimens were taken from the crack. The locations of the specimens can be seen in Figure 1.

  Specimen 1 was located approximately in the middle of the crack and Specimen 2 was taken near the crack tip. Photo 10 shows an overview of the fracture surface of Specimen 1. The crack propagation direction cannot be clearly identified from this section of the fracture surface. The fracture morphology of this section of the crack can be seen in Photo 11. The fiber-like structure that was resulted from the slow crack growth mechanism by break down of the craze is clearly shown on the fracture surface. The small size of the fibers (the photo was taken under 1,000 magnification) suggests that the stress causing the cracking was comparatively low. There was no obvious crack initiation along the inner surface of the duct; however, three impurities were observed. A close-up view of the impurities can be seen in Photos 12 and 13. These impurities seem to have different fracture morphology than the polyethylene. The impurities could have been mixed in with the polyethylene during the duct processing.

  An overview of the fracture surface of Specimen 2 is shown in Photo 14. Based on the crack tip geometry, the crack probably initiated from the inner surface and grew through the thickness of the pipe as well as along the pipe longitudinal axis. Photo 15 shows the fracture morphology of Specimen 2, which is similar to that of Specimen 1, revealing a fibril structure that resulted from a slow crack growth mechanism. Possible crack initiations were observed in this section of the sample at areas “B” and “C”. At both crack initiation areas, an impurity was found (see Photos 16 and 17).

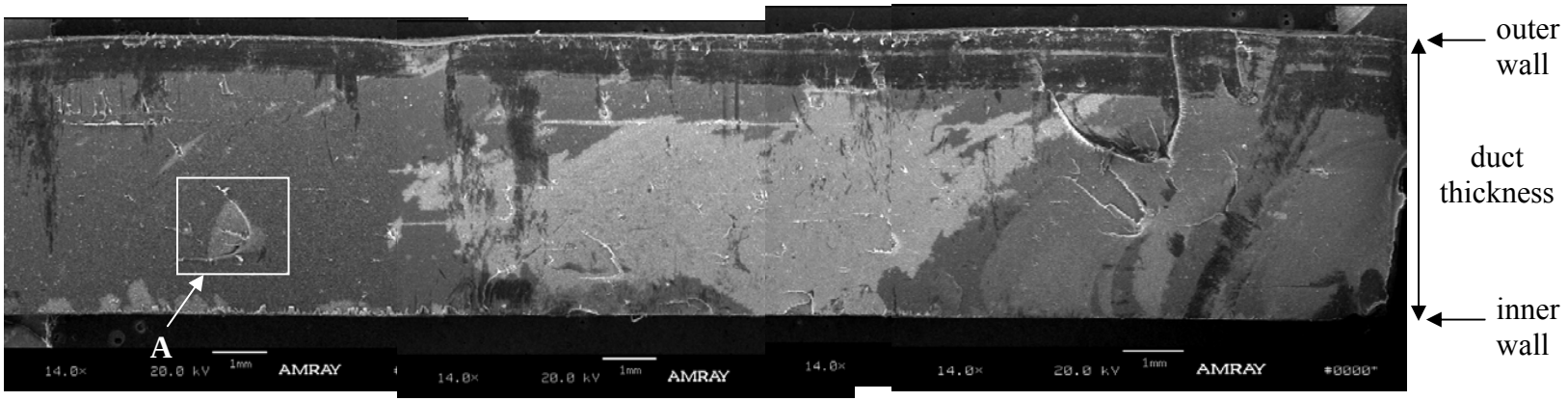

Photo 10. A general view of the fracture surface of Specimen 1 from Sample 67-5-A

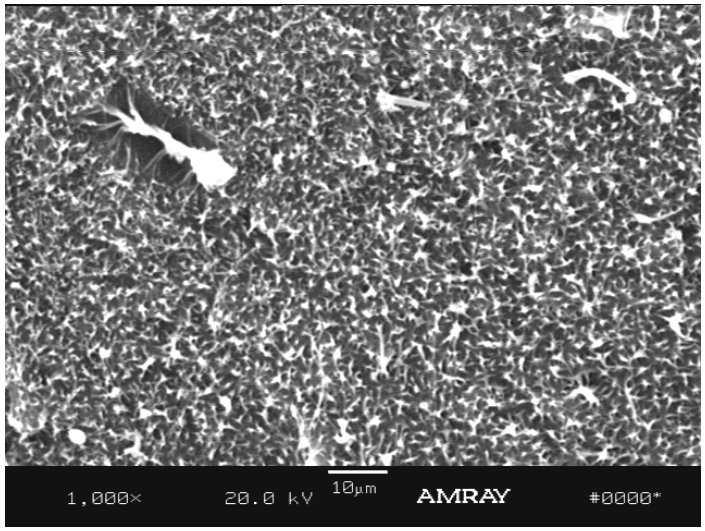

Photo 11. The fracture morphology in area marked "A" of Specimen 1 from Sample 67-5-A.

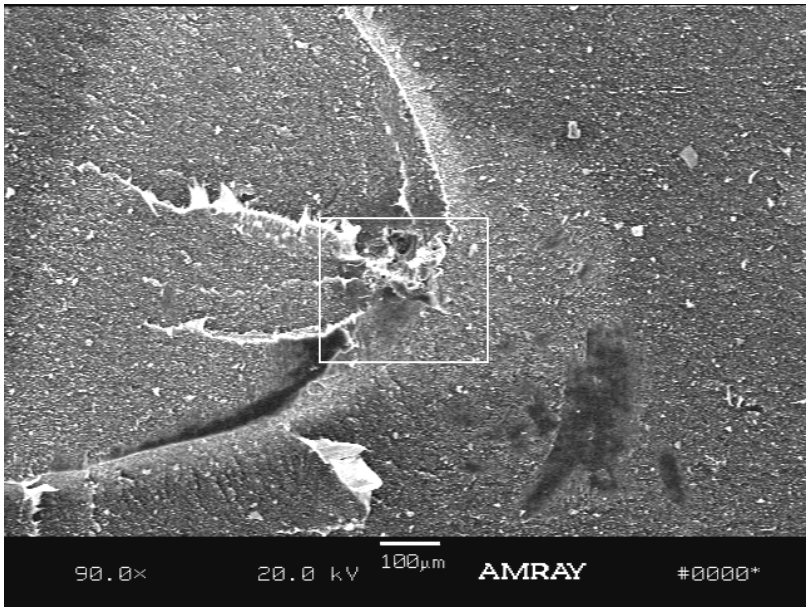

Photo 12. A close-up view of the microstructure in area "A" in Specimen 1 from Sample 67-5-A

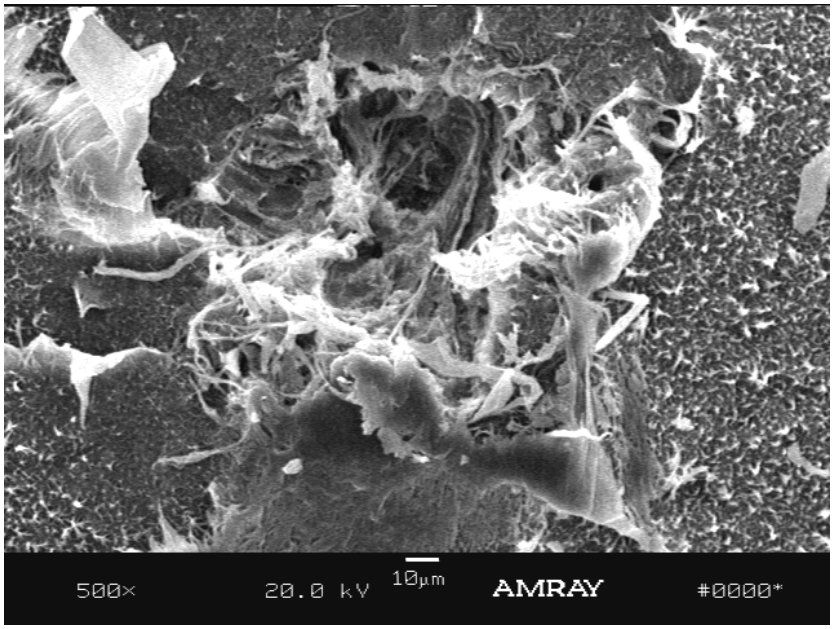

Photo 13. A detailed view of the highlighted area in Photo 12

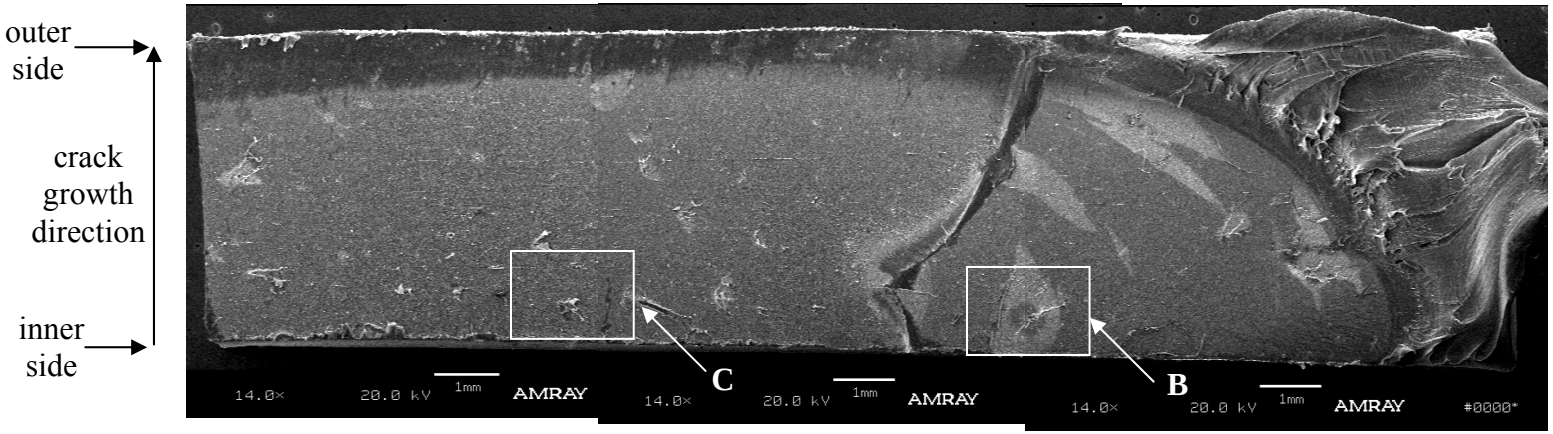

Photo 14. A general view of Specimen 2 from Sample 67-5-A

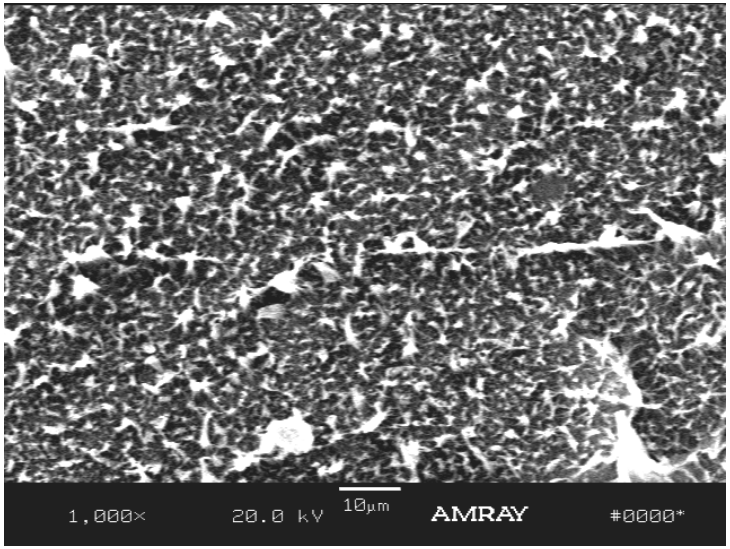

Photo 15. The fracture morphology of Specimen 2 from Sample 67-5-A

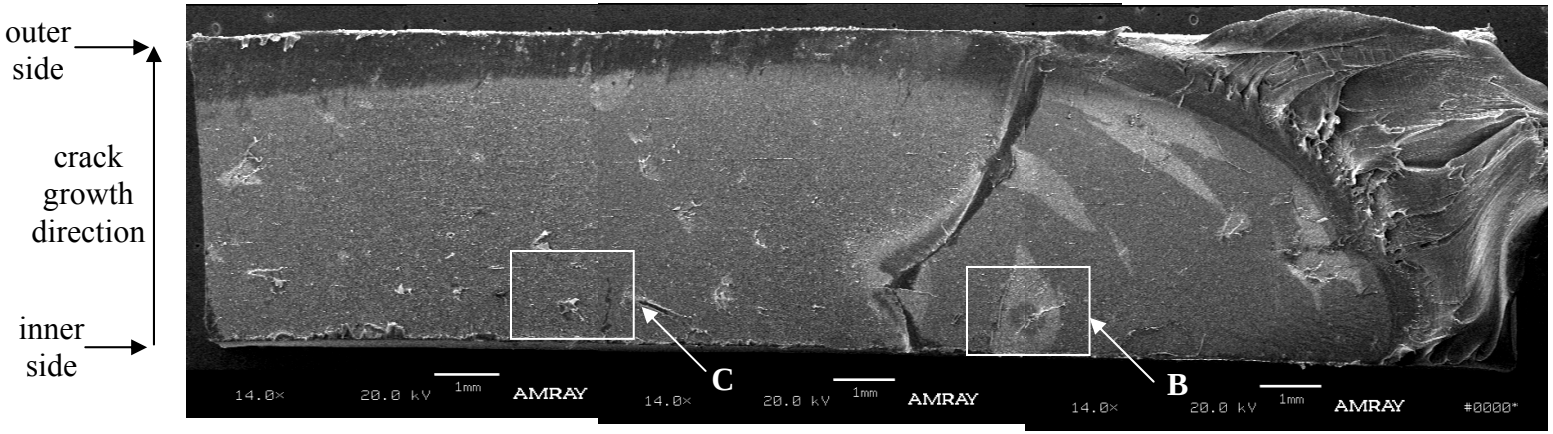

Photo 14. A general view of Specimen 2 from Sample 67-5-A

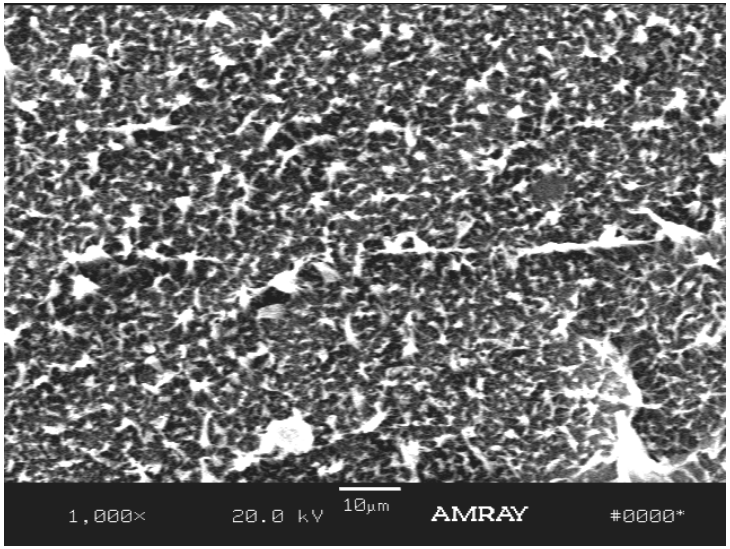

Photo 15. The fracture morphology of Specimen 2 from Sample 67-5-A

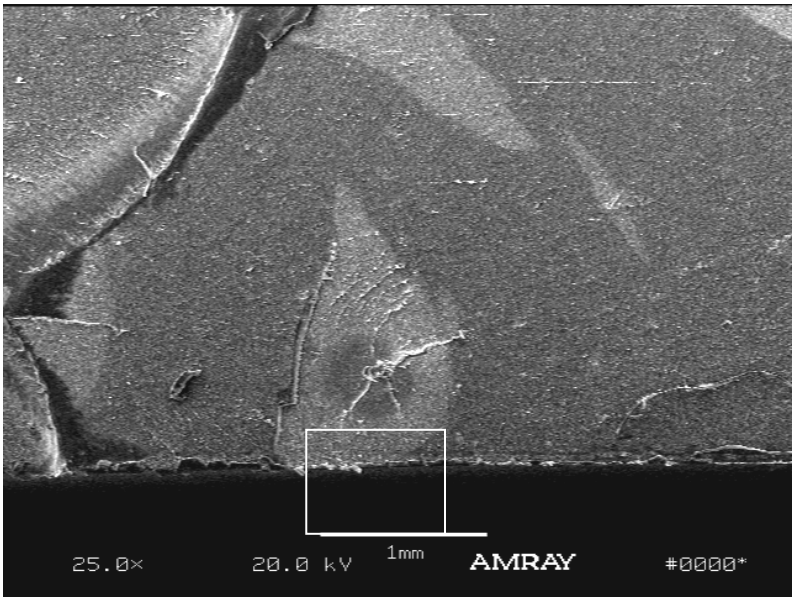

Photo 16. A close-up view of the area "B" in Specimen 2 from Sample 67-5-A

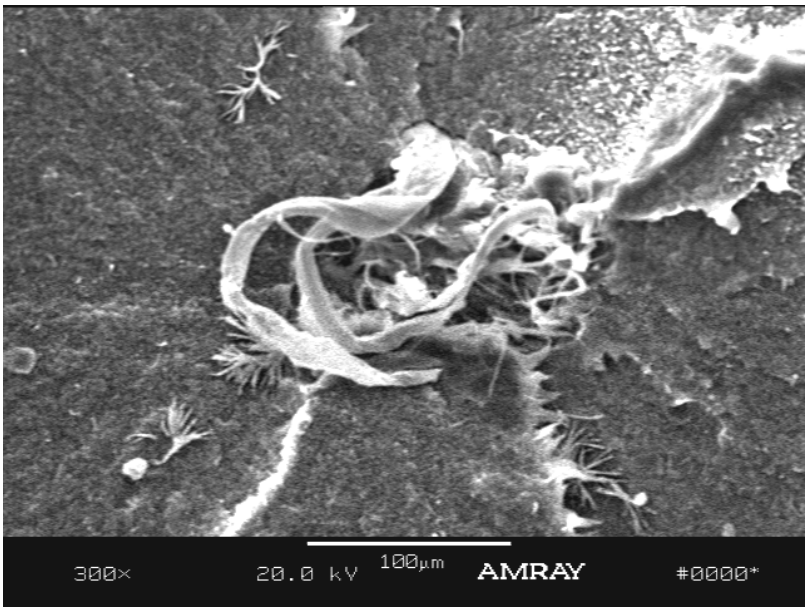

Photo 17. A detailed view of the highlighted area in Photo 16.

- Sample MBB 38-4-A – Four specimens were taken along various positions of the crack, as shown in Figure 2.

The general view of Specimen 1 can be seen in Photo 18. Few air bubble voids can be seen in this section of the crack. The horizontal line in the upper half of the fracture surface was resulted from crack arresting. There was no obvious crack initiation point in this section of the surface. The overall fracture morphology in Specimen 1 was a fibril structure resulting from a slow crack mechanism, as revealed in Photo 19.

A general view of the fracture surface of Specimen 2 is shown in Photo 20. The fracture surface of this section of the crack was covered by the fibril morphology, as can be seen in Photo 21. There was no clear crack initiation point observed in this region of the crack surface. However, a close view of the fracture surface near the inner duct wall revealed fatigue crack propagation behavior, as shown in Photos 22 and 23.

For Specimen 3, Photo 24 shows a hemispherical pattern on the entire fracture surface of the specimen. The initiation of such a pattern was around an impurity at area "A" near the inner pipe surface. An enlarged view of the impurity can be seen in Photo 25. In addition, there were many small unknown black particles near the inner fracture surface, as shown in Photo 26. The overall fracture morphology of Specimen 3 was the fibril structure, as shown in Photo 27.

In Specimen 4, two crack initiations could be identified on the right hand side of the fracture surface, as indicated in Photo 28. The enlarged area "A" can be seen in Photo 29. A similar impurity could also be seen on the left hand of the fracture surface, at the area "B". In addition, two air bubbles were observed in this section of the surface, but they did not initiate the cracking. In addition, a few fatigue lines were observed at the inner duct surface near the area "B", as shown in Photo 30. The fracture surface of Specimen 4 was covered by the fibril structures, as shown in Photo 31.

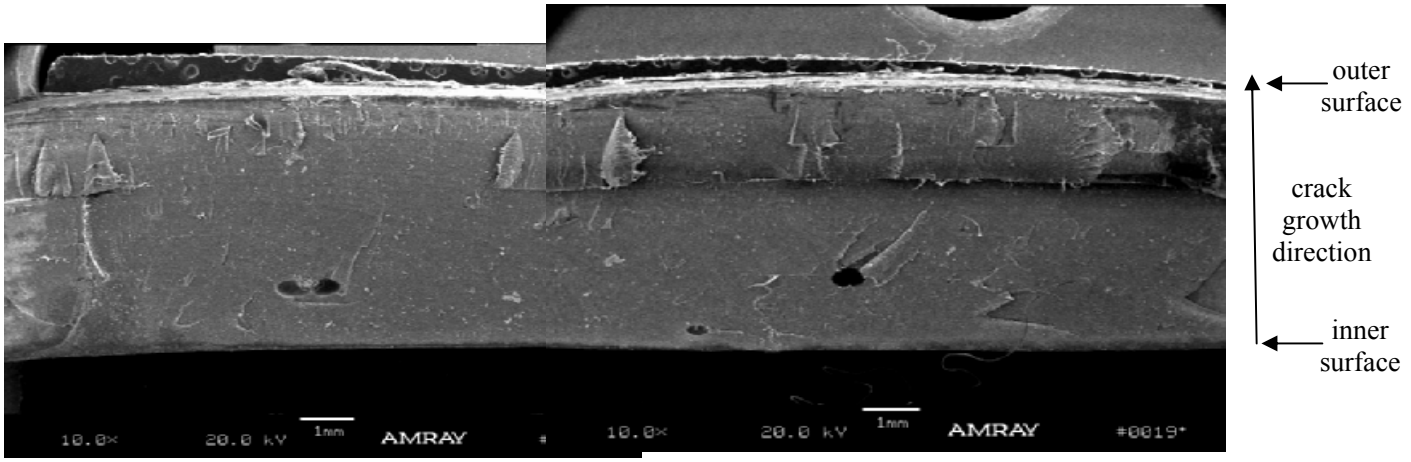

Photo 18. A general view of Specimen 1 from Sample 38-4-A

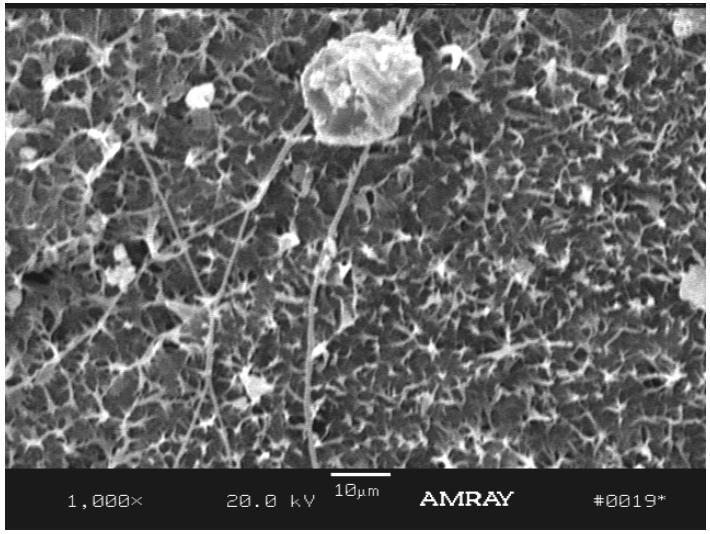

Photo 19. The fracture morphology of Specimen 1 from Sample 38-4-A

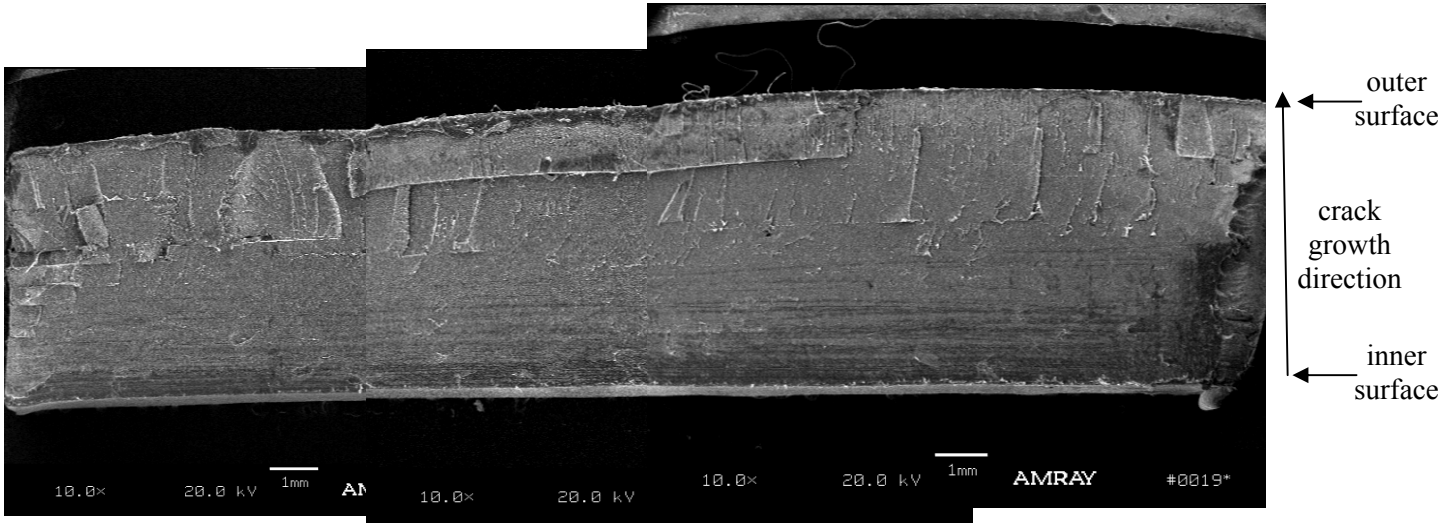

Photo 20. A general view of the fracture surface of Specimen 2 from Sample 38-4-A

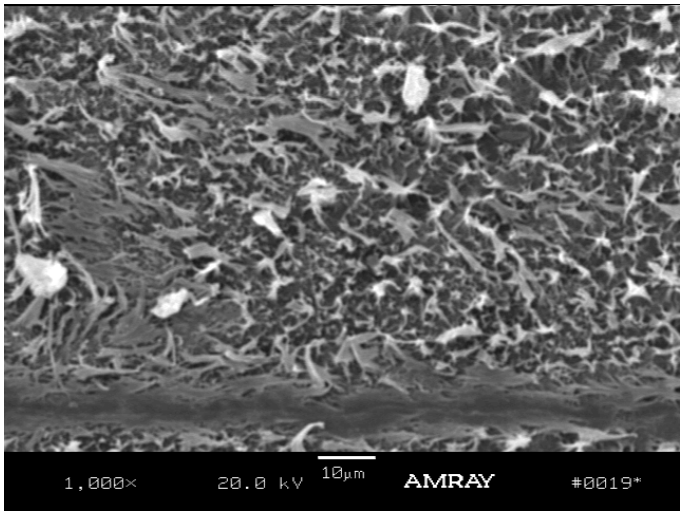

Photo 21. Fracture morphology of Specimen 2 from Sample38-4-A

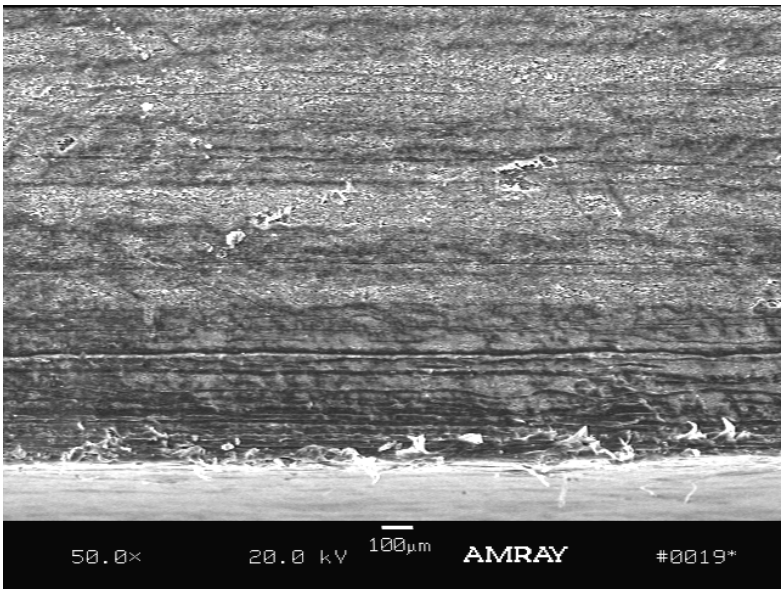

Photo 22. A close view on the inner duct surface of Specimen 2 form Sample 38-4-A.

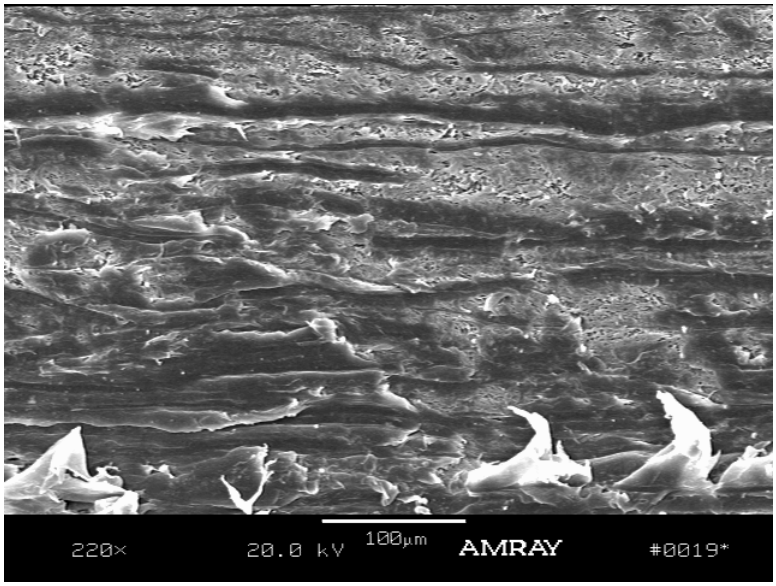

Photo 23. A detailed view of the line morphology in Photo 22.

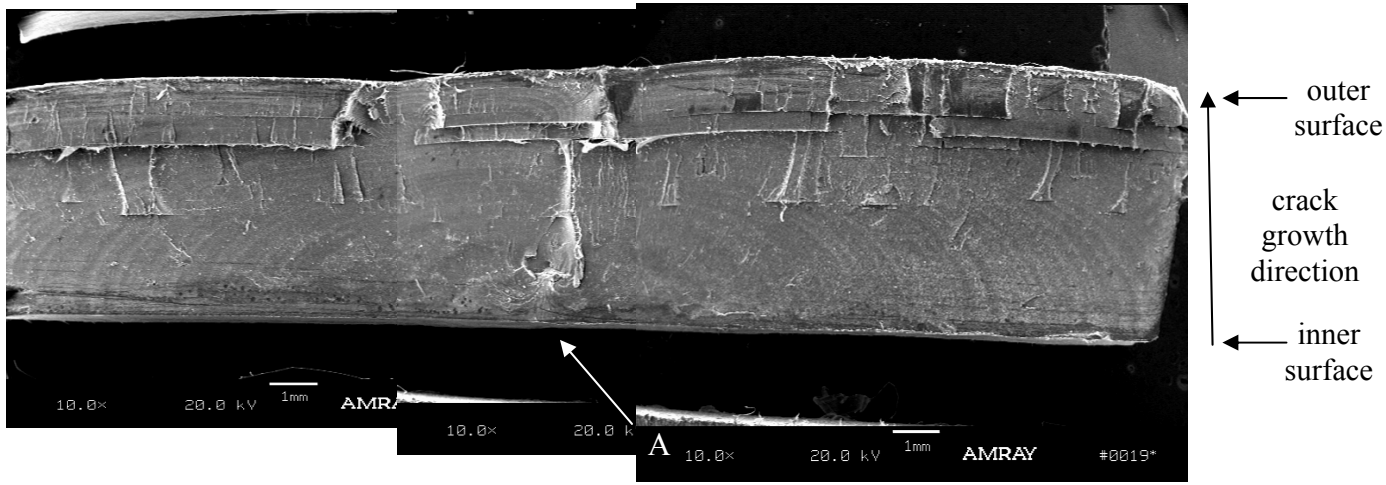

Photo 24. A general view of the fracture surface of Specimen 3 from Sample 38-4-A

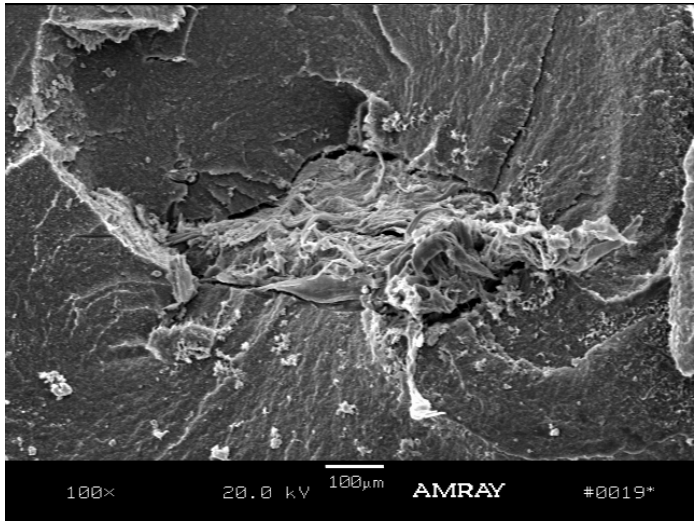

Photo 25. The close view of area A in Photo 24

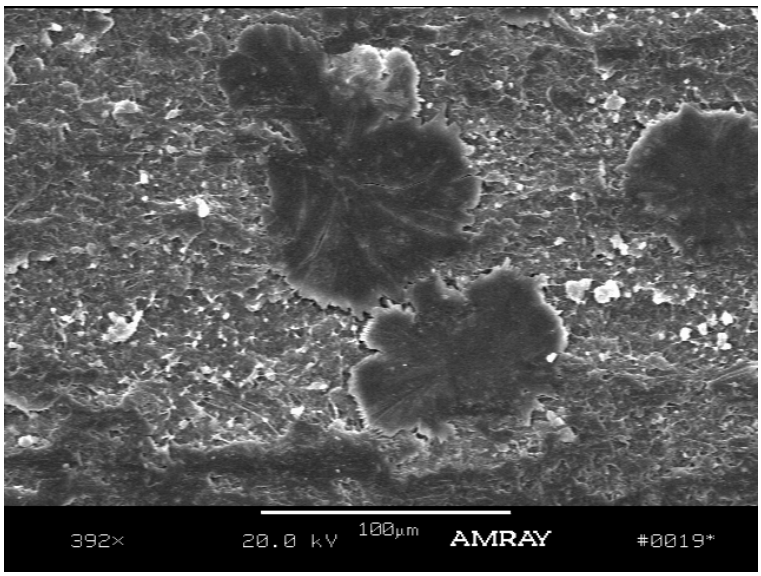

Photo 26. A close view of an unknown feature on the surface of Specimen 3

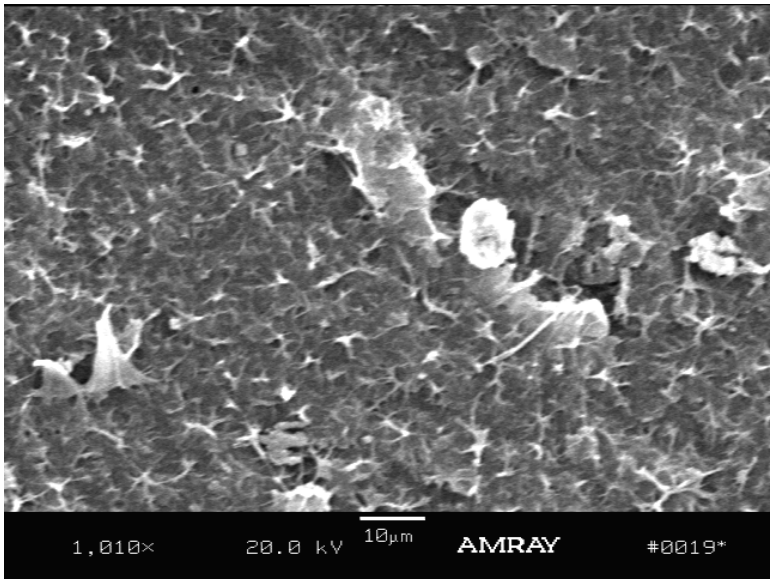

Photo 27. The fracture morphology of Specimen 3 from Sample 38-4-A

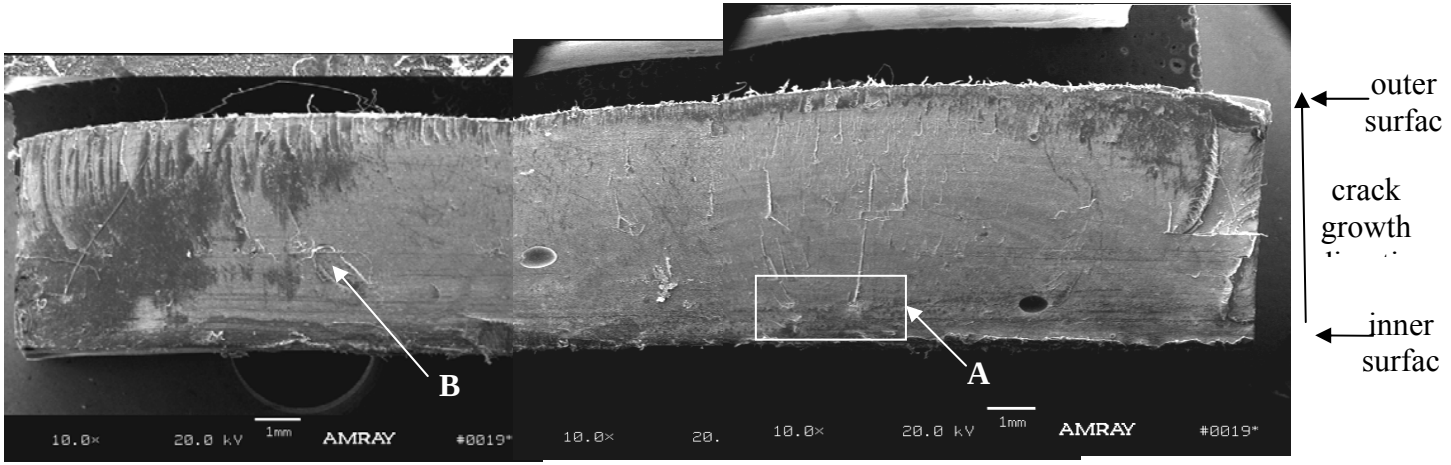

Photo 28. A general view of the fracture surface of Specimen 4 from Sample 38-4-A

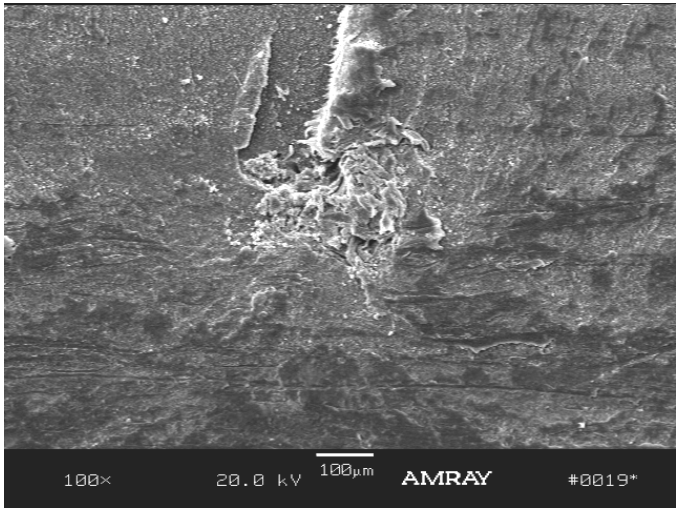

Photo 29. A close-up view of area "A" revealing the imperfection

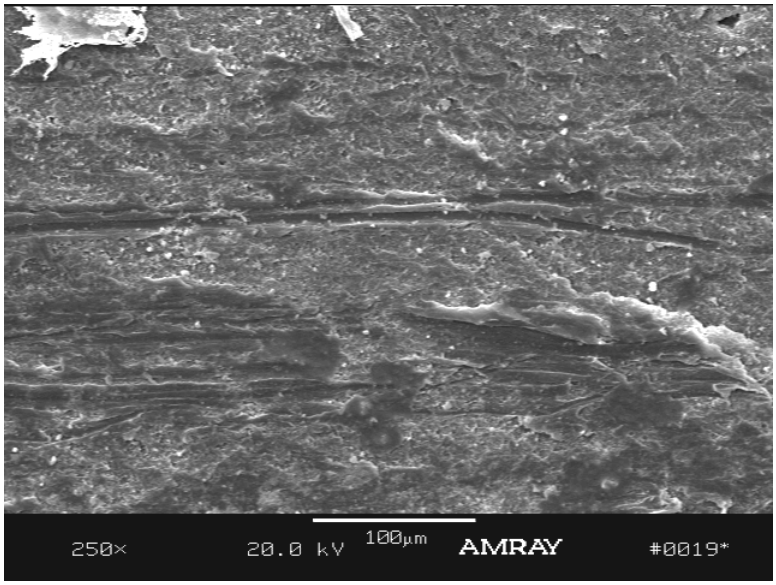

Photo 30. A close-up view of the fracture surface near the inner duct surface

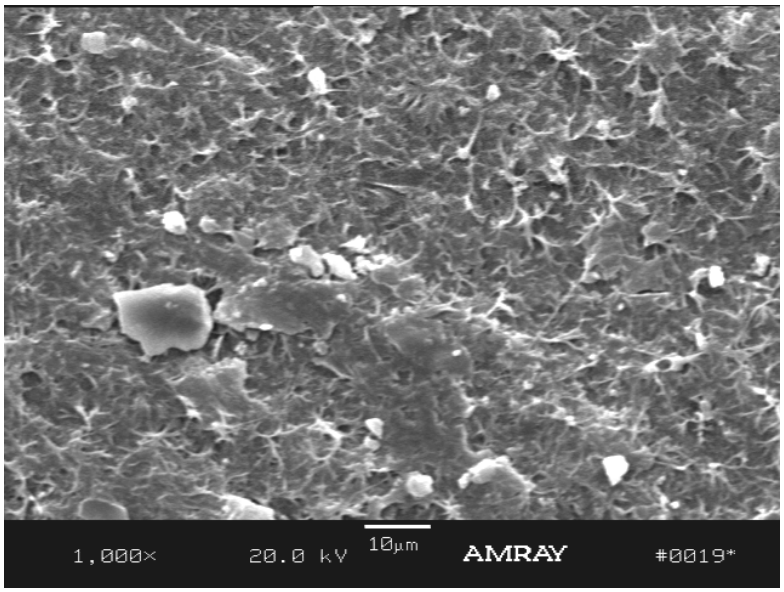

Photo 31. The fracture morphology of Specimen 4 from Sample 38-4-A

- Sample MBB 126-4-A – Four specimens were taken along various positions of the crack, as indicated in Figure 3.

  The general view of Specimen 1 can be seen in Photo 32. Part of this section of the crack was initiated from area "A" near the inner surface of the pipe wall. The fracture morphology of Specimen 4 was dominated by fibril structures, as shown in Photo 33. A close-up view of area "A" is depicted in Photo 34. The cracking seems to have been initiated from a small impurity, as revealed in Photo 35.

  In Specimen 3, a hemispherical crack initiation pattern was observed in area "A" near the inner surface of the pipe wall, as depicted in Photo 36. An enlarged view of the impurity is shown in Photo 37. The fracture morphology within the hemispherical area exhibited a fibril structure, as shown in Photo 38; however, a flake structure (see Photo 39) was observed in the "B" region. The flake structure was resulted from rapid crack propagation, which may have been caused by impact loading and/or low temperature. In region "C", many fatigue lines can be seen, as revealed in Photos 40 and 41.

  Photo 42 reveals the fracture surface of Specimen 3. Part of the crack was initiated at "A", as shown in Photo 43. The fracture surface of this particular specimen was covered by many white particles, as can be seen in Photo 44. These were not apparent in any other specimens. Some of the fracture morphology was covered by white particles and unable to observe under the microscopic examination. Nevertheless, the fracture surface was covered by the fibril structure (see Photo 45) indicating that the crack propagated via a slow crack growth mechanism.

  The fracture surface of Specimen 4 can be seen in Photo 46. The fibril structure dominated fracture morphology, as can be seen in Photo 47. A part of the crack was initiated from area "A", as indicated by the close view of area "A" in Photo 48. The initiation was again caused by an impurity (see Photo 49), as observed in many other examined duct samples. Photos 50 and 51 show fatigue propagation in regions "B" and "C" of the fracture surface, respectively.

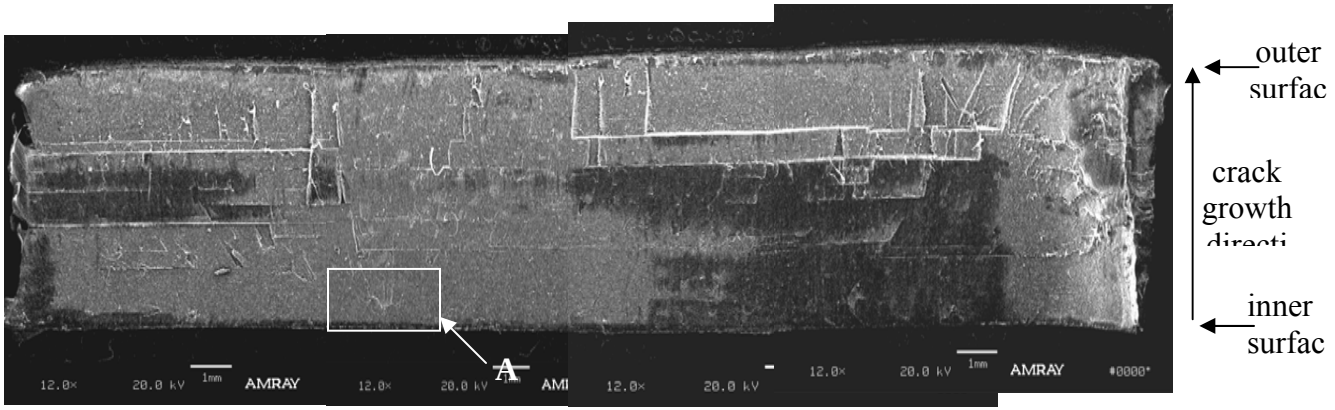

Photo 32. A general view of the fracture surface of Specimen 1 from Sample 126-4-A.

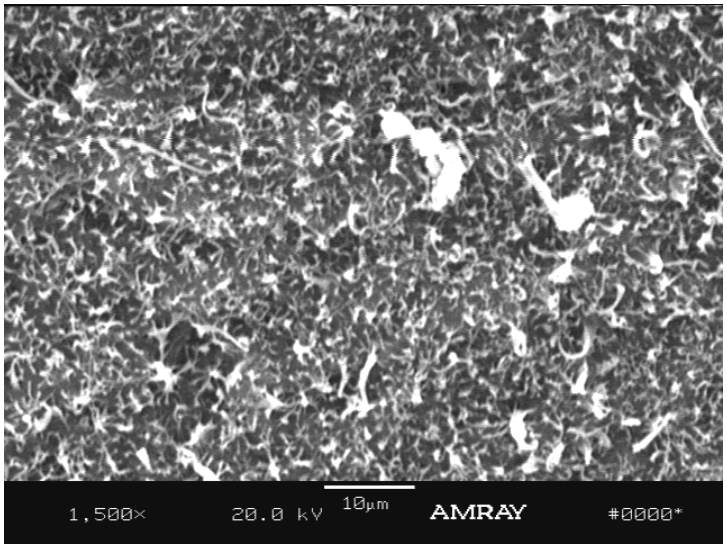

Photo 33. The fracture morphology of Specimen 1 from Sample 126-4-A.

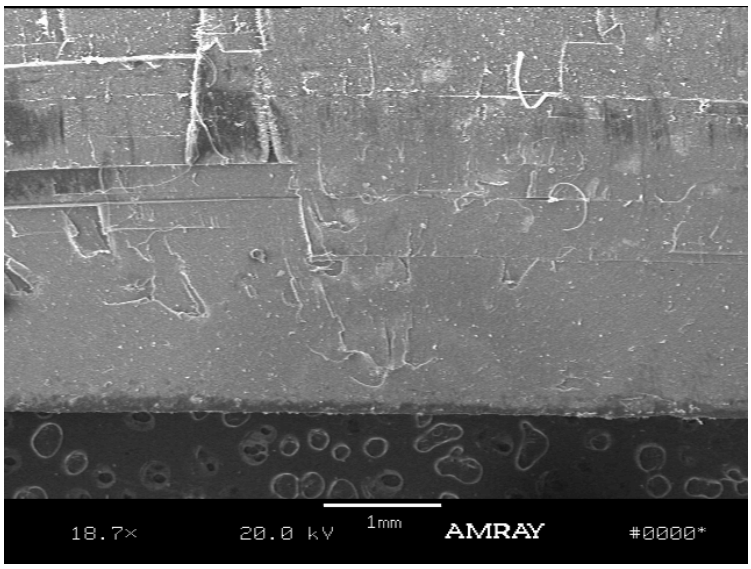

Photo 34. A close-up view of area "A" in Photo 31

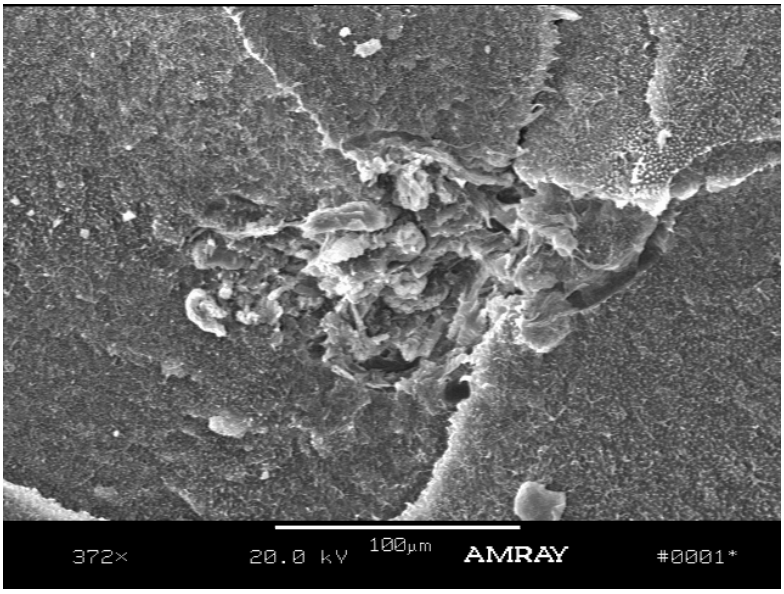

Photo 35. An enlarged view of the imperfection in area "A" of Specimen 1 from Sample 126-4-A

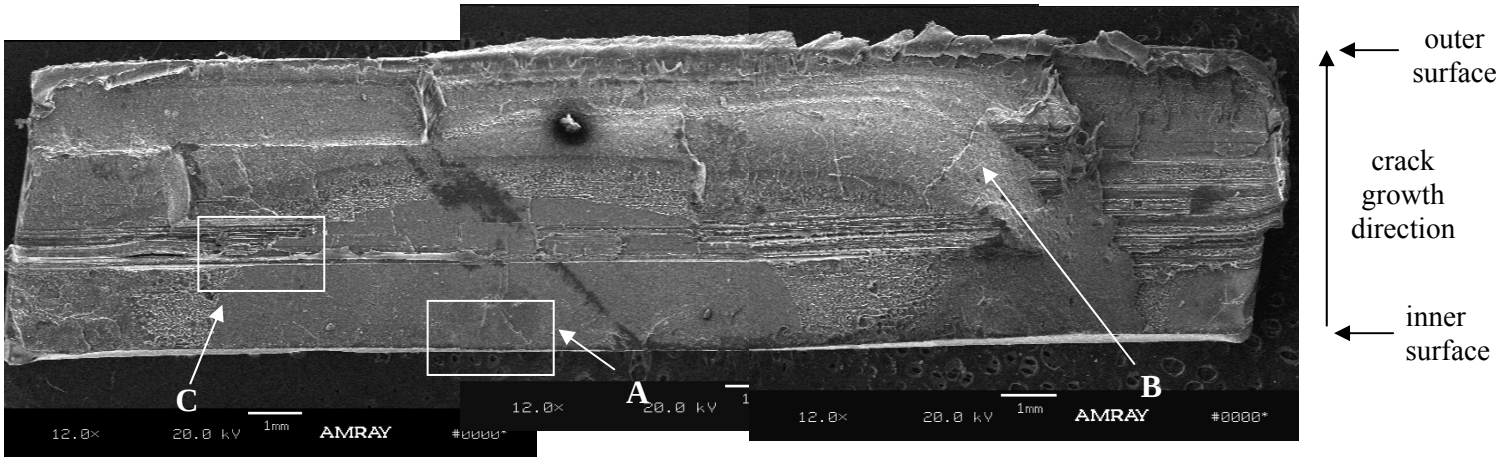

Photo 36. A general view of the fracture surface of Specimen 2 from Sample 126-4-A

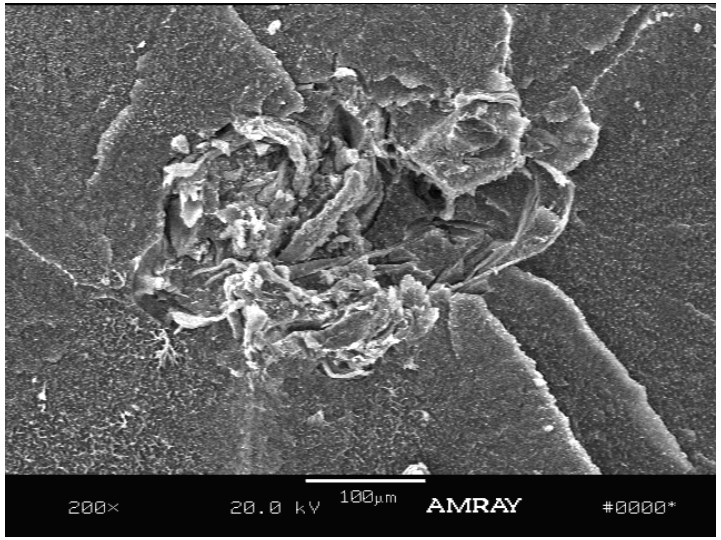

Photo 37. An enlarged view of area "A" in Photo 36

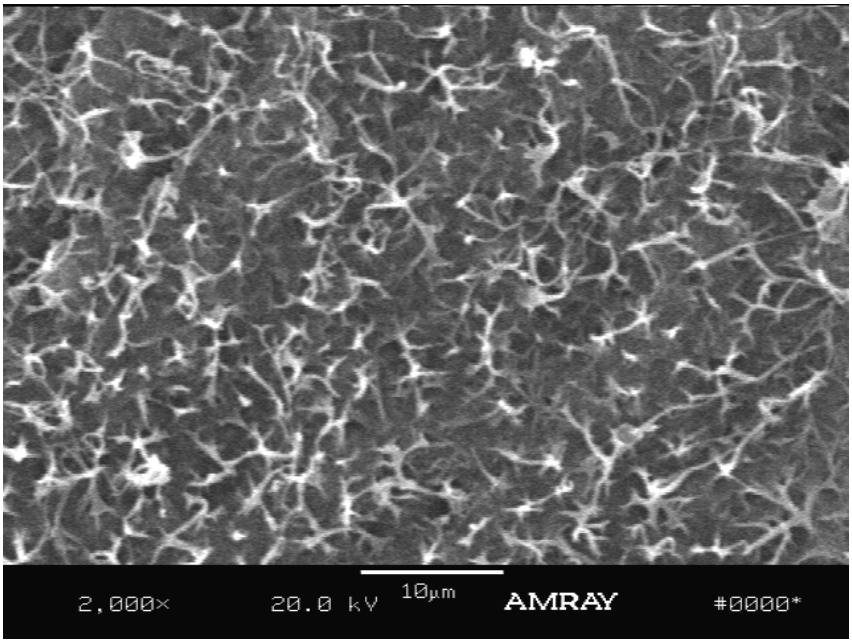

Photo 38. The fracture morphology around the area "A" of Specimen 2

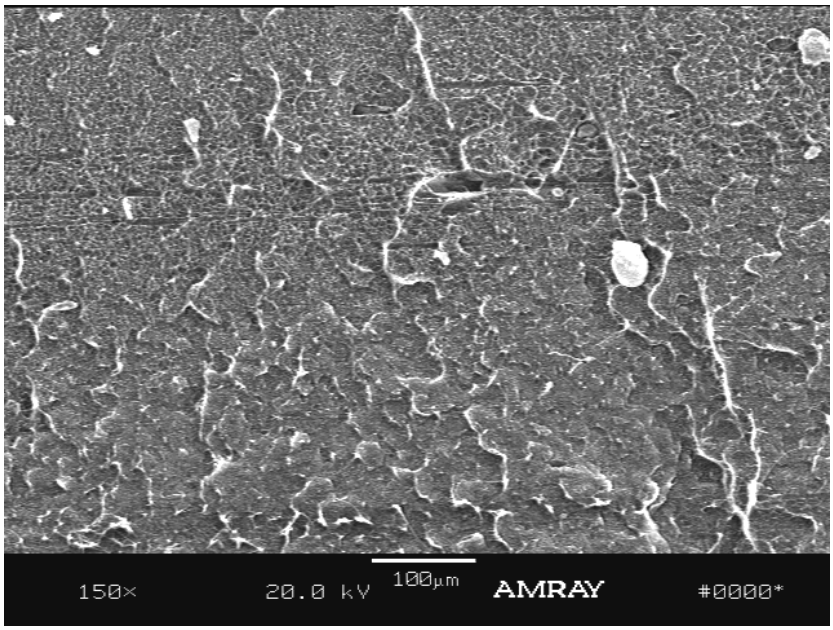

Photo 39. The fracture morphology of rapid crack propagation in area "C" of Specimen 2 from Sample 126-4-A

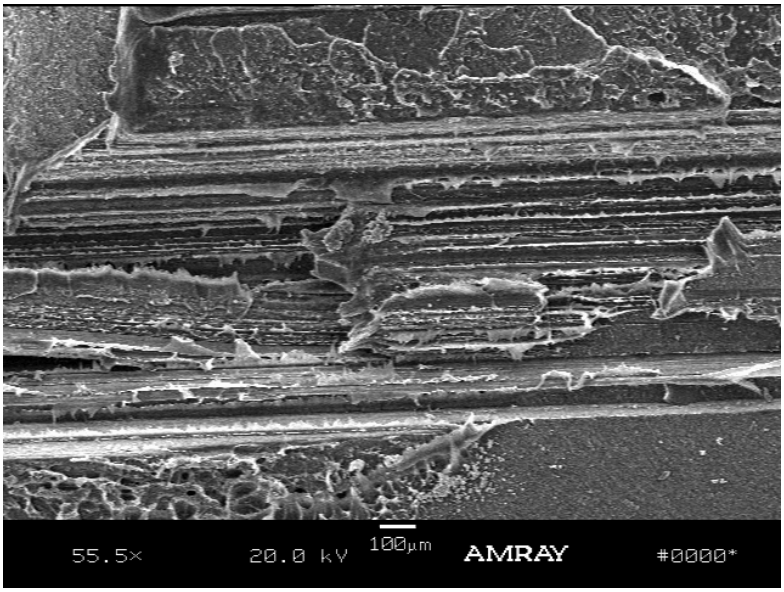

Photo 40. A close-up view on the fatigue line structure in area "B" of Specimen 2 form Sample 126-4-A

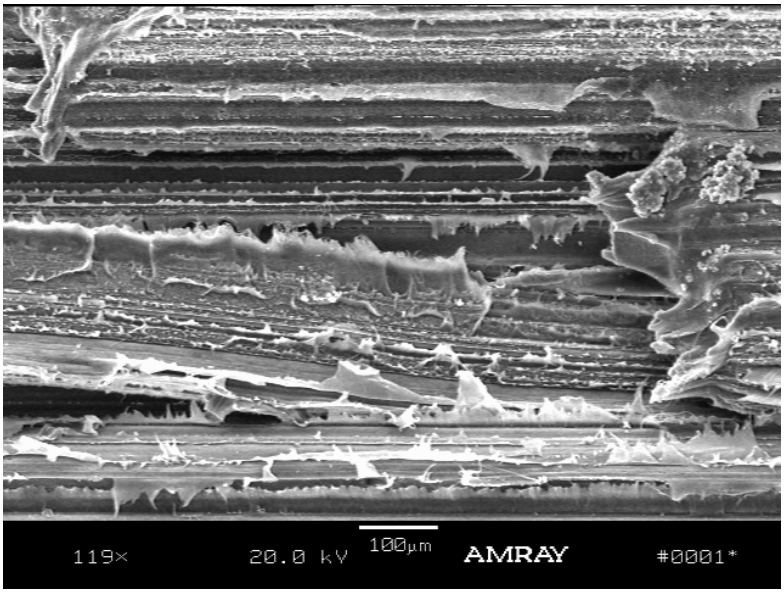

Photo 41. An enlarged view of the fatigue lines on the fracture surface of Specimen 2 from Sample 126-4-A

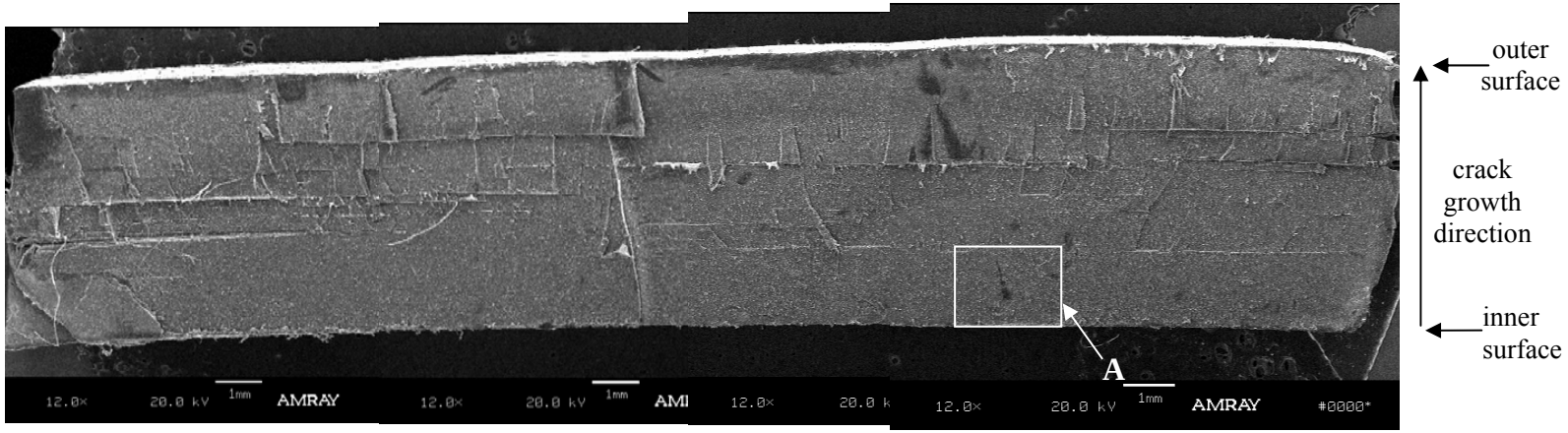

Photo 42. A general view of the fracture surface of Specimen 3 from Sample 126-4-A

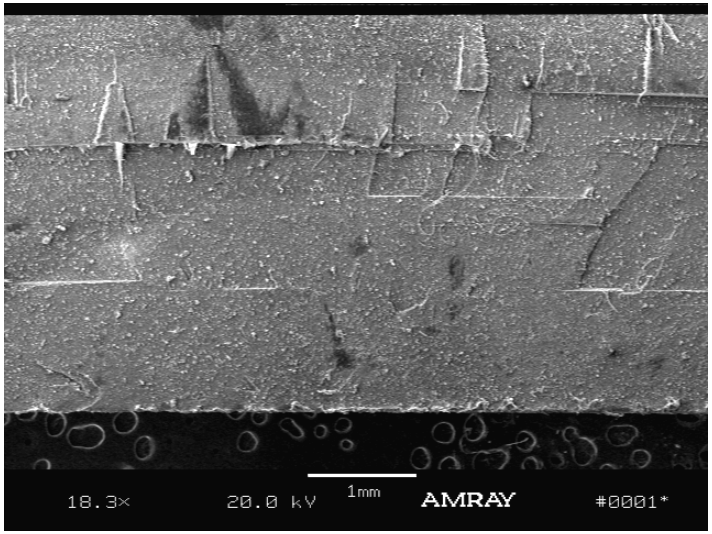

Photo 43. A close of the area "A" in Photo 42 of Specimen 3 from Sample 126-4-A

Photo 44. A close-up view on the fracture surface revealing many small white particles

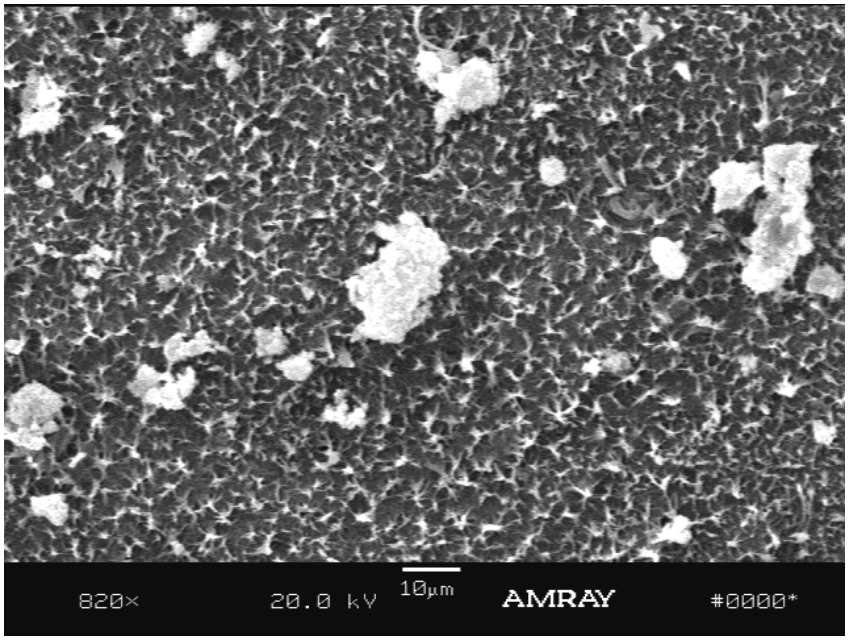

Photo 45. The fracture morphology of Specimen 3 from Sample 126-4-A

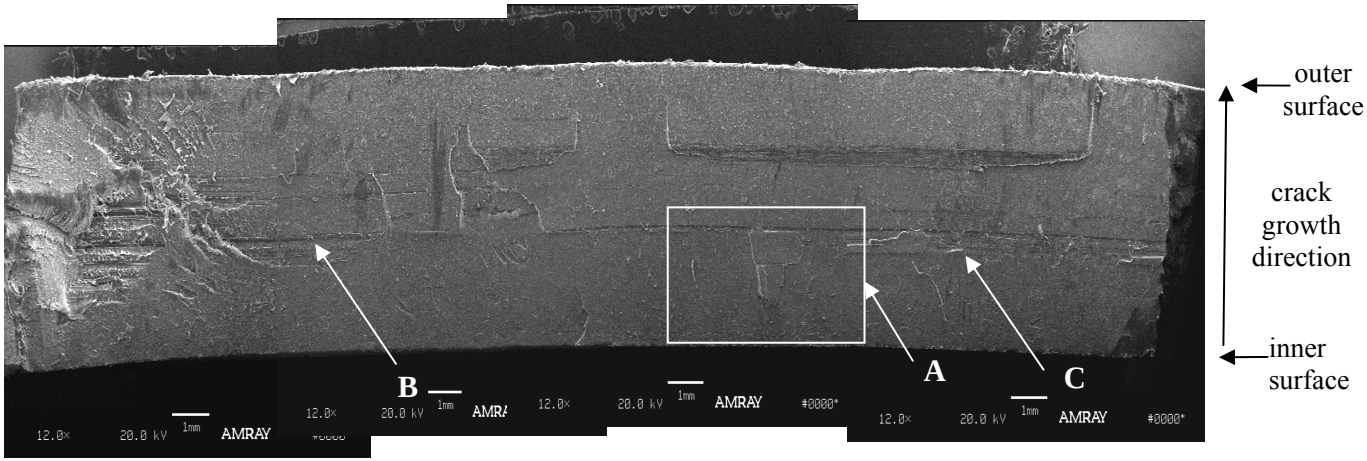

Photo 46. A general view of the fracture surface of Specimen 4 from Sample 126-4-A

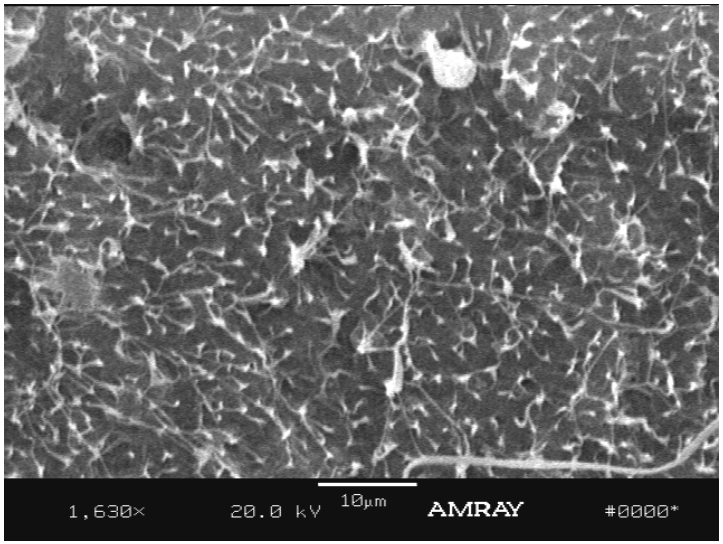

Photo 47. The fracture morphology of Specimen 4 from Sample 126-4-A

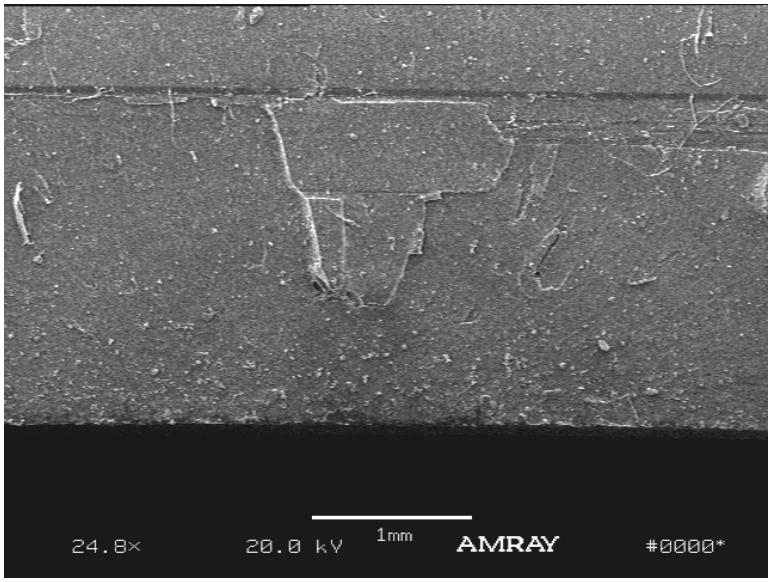

Photo 48. A close-up view of the area in Photo 46 of Specimen 4

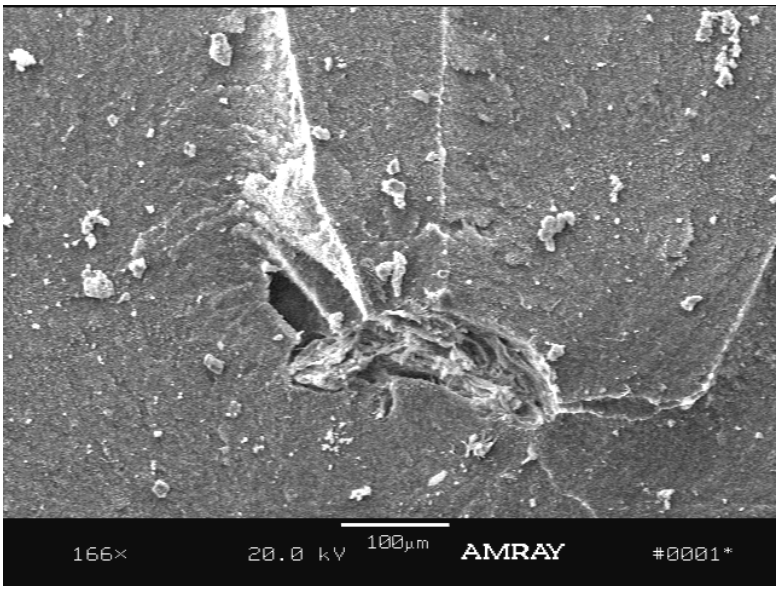

Photo 49. An enlarged view of the imperfection at the area "A"

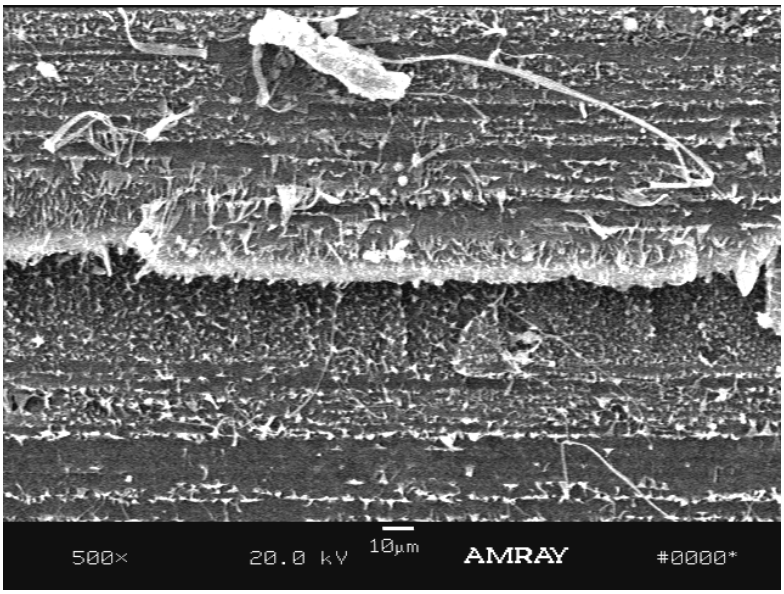

Photo 50. Fatigue lines in region “B” of Specimen 4

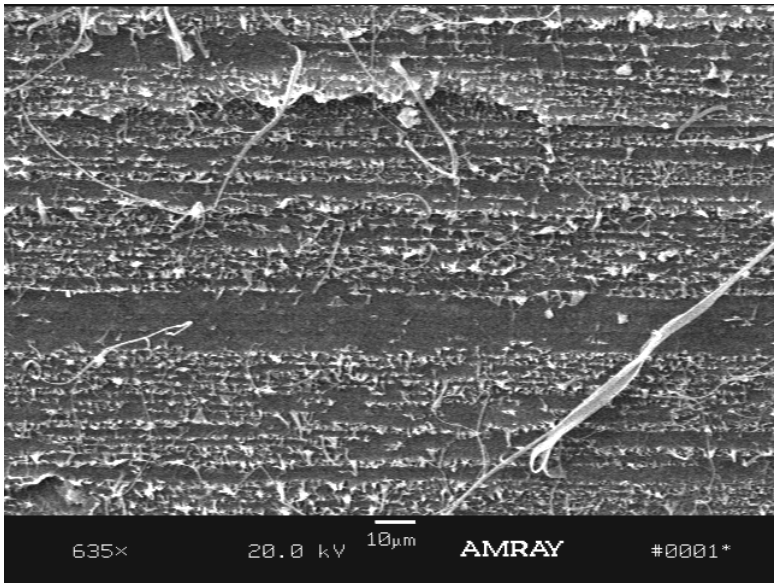

Photo 51. Fatigue lines in region “C” of Specimen 4

Summary of the Cracking Mechanism

The microstructure of the fracture surfaces provided significant information regarding the cracking mechanism of the three duct samples. In all three cases, cracking started from the inner surface and propagated through the wall thickness. The direction of the crack growth suggests that the inner duct surface was subjected to a tensile stress. The probable cause of the tensile stress was investigated as part of this research project and is described in the report body.

Crack initiations were found to have occurred at points of impurities or air bubble voids, where a tensile stress was also present. In Samples MMB 38-4-A and MMB 126-4-A, which contained cracks, numerous initiation points were observed. Such an observation suggests that the long crack resulted from joining together of multiple small cracks. These small cracks might have started at different times during the service period. The formation of multiple small cracks may reflect a localized tensile stress, which shifted from region to region as cracking was taking place.

It was difficult to identify the chemical composition of the impurity particles. However, the fracture morphology of the impurities was different from that of the polyethylene duct material itself. In addition, a small amount of black particles was observed in Sample 38-4-A (Photo 26). The smooth fracture surface suggests that the black particles may have been harder than the surrounding polyethylene material. These particles could be the residual of a carbon black master package that was not properly dispersed.

The fracture morphology of all examined specimens was dominated by the fibril structure. Although the appearance of the fibril structures may seem different, the slow crack growth was the mechanism that caused this structure. The appearance of the fibril structure is stress dependent, whereby a high stress tends to yield long fibers. In addition, some of the fibril structure could be damage from abrasion between two opposite fracture surfaces. Of the three samples, only one specimen of Sample 126-4-A revealed a small area that had failed by rapid crack propagation. This could have been caused by an impact stress. However, fatigue lines running parallel to the longitudinal axis of the duct were observed on some of the fracture surfaces of Samples 126-4-A and 38-5-A. The combination of the fibril structure and fatigue lines indicates that certain parts of the crack in Samples 126-4-A and 38-5-A were generated by a mixture of steady slow crack growth and fatigue crack growth.

Verification of the cracking mechanism (i.e., slow crack growth) was essential for selecting proper tests in the material evaluation part of this study. The two stress crack resistance tests (environmental stress crack resistance (ESCR) and single point tensile load (SP-NCTL) test) that have been included in this study were specifically designed to assess the steady slow crack growth.

Material Properties

Material properties of the retrieved field ducts were evaluated using the specification that was applied at the time of construction. A copy of the specification was provided by Mr. Vest from the Mid-Bay Bridge Authority, in which the material properties of HDPE duct are specified in Section 2 – Part 2. 3d. This states that ***"Smooth plastic duct shall be made of polyethylene material and shall conform to the requirement of ASTM D 2239 or D 3350 with a cell classification PE 3454336 or ASTM D 1248, Type 3, Grade 34, Category 5."*** However, it is believed that the last cell class number (6) in ASTM D 3350 was a typographical error. The character should be (C) referring to the carbon black level; thus, the cell classes should be ***345433C.*** Table 1 shows the required properties and corresponding value according to both ASTM D 3350 and ASTM D 1248. The information listed in Table 1 indicates that the specified properties in these two specifications are relatively similar but not identical. If ASTM D 3350 was used to specify the field duct samples, then tests involving brittle temperature and tensile elongation at break would not be required. On the other hand, the flexural modulus, hydrostatic design basis (HDB) and carbon black tests are not required by the ASTM D 1248. Since ASTM D 3350 is a more comprehensive specification for assessing pipe properties than is ASTM D 1248, it was used in this program to evaluate the retrieved field duct samples. Nevertheless, the tensile break elongation was also recorded during the tensile test.

As noted in the report body, the HDB test was eliminated from the present program. This test can only be performed on an whole uncracked pipe section; and samples of this type were not available.

Four additional tests, the SP-NCTL test, OIT test, determination of antioxidant, and carbonyl analyses, were also included (see Table 1). The SP-NCTL test was recently adopted to replace the ESCR test (ASTM D1693) for corrugated polyethylene non-pressured pipe in the AASHTO M294 specification. The reason this is the large standard deviation and qualitative nature of the test. In this test program, the SP-NCTL test was employed even though it is not included in the ASTM D3350 specification. The test

data were beneficial for comparing different grades of HDPE resins and to development of future duct specifications.

Table 1. Properties of PE duct according to ASTM specifications.

Property	Test Method	ASTM D 3350 Classification	ASTM D 1248 Classification	Required Value
Density	ASTM D 1505 or D 792	3	Type 3	>0.940-0.955 (g/cc)
Melt index	ASTM D 1238	4		< 0.15 (g/10 min.)
			Category 5	<0.4 (g/10 min.)
Flexural Modulus	ASTM D 790	5		110,000 - <160,000 psi
			Not defined	
Tensile yield strength	ASTM D 638 Type IV	4		3000 -<3500 psi
			Grade P34	> 3200 psi
Tensile break elongation	ASTM D 638 Type IV	Not required	Grade P34	> 500%
Brittle temperature	ASTM D746-A	Not required	Grade P34	-75°C
ESCR	ASTM D 1693	3	Grade P34	F_{20} = 192 hr.
HDB	ASTM D 2837	3	Not defined	1250 psi
Carbon black	ASTM D 4218	C	Not required	> 2%
Additional Tests				
SP-NCTL	AASHTO M294	na	na	> 24 hours
OIT	ASTM D3895	na	na	Not defined
Antioxdant Content	ASTM D5524 HPLC	na	na	na
Carbonyl Analysis	FTIR	na	na	na

Note: ESCR – environmental stress crack resistance.
HDB – hydrostatic design basis.
SP-NCTL – single point notched constant tensile load test.
OIT – oxidative induction time.
HPLC – high pressure liquid chromatography
FTIR – Fourier transform infrared analysis
na – non-applicable

The second additional test involved determination of the oxidative inductive time (OIT). This test assesses the amount of antioxidant remaining in the polymer. A short OIT value indicates a low amount of antioxidants present in the formulation and vise versa. The results of this test can provide an indication of the level of antioxidant remaining in the duct samples, as well as in compression molded plaques which

were used for the material property evaluation. However, OIT is not a quantitative analysis in that the exact amount of antioxidants in part-per-million (ppm) cannot be determined. In addition, the sensitivity of the OIT decreases when the amount of antioxidant in the duct is near depletion.

In order to quantify the amount of antioxidant in the polymer, a chemical analysis, ASTM D5524, is required; and this is the third additional test in this program. The antioxidant was extract from the polymer using warm cyclohexane and then was analyzed for using High Pressure Liquid Chromatography (HPLC) to determine the concentration of antioxidants. The fourth additional test assessed the presence of the carbonyl functional group (–COO) in the HDPE duct using Fourier Transform Infrared (FTIR). Carbonyl results from oxidation of polyethylene, which induces chain scission. As oxidation propagates in the polymer, the mechanical properties change accordingly. For polyethylene, the first indication is a decrease of breaking elongation as a consequence of increased brittleness.

1. Test plaque preparation.

An uncracked section of the duct samples was cut into approximately one inch square pieces, and compression molded plaques were prepared from these. The molding procedure was according to ASTM D1928 Procedure C (at a cooling rate of 15±5^{o}C). Four plaques with thickness of approximately 0.075 inches and one with a thickness of approximately 0.125 inches were made for each duct sample. From these plaques, various test specimens were die cut and used for subsequent physical and mechanical testing so that properties could be compared to requirements of the relevant project specification.

2. ASTM D3350 specified tests.

The procedure and results of the each specified test are presented below:

- Density: The density test was performed according to ASTM D792 procedure B. The liquid used was 1-Propanol with density of 0.781 g/cc. The measurement was made using an analytical balance with an accuracy of 0.0001g. Two replicates were evaluated for each sample. Note that the "true" resin density cannot be obtained due to the added carbon black in the product. The average density values shown in Table 2 were obtained by subtracting the amount of carbon black from the density of the tested specimens according to Equation 1,

$$\rho_{(resin)} = \rho_{(product)} - 0.0044C \quad (1)$$

where C = % carbon black in the product.

- Melt index: The melt index test was performed according to ASTM D1238 using a condition of 2.16 kg/190°C. Two replicates were evaluated for each sample. The average value of each sample is given in Table 2. All three samples have values above the specified 0.15 g/10 min. The results suggest that the molecular weight of the examined duct resins could be lower than resins with melt index of 0.15 g/10 min.

- Flexural modulus: The flexural modulus test was performed according to ASTM D 790, Method 1, Procedure B. Five replicates were tested for each pipe sample. The average flexural modulus of each sample is shown in Table 2. The average values are all within the specified range.

- Tensile yield strength: The tensile yield strength test was performed according to ASTM D 638 Type IV. The required number of replicates for this test is five. However, it was found that some of the specimens were extremely brittle in that they broke before or near yielding. Subsequently, additional specimens were tested in order to obtain an average value from five replicates. The average tensile yield strength of each sample is shown in Table 2. All three samples exhibit yield strengths above the specified range.

- ESCR: The ESCR test was performed according to ASTM D 1693 Procedure C, which requires that test specimens be immersed in 100 percent Igepal at 100°C. The cell Class 3 requirement is that F_{20} be 192 hours. In other words, no more than two of the 10 test specimens (20 percent) are allowed to crack within the testing duration of 192 hours. The results are shown in Table 2. For all three duct samples, the 10 test specimens cracked within 0.25 hours; thus, F_{20} was less than 0.25 hour, which is significantly below the specified value.

- Carbon Black: The carbon black content test was determined according to ASTM D 4812. Two replicates were evaluated for each sample. The average values are shown in Table 2. All three samples have carbon black contents slightly below the specified value of 2 percent.

Table 2. Results of specified properties for PE duct according to ASTM 3350.

Property	ASTM Method	ASTM D 3350 Classification	Required Value	Average Test Value		
				MBB 67-5-A	MBB 38-4-C	MBB 126-4-A
Density (g/cc)	D 792-B	3	**>0.940-0.955**	0.948*	0.952*	0.949*
Melt index (g/10 min)	D 1238	4	**< 0.15**	0.67	0.60	0.60
Flexural Modulus (psi)	D 790	5	**110,000 - <160,000**	127,000	129,800	145,000
Tensile yield strength (psi)	D 638 Type IV	4	**3000 - <3500**	4,000	4,290	4,312
ESCR $(F_{20})^{+}$ (hr)	D 1693	3	**F_{20} = 192 hr.**	< 0.25	< 0.25	< 0.25
Carbon black (%)	D 4218	C	**> 2**	1.3	1.5	1.6

* Density obtained by calculation (see Appendix B)

$^{+}$ ESCR (F_{20}) – environmental stress crack resistance.(20% failure time)

3. Additional non-specified tests.

The procedure and results of the four additional tests that were performed are presented below:

- SP-NCTL test: The test was performed according to the AASHTO M294 specification, which was developed based on the ASTM D 5397-Appendix. A set of five notched specimens was subjected to tensile loads while immersed in a solution of 10 percent Igepal at 50°C. The applied tensile load was equal to 15 percent of the yield strength of the material at room temperature. The notch depth was 20 percent of the thickness of the specimen. The failure time of each specimen was automatically recorded to the nearest 0.1 hour. The average failure time was around 3.5 hours as shown for each sample in Table 3.

  Although currently there is no specified value for polyethylene duct material, the AASHTO M294 specification requires a minimum 24 hours failure time for corrugated HDPE pipes. However, the ESCR cell class requirement for corrugated HDPE pipes is "2" (F_{50} = 24), which is one class lower than the requirement for the duct material. Therefore, it seems that the failure time of the polyethylene duct material should be higher than the 24-housr specified by the SP-NCTL test.

- OIT test: The test was performed according to ASTM D3895 and assesses the time required to oxidize a test specimen at an isothermal temperature of 200°C. A specimen weighing approximately 2 to 3 mg was heated to 200°C at a constant rate of 20°C/min under a nitrogen atmosphere. The temperature was then held at 200°C while the gas was changed from nitrogen to oxygen. The test was terminated after oxidation of the polymer was detected.

  Both the pipe and plaque materials were tested. The average OIT values are shown in Table 3. Since the plaque had gone through another heating cycle in sample preparation, its OIT value was expected to be slightly lower than for the corresponding pipe material. The OIT values of the pipes, as well as the plaques, are very low in all three samples. The low OIT values indicate that the overall amount of antioxidants remaining in these duct samples was very small. However, this test does not provide information regarding the oxidation degradation status of the pipe.

- Antioxidants Quantity: This test was performed by the Exxon-Mobile Corp., a polyethylene resin producer. The test procedure basically followed ASTM D5524, except that high pressure liquid

Table 3 – Result of the four non-specified properties for PE duct.

Property	ASTM Meth	Average Test Value		
		MBB 67-5-A	MBB 38-4-A	MBB 126-4-A
SP-NCTL (hr.)	ASTM 5397-Ap	3.8	3.9	3.0
OIT (min.)	ASTM D 3895	4.05 (pipe) 1.47 (plaque)	3.76 (pipe) 1.37 (plaque)	1.64 (pipe) 1.22 (plaque)
Antioxidant (ppm) Irganox 1010 Irganox 1076	HPLC	 0 0	 201 0	 0 102
Carbonyl Content (ppm)	FTIR	407 (outside layer) 379 (inside layer) 416 (overall)	367 (outside layer) 322 (inside layer) 353 (overall)	312 (outside layer) 202 (inside layer) 239 (overall)

[+] SP-NCTL – single point notched constant tensile load test at 15% yield stress

[++] OIT – oxidative induction time test.

chromatography was used to increase the sensitivity of the test. In addition, the analysis was not limited to the phenolic types of antioxidants, such as Irganox 1010 and Irganox 1076, in that testing for a phosphite compound, Irgafos 168, was also performed. Irganox 1010 and Irganox 1076 are two common phenolic antioxidants used in commercial polyethylene products. Their functional temperature ranges from room temperature to 300^{o}C; thus, they can be used as short term processing stabilizers as well as long-term antioxidants to protect product during the service life. The difference between these two antioxidants is that Irganox 1076 has a lower molecular weight than the Irganox 1010. Therefore, Irganox 1076 in some cases is used as a short-term stabilizer, whereas Irganox 1010 is used as a long term stabilizer. On the other hand, Irgafos 168 is used solely for processing stabilization due to its high effective temperature.

The amount of antioxidants in the three retrieved field samples is shown in Table 3. Neither Irganox 1010 nor Irganox 1076 were detected in Sample 67-5-A. In Sample 38-4-A, approximately 200 ppm of Irganox 1010 and no Irganox 1076, was detected, whereas 100 ppm of Irganox 1076 was found in Sample 126-4-A. No Irgafos 168 was detected in any of the three samples. The amount of antioxidant remaining in the duct samples was relatively low or even zero. By comparison, the typical formulation of HDPE geomembranes for landfill applications consists of 1500 to 3000 ppm of Irganox 1010 and 750 ppm of Irgafos 168. Such a formulation yields OIT value ranging from 80 to 130 minutes.

However, the HPLC data does not seem to be consistence with the OIT data. Sample MBB 67-5-A, which exhibited zero antioxidants, still had an OIT value of 4 minutes. On the other hand, Sample 126-4-A had the lowest OIT value, but it still contained 100 ppm of Irganox 1076. This inconsistency between OIT and HPLC tests can be caused by a) uneven distribution of antioxidant in the duct samples and b) error in marking sample codes.

- Carbonyl Group Analysis: Carbonyl group results from the oxidation of polyethylene. Since the amount of antioxidants was found to be relatively low or non-existent, the HDPE duct could already have been oxidized, particularly near the surface. A common method to verify oxidation of polyethylene is to evaluate the existence of carbonyl groups. A thin layer of material was removed from the inside and outside of the duct surface and was analyzed using FTIR. In addition, a section of the material was cut across the duct wall thickness and then compressed into a thin film for analysis. The results are shown in Table 3. Carbonyl group was detected in all three duct samples. The outer surface of the duct had a slightly higher concentration than the inside surface, as expected. In addition, Sample 67-5-A, which showed zero antioxidant in the

HPLC analysis, also exhibited slightly higher carbonyl content than the other two samples (note that there may have been an error in marking the tested sample as stated above). The results suggest that some amount of oxidation has occurred in the duct samples. However, extruded products, like ducts, do contain a small amount of carbonyl groups. Since there is no original product to provide a base line for comparison, the extent of the oxidation in these duct samples cannot be quantified.

Summary of the Material Properties Evaluation

The properties of the three field duct samples were evaluated according to the material specification ASTM D3350. The required cell class specification for the duct material was 345433C; however, one of the tests (HDB) was not performed. Therefore, the field duct samples were tested for the other six properties only, which included density, melt index, flexural modulus, tensile yield stress, ESCR, and carbon black. With the exception of density and flexural modulus, the properties did not meet the specified value. The melt index was much higher than specified, suggesting that the molecular weight of the polymer probably was lower than the specified material. The tensile yield stress was well above the specified value; however, this is usually acceptable. The ESCR is significantly below the required value, indicating that the tested duct materials were highly susceptible to stress cracking. Finally the carbon black is slightly below the required percentage.

In addition, four non-specified properties were of the duct samples were evaluated. The SP-NCTL test has the same purpose as the ESCR; that is, to assess the slow crack growth resistance of the material. The SP-NCTL test is considered to be a better controlled and more quantifiable test than the ESCR. However, a correlation between the SP-NCTL test and the specified ESCR test has not yet been developed. Nevertheless, the average failure times of the duct samples ranged between 3 to 4 hours at an applied stress of 15 percent of the yield stress. For the OIT test, the values of the duct samples range from 1.6 to 4 minutes, while the values for the compression molded plaques averaged about 1.3 minutes. These OIT values are very low, and they suggest that the overall average amount of antioxidants in these duct samples was very limited. The HPLC test results also confirm this finding, although at this time the correlation between OIT and HPLC has not been established. However, it is not certain over what period of time the antioxidant was consumed, since an original duct sample was not available for comparison. It is possible that the duct samples contained a low level of antioxidants from the very beginning. It should be noted that the OIT test does not provide information regarding the oxidation degradation status of the duct samples.

The oxidation degradation status in the duct samples was also assessed by the presence of carbonyl functional group. All three samples showed some amount of carbonyl group. The highest concentration was found in Sample MBB 67-5-A, which exhibited zero antioxidants. However, without knowing the carbonyl content in the original (unaged) duct sample, the extent of the oxidation cannot be confirmed.

CONCLUSIONS

Three polyethylene duct samples with various lengths of longitudinal cracks were examined for their fracture morphology as well as material properties. The microstructure of the fracture surfaces verified that these cracks were generated via a slow crack growth mechanism. A majority of the cracking started from the inner surface of duct wall and then grew through the wall thickness, as well as extending along the longitudinal axis of the duct. The initiations of the cracks were observed to be near impurity particles or air bubbles in the duct material.

Four of the six tested material properties did not conform to the specified value. Most importantly, the stress crack resistance of the three tested duct samples was extremely poor based on the results from both ESCR and SP-NCTL tests.

The amount of antioxidant remaining in the three duct samples was also found to be very low. In addition, some amount of carbonyl functional group was detected. However, the extent of oxidative degradation cannot be quantified due to the lack of reference data.

APPENDIX B

EVALUATION OF HIGH DENSITY POLYETHYLENE DUCTS FROM THE GARCON POINT AND SEVEN MILES BRIDGES

INTRODUCTION

The objective of this test program was to determine material properties of retrieved field high-density polyethylene (HDPE) duct samples from the two indicated bridges. The material properties that were included are largely based on the ASTM D3350 specification with one of the specified tests being omitted. Furthermore, three tests have been added to evaluate the stress crack resistance and antioxidant content of the materials.

TEST MATERIALS

Two different duct samples were provided by the Florida Department of Transportation (FDOT) for evaluation. One of the samples was retrieved from the Garcon Point Bridge and the other from the Seven-Mile Bridge. The two ducts were coded in this report as Garcon-Point and Seven-Mile samples. None of the duct samples contained cracks, and no cracking was observed in the external ducts of either bridge.

For the Garcon-Point duct sample, PE 3408 and ASTM F 714 were labeled on the outer surface. PE 3408 is the plastic pipe material designation, indicating that the material shall yield a HDB value of 1600 psi according to ASTM D 2513. ASTM F 714 is a standard specification for "Polyethylene Plastic Pipe (SRD-PR) Based on Outside Diameter". All pipes produced under this specification are pressure-rated according to the ASTM 2837 hydrostatic design basis (HDB) test. Three HDB values are defined in the specification, 1250, 1450 and 1600 psi. Furthermore, ASTM F 714 provides the ASTM 3350 cell classification for the 1600 psi pipe materials (i.e., PE 3408) as shown in Table 1. However, the cell classes are very broad.

For the Seven-Mile Bridge duct samples, no printed label was found on the outer surface, although the pipe supplier (Vstructural, LLC) did provide the resin specification of the duct, as shown in Table 2. The specification indicates Driscopipe as the duct manufacturer.

EVALUATION OF RETRIEVED DUCT SAMPLES

The retrieved field duct samples were examined to determine their material properties and the extent they conformed to specification. The results are described in the following sections.

Table 1: Classification of Polyethylene Pipe Material (Ref. ASTM 714, Table 4).

Properties	Cell Class for 1600 psi pipe material
Density	2 or 3
Melt Index	3, 4, or 5
Flexural modulus	4 or 5
Tensile Strength	3, 4, or 5
ESCR	3
UV stabilizer	C or E

Table 2: Classification of Seven-Mile Duct Material.

Properties	Cell Class	Value
Density	3	0.941 – 0.955 g/cc
Melt Index	3	<0.4 – 0.15 g/10 min
Flexural modulus	5	120,000 to <160,000 psi
Tensile Strength	4	3,000 - <3,500 psi
ESCR	3	Condition C, F_{20} = 192 hours
HDB	3	1250 psi
UV stabilizer	C	2% minimum carbon black

Material Properties

Material properties of the retrieved field ducts were evaluated based on the test methods defined in the ASTM D 3350. As stated in the Introduction, the HDB test was omitted from this program. This test requires extremely long testing time (at least 10,000 hours) and is performed using a sophisticated testing device that monitors pressure and failure time.

The three tests that were added to the test program are described in Table 3. Of these, the NCTL test was recently adopted to replace the ESCR test, ASTM D1693, for corrugated polyethylene non-pressured pipe in the AASHTO M294 specification. The reason for replacing the ESCR test was the large standard deviation and qualitative nature of the test. The NCTL test was included in the present program even though it is not included in the ASTM D3350

specification. The test data will be seen to be beneficial for comparing results from different grades of HDPE resins and for establishing future duct specifications. The PENT test is designed to evaluate gas pipe resins. The test conditions are relatively aggressive in order to shorten the testing time. Also, the test is difficult to perform due to specimen preparation procedures and to the sophisticated nature of the test device, which the research team did not have. In this report, the PENT test was carried out by one of resin manufactures (BP-Solvay Polyolefin Company).

Table 3: Additional Tests to Evaluate Properties of Duct Materials.

Test	Test Method	Property
NCTL test	ASTM D 5397	Slow crack resistance
PENT test	ASTM F 1473	Slow crack resistance
OIT	ASTM D3895	Antioxidants

Note: NCTL – notched constant tensile load test.
PENT – Pennsylvanian test
OIT – oxidative induction time.

The third additional test was the oxidative inductive time (OIT) test. This assesses the amount of antioxidant remaining in the polymer. A short OIT value indicates a low amount of antioxidants in the formulation. The result of this test can provide an indication as to the level of antioxidant remaining in the duct samples, as well as for compression molded plaques which were used for the material property evaluation. However, OIT is not a quantitative analysis; and the exact amount of each antioxidant in part-per-million (ppm) cannot be determined. In addition, the sensitivity of the OIT decreases when the amount of antioxidant in the duct is close to depletion.

4. Test plaque preparation.

   The duct samples were cut into approximately one inch square pieces and compression molded plaques prepared from these. The molding procedure was according to ASTM D1928 Procedure C (at a cooling rate of 15±5^{o}C). Four plaques with thickness of approximately 0.075 inches and one with a thickness of approximately 0.125 inches were made for each duct sample. From these plaques, various test specimens were die cut and used for subsequent physical and mechanical testing and the results compared to the relevant project specification.

5. ASTM D3350 specified tests.

The procedure and results of each specified test are presented below:

- Density: The density test was performed according to ASTM D792 procedure B. The liquid used was 1-Propanol with a density of 0.781 g/cc. The measurement was obtained using an analytical balance with an accuracy of 0.0001g. At least two replicates were evaluated for each sample. Note that the "true" resin density cannot be measured directly due to the added carbon black in the product; however, it can be calculated according to the equation,

$$\rho_{(resin)} = \rho_{(product)} - 0.0044C, \quad (1)$$

where C = % carbon black in the product. Tables 4(a) and (b) show the measured product density, carbon black content, and the calculated resin density for the Garcon-Point and Seven-Mile samples, respectively. The density values of the two duct materials are very similar, approximately 0.945 g/cc, and within the cell class 3 of the specification.

- Melt index: The melt index test was performed according to ASTM D1238 using a condition of 2.16 kg/190^{o}C. Two replicates were evaluated for each sample. The test values are given in Tables 5(a) and (b) for the Garcon-Point and Seven-Mile samples, respectively. There is a large different between two field samples. The MI value of the Seven-Mile duct material is much higher than that of the Garcon-Point duct, indicating that a lower molecular weight resin was used in the Seven-Mile duct. However, the MI value of Seven-Mile duct material does conform to the resin specification.

- Flexural modulus*:* The flexural modulus test was performed according to ASTM D 790, Method 1, Procedure B. Five replicates were tested for each pipe sample. The flexural test data of the Garcon-Point and Seven-Mile duct samples are shown in Tables 6(a) and (b), respectively. Interestingly, the flexural modulus of the Seven-Mile sample exhibits a slightly higher value than that of Garcon-Point, even through the density of two duct materials was very similar.

- Tensile yield strength: The tensile yield strength test was performed according to ASTM D 638 Type IV. The tensile properties of Garcon-Point and Seven-Mile duct samples are shown in Tables 7(a) and (b), respectively. Similar to the behavior of flexural modulus,

Table 4(a): Density, carbon black content, and calculated resin density of the field duct sample from the Garcon-Point Bridge.

Density Test via ASTM D 792		
Specimen	Density (g/cc)	**Average (g/cc)**
1	0.955	**0.954**
2	0.953	

Carbon Black Test via ASTM D 4218		
Specimen	Carbon Black (%)	**Average (%)**
1	2	**2**
2	2	

Calculate the Density of the Resin based on Equation provided in the ASTM D 3350 **$\rho_{(resin)} = \rho_{(product)} - 0.0044C$, C = % carbon black**			
Specimen	Density (g/cc)	Carbon Black (%)	**Resin Density (g/cc)**
1	0.954	2	**0.945**

Table 4(b): Density, carbon black content, and calculated resin density of the field duct sample from the Seven-Mile Bridge.

Density Test via ASTM D792-Procedure B				
Specimen	Density (g/cc)			**Average (g/cc)**
1	0.952	0.953	0.952	**0.952**
2	0.952	0.953	0.953	**0.953**
3	0.952	0.953	0.953	**0.953**
Carbon Black Test via ASTM D4218				
Specimen	Carbon Black (%)			**Average (%)**
1	2.0	2.1	2.0	**2.0**
2	2.0	2.0	2.0	**2.0**
3	2.0	2.0	2.0	**2.0**

Calculate the Density of the Resin based on Equation provided in the ASTM D 3350 **$\rho_{(resin)} = \rho_{(product)} - 0.0044C$, C = % carbon black**				
Specimen	Density (g/cc)	Carbon Black (%)	Resin Density (g/cc)	**Average (g/cc)**
1	0.952	2.0	0.944	**0.944**
2	0.953	2.0	0.944	
3	0.953	2.0	0.944	

Table 5(a): Melt index values of the field duct sample from the Garcon Point Bridge.

Melt Index Test via ASTM D 1238 Condition 190°C/2.16kg		
Specimen	Melt Flow (g/10 min)	Average MI (g/10 min)
1	0.05	0.06
2	0.07	

Table 5(b): Melt index values of the field duct sample from the Seven-Mile Bridge.

Melt Index Test via ASTM D1238, Condition 190°C/2.16kg		
Specimen	Melt Flow (g/10 min)	Average MI (g/10 min)
1	0.25	0.25
2	0.26	

Table 6(a): Flexural test data of the field duct sample from the Garcon-Point Bridge.

Flexural Test via ASTM D 790 Method 1, Procedure B			
Test Specimens	Specimen Depth (inches)	Specimen Width (inch)	2% Secant Modulus (psi)
1	0.133	0.5055	88490
2	0.130	0.5055	98200
3	0.133	0.5055	98540
4	0.125	0.5055	101500
5	0.125	0.5055	105200
Average	0.129	0.50	98386

Table 6(b): Flexural test data of the field duct sample from the Seven-Miles Bridge.

Flexural Test via ASTM D 790 Method 1, Procedure B			
Test Specimens	Specimen Depth (inches)	Specimen Width (inch)	2% Secant Modulus (psi)
1	0.111	0.5	117800
2	0.114	0.5	114100
3	0.110	0.5	120100
4	0.114	0.5	111300
5	0.110	0.5	115800
Average	0.112	0.5	115820

Table 7(a): Tensile test data of the field duct sample from the Garcon-Point Bridge.

Tensile Test via ASTM D 638 Type IV					
Test Specimens	Specimen Thickness (inches)	Yield Stress (psi)	Yield Elongation* (%)	Break Stress (psi)	Break Elongation* (%)
1	0.080	3085	17.1	4365	1235
2	0.080	3013	17.0	4677	1335
3	0.077	3032	16.6	4400	1259
4	0.077	2991	17.5	4964	1383
5	0.079	3038	16.6	4531	1282
Average	0.079	3032	17.0	4587	1299

* the value is calculated based on cross head movement and 1.3 inch gauage length

Table 7(b): Tensile test data of the field duct sample from the Seven-Miles Bridge.

Tensile Test via ASTM D 638 Type IV					
Test Specimens	Specimen Thickness (inches)	Yield Stress (psi)	Yield Elongation* (%)	Break Stress (psi)	Break Elongation* (%)
1	0.076	3623	14.6	2656	923
2	0.076	3445	14.3	2475	834
3	0.076	3394	14.8	2105	219
4	0.074	3345	14.2	2071	764
5	0.074	3419	14.8	1907	729
Average	0.075	3452	14.5	2327	685

* the value is calculated based on cross head movement and 1.3 inch gauage length

the yield strength of the Seven-Mile material is higher than that of the Garcon-Point.

- ESCR: The ESCR test was performed according to ASTM D 1693 Procedure C, which requires test specimens to be immersed in 100% Igepal at 100°C. The cell Class 3 requirement is that F_{20} be a minimum of 192 hours. In other words, no more than two of the 10 test specimens (i.e., 20%) are allowed to crack within the testing duration of 192 hours. The results of the tests are shown in Tables 8(a) and (b) for the Garcon-Point and Seven-Mile ducts, respectively. Both duct materials passed the specification with no cracked specimen after 192 testing hours. The testing time was extended to 600 hours (cell class 4), and no cracking in any of the specimens occurred for either duct material.

- Carbon Black: The carbon black content test was performed according to ASTM D 4812. At least two replicates were evaluated for each sample. The test data of the Garcon-Point and Seven-Mile duct materials are shown in Tables 4(a) and (b), respectively. Both materials contain the specified value of 2 percent.

Table 8(a) – ESCR test data of the field duct sample from Garcon-Point Bridge.

ASTM D 1693 Condition C: 100% Igepal at 100°C	
Testing Time (hour)	No. of Failed Specimens
3	0
17	0
24	0
48	0
72	0
96	0
120	0
144	0
168	0
192	0
F_{20}	**0**

Table 8(b) – ESCR test data of the field duct sample from Seven-Miles Bridge

ASTM D1693 Condition C = 100% Igepal at 100°C	
Testing Time (hour)	No. of Failed Specimens
2	0
24	0
48	0
72	0
120	0
168	0
192	0
F_{20}	**0**

3. Additional non-specified tests.

The procedure and results of the four additional tests that were performed are presented below:

- SP-NCTL test: The test was performed according to the AASHTO M294 specification, which was developed based on the ASTM D 5397-Appendix. A set of five notched specimens was subjected to tensile loads while immersed in a solution of 10 percent Igepal at 50°C. The applied tensile load was equal to 15 percent of the yield strength of the material at room temperature. The notch depth was 20 percent of the thickness of the specimen. The failure time of each specimen was automatically recorded to the nearest 0.1 hour. The test data are shown in Tables 9(a) and (b) for the Garcon-Point and Seven-Mile duct samples, respectively. The average failure time of the Seven-Mile duct material was 80 hours. On the other hand, the Garcon-Point duct material did not fail even after 1000 hours. This result clearly indicates that the HDPE resin used in the Garcon-Point duct has much higher stress crack resistance than that in the Seven-Mile duct. Note that the ESCR test (ASTM D 1693) could not provide any conclusive information, since both materials passed the required specification.

  In order to further evaluate the slow crack behavior of the two duct materials, additional tests were performed using different applied stresses. Figure 1 shows the ductile-to-brittle curve of the Garcon-Point duct material. The transition between ductile and brittle failure occurred in the stress range of 30 to 35 percent. Specimens tested at stresses higher than 35 percent failed in a ductile mode, whereas those tested at less than 30 percent yield stress failed in a brittle mode. The ductile region exhibits a flatter slope than the brittle region. For the Seven-Mile duct material, only the brittle portion of the curve was generated and is superimposed in Figure 1. The slope of the brittle curve is similar to that of the Garcon-Point duct material, indicating that the same failure mechanism was taking place in both materials. At an applied stress of 25 percent, the Garcon-Point duct material lasted 25 times longer than the Seven-Mile duct material.

- PENT test: This test was performed according to the ASTM F 1473. The compression molded plaque was prepared according to the procedure described in ASTM F1473 using a very slow cooling rate to achieve maximum crystallinity in the plaque. The thickness of the plaque (same as the specimen thickness) was 10 mm (0.4 inch). Due to the large thickness, test specimens must be machined to form the rectangular bar. The applied stress of the test was a constant value of 2.4 MPa (348 psi or approximately 10 percent of the yield stress of the two duct materials). The test was performed in a forced air oven at

- Table 9(a): NCTL test data of the field duct sample from the Garcon-Point Bridge.

SP-NCTL Test per ASTM D 5397						
Applied Stress (psi)	Test Specimens	Specimen Thickness (inches)	Ligament Thickness (inches)	Applied Load (grams)	Failure Time (hours)	Average Failure Time (hour)
455 (15%)	1	0.078	0.063	541	> 1000	> 1000
	2	0.078	0.063	541	> 1000	
	3	0.078	0.063	541	> 1000	
	4	0.077	0.062	533	> 1000	
	5	0.077	0.062	533	> 1000	
606 (20%)	1	0.077	0.062	710	> 1000	> 1000
	2	0.077	0.062		> 1000	
	3	0.077	0.062		> 1000	
758 (25%)	1	0.077	0.062	888	461.6	524.0
	2	0.077	0.062		512.9	
	3	0.077	0.062		597.6	
910 (30%)	1	0.079	0.064	1101	296.6	295.2
	2	0.078	0.063		306.6	
	3	0.078	0.063		282.4	

Table 9(b): NCTL test data of the field duct sample from the Seven-Miles Bridge.

NCTL Test per ASTM D5397						
Applied Stress (psi)	Test Specimen	Average Five Specimen Thickness (inches)	Ligament Thickness (inches)	Applied Load (grams)	Failure Time (hours)	Average Failure Time (hours)
517 (15%)	1	0.077	0.062	0	78.3	79.54
	2	0.077	0.062	0	90.2	
	3	0.077	0.062	0	75.9	
	4	0.077	0.062	0	82.6	
	5	0.077	0.062	0	70.7	
689 (20%)	1	0.079	0.064	0	38.9	34.58
	2	0.079	0.064	0	34.2	
	3	0.079	0.064	0	34.3	
	4	0.079	0.064	0	31.2	
	5	0.079	0.064	0	34.3	
861 (25%)	1	0.078	0.063	0	18.3	19.18
	2	0.078	0.063	0	19.5	
	3	0.078	0.063	0	19.3	
	4	0.078	0.063	0	18.5	
	5	0.079	0.064	0	20.3	

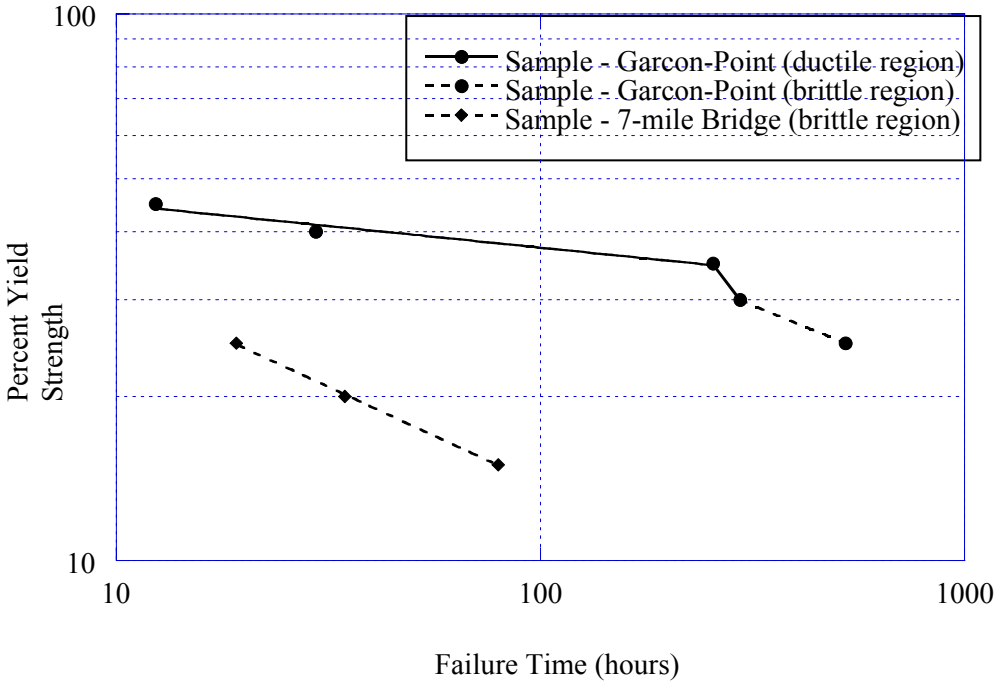

Figure 1 - NCTL test curves for duct samples from the Garcon-Point and Seven Mile Bridges.

80°C. Since the project team did not have the PENT test apparatus, the test was performed by another laboratory (BP-Solvay Polyolefin Company). Only the Garcon-Point duct material was evaluated. Two specimens were tested, and their failure times were 110.4 and 113.2 hours.

- OIT test: This test was performed according to ASTM D3895. The test is used to assess the time required to oxidize a test specimen at an isothermal temperature of 200°C. A specimen weighing approximately 2 to 3 mg was heated to 200°C at a constant rate of 20°C/min under a nitrogen atmosphere. The temperature was then held at 200°C while the gas was changed from nitrogen to oxygen. The test was terminated after oxidation of the polymer was detected.

  Both the pipe and plaque materials were tested. The OIT values are shown in Tables 10(a) and (b) for Garcon-Point and Seven-Mile ducts, respectively. Since the plaque had

gone through another heating cycle in the preparation, its OIT value is expected to be slightly lower than the corresponding pipe material.

The OIT value of the Seven-Mile duct material is much lower than that of the Garcon-Point. If the types of antioxidants are the same in both duct materials, then the Garcon-Point duct would have a longer lifetime than the Seven-Mile under the identical exposure condition. Currently, there are still antioxidants remained in the Seven-Mile duct sample. However, there is insufficient technical information available at this time to predict the depletion rate of the antioxidant in the service environment.

Table 10(a): OIT test data of the field duct sample from the Garcon-Point Bridge:

OIT Test via ASTM D3895			
Material	OIT (min)		Average OIT (min)
	1	2	
Pipe	111.3	108.9	110.1
Plaque	109.9	108.7	109.3

Table 10(b): OIT test data of the field duct sample from the Seven-Miles Bridge.

OIT Test via ASTM D3895			
Material	OIT (min)		Average OIT (min)
	1	2	
Pipe	15.1	13.4	14.2
Plaque	12.4	10.7	11.6

Summary of the Material Properties

The properties of the two field duct samples were evaluated according to the material specification ASTM D3350 together with three additional tests. The cell classes of the two duct materials are shown in Table 11. The Garcon-Point duct material has a cell class series of **3, 4, 4, 4, 3 (or 6), _, C** which falls in the range defined by the ASTM F714. For the Seven-Mile duct material, the cell class series is **3, 3, 5, 4, 3, _, C** which conforms to the resin manufacture's specification.

Table 11: Material Characteristic via Cell Class of ASTM D3350.

Property	Garcon-Point		Seven-Mile	
	Test Value	Cell Class	Test Value	Cell Class
Density (g/cc)	0.945	**3**	0.944	**3**
Melt Index (g/10 min)	0.06	**4**	0.25	**3**
Flexural modulus (psi)	98,386	**4**	115,820	**5**
Tensile Strength (psi)	3032	**4**	3,452	**4**
ESCR (F_{20} = 192)	0	**3**	0	**3**
SP-NCTL (hours) at 25% yield stress	524	**Non applicable**	19.2	**Non - applicable**
PENT (hours) at 348 psi (~ 10% yield stress)	111.8	**6**	None	**Not available**
HDB (psi)	Not tested	**Not available**	Not tested	**Not available**
UV stabilizer (%)	2	**C**	2	**C**
OIT (pipe) (min)	110.1	**Non applicable**	14.2	**Non applicable**

CONCLUSIONS

A section of the external duct was retrieved from the Garcon-Point and Seven-Mile Bridges. The material properties were evaluated according to the ASTM D 3350 together with three additional tests, which were SP-NCTL test, PENT test, and OIT test. The cell class series of both duct materials conforms to the respective specification. However, significant difference was found in the stress crack resistance and OIT value. The Garcon-Point duct sample exhibited 25 times higher stress crack resistance than the Seven-Mile duct sample, while both materials passed the ESCR requirement. Thus, the data indicate that the ESCR test cannot properly evaluate the stress crack resistance of all duct materials. The sensitivity of the ESCR test is not sufficient to distinguish HDPE duct resins with medium to high levels of stress crack resistance. Either the SP-NCTL or PENT test should be used to assess this property.

The large difference in the OIT values indicates that the antioxidant package of the two duct samples was not the same. However, the appropriate OIT value for ensuring a service lifetime of 100 years has not been defined at this time.

APPENDIX C

EVALUATION OF THE HIGH DENSITY POLYETHYLENE DUCTS IN THE CHANNEL FIVE, LONG KEY, AND NILES CHANNEL BRIDGES

INTRODUCTION

For this evaluation, six duct samples that were retrieved from the Channel Five, Long Key, and Niles Channel Bridges were evaluated, as described below.

TEST MATERIALS

The majority of the tests were based on the ASTM D 3350 specification with additional physical and chemical properties being determined to assess the durability of the ducts. No cracks were observed in the HDPE ducts of all three bridges. Approximately three-foot long samples were removed from the ducts for material characterization purpose. The locations of the field samples and material information printed on the ducts are shown in Table 1.

Table 1: Identification of the Six Field Samples.

Bridge	Sample Location	Code on the Duct
Nile Channel	Span 5_Tend 4_Gulf side_Seg 1 Span 39_Tend 1_Gulf side_Seg 1	PE 3406 PE 3406
Channel 5	Span 1_Tend 1_Gulf side_Seg 1-5	ASTM 3350 "335433C"
Long-Key	Span 99_Tend 4_Ocean side_Seg 1 Span 99_Tend 4E_Ocean side_Seg 1 Span 1_Tend 3_Ocean side_Seg 1-7	PE 3406 PE 3408 PE 3406

EVALUATION OF MATERIAL PROPERTIES OF RETRIEVED DUCT SAMPLES

The specification that was adapted by the FDOT in April, 2003 was used to characterize the six retrieved field duct samples. This requires ASTM D3350 cell classes of 344404C with conformance to two additional tests. The two additional tests are the Notched Constant Ligament Stress (NCLS) test for measuring stress crack resistance and the Oxidative Induction Time (OIT) test for assessing oxidation resistance properties. The specified value of each test is listed in Table 2. In this study, the HDB test was not performed, since it requires a complete duct sample which was not available.

Another item that should be noted is the difference between the PE 3408 and FDOT specification. Commonly for the gas pipe industry, the slow crack growth resistance (SCGR) test (also called

the PENN Test), ASTM F4218, is used to assess the stress crack resistance (SCR) of a resin. In the latest FDOT specification, the NCLT test is required to assess the SCR of the duct resin. Both tests are used to

Table 2: Properties for PE duct according to the FDOT Specification.

Property	Test Method	ASTM D 3350 Classification	Required Value	PE 3408	PE 3406
Density (g/cc)	ASTM D 792	3	>0.940-0.955	3	3
Melt index (g/10 min.)	ASTM D 1238	4	< 0.15	3	3
Flexural Modulus (psi)	ASTM D 790	4	80,000 - <110,000	4	4
Tensile yield strength (psi)	ASTM D 638 Type IV	4	3000 - <3500	4	4
ESCR*	ASTM D 1693	0	Not specified	3	3
SCGR** (hr)	ASTM F 1473	0	Not specified	0	0
HDB*** (psi)	ASTM D 2837	4	1600	0	0
Carbon black (%)	ASTM D 4218	C	> 2	C	C
NCLS^{+} test (hour)	ASTM F 2136 at 800 psi	na	500	na	na
OIT^{++} (min)	ASTM D3895	na	40	na	na

* ESCR – environmental stress crack resistance.
** SCGR – slow crack growth resistance
*** HDB – hydrostatic design basis.
$^{+}$ NCLS – notched constant ligament test.
$^{++}$ OIT – oxidative induction time.
na not available

evaluate the same material property; however, the test conditions are completely different. In this report, the NCLS test was used to evaluation all duct samples.

Test plaque preparation

All field duct samples were cleaned and cut into small pieces approximately one inch square in size. Compression molded plaques were prepared from these small pieces. The molding procedure was according to ASTM D1928 Procedure C (at a cooling rate of 15 ± 5^{o}C). Two to

three plaques with thickness of approximately 0.075 inches and one with a thickness of approximately 0.125 inches were made for each duct sample. From these plaques, various test specimens were cut using appropriate dies and used for subsequent physical and mechanical testing with the results being compared to the relevant project specification.

ASTM D3350 specified tests

The procedure and results of each specified test are presented below:

- Density: The density test was performed according to ASTM D792 procedure B. The liquid used in the test was Iso-Propanol with density of 0.781 g/cc at 23°C. The measurement was obtained using an analytical balance with an accuracy of 0.0001g. At least two replicates were evaluated for each sample. Note that the "true" resin density cannot directly be measured due to the added carbon black in the product; however, it can be calculated according to the equation,

$$\rho_{(resin)} = \rho_{(product)} - 0.0044C \qquad (1$$

where: C = % carbon black in the product. Table 3 shows the measured product density, carbon black content, and the calculated resin density of tested samples. The density values of the six duct samples were relatively similar, ranging from 0.939 to 0.942 g/cc, which falls near the lower limit of the required density cell class.

Table 3: Calculated resin density of seven duct samples.

Bridge	Sample	Product Density (g/cc)	Carbon Black (%)	Resin Density (g/cc)
Nile Channel	Span5_Tend4_Gulf_Seg1	0.955	3.30	0.940
	Span39_Tend1_Gulf_Seg1	0.944	1.20	0.939
Channel 5	Span1_Tend1_Gulf_Seg1-5	0.951	2.50	0.940
Long-Key	Span99_Tend4_Ocean_Seg1	0.951	2.60	0.940
	Span99_Tend4E_Ocean_Seg1	0.950	1.80	0.942
	Span1_Tend3_Gulf_Seg1-7	0.951	2.50	0.940

- Carbon Black: The carbon black content test was performed according to ASTM D 4812. At least two replicates were evaluated for each sample. The test data are included in

Table 4. Two samples, one from the Nile Channel Bridge and one from Long-key Bridge, contain carbon black less than 2 percent which is the minimum requirement defined in the ASTM D3350. The carbon black content in the other five samples was approximately 2.5 percent. The function of the carbon black is to protect the duct from ultraviolet (UV) light. Once the duct is installed inside the concrete segment box and shield from sunlight light, UV protection is not required. Thus, less than 2 percent carbon black content may not affect the longevity of the duct in the field.

Table 4: Carbon black content of seven tested duct samples.

Bridge	Sample	Carbon Black (%)		Average
		1	2	(%)
Nile Channel	Span5_Tend4_Gulf _Seg1	3.3	3.3	3.3
	Span39_Tend1_Gulf_Seg1	1.2	1.2	1.2
Channel 5	Span1_Tend1_Gulf_Seg1-5	2.5	2.5	2.5
Long-Key	Span99_Tend4_Ocean_Seg1	2.6	2.6	2.6
	Span99_Tend4E_Ocean_Seg1	1.8	1.8	1.8
	Span1_Tend3_Gulf_Seg1-7	2.6	2.5	2.6

- Melt index: The melt index (MI) test was performed according to ASTM D1238 using a condition of 2.16 kg/190^{o}C. Four replicates were evaluated for each sample. The test results for the six samples are shown in Table 5. With the exception of the Long-Key Bridge Span 99_Tend4E_Ocean side_SEG 1 sample, the MI values are similar (approximately 0.2 g/10 min) and conform to cell class (3) - <0.4 to 0.15 g/10 min, as defined in PE 3406. However, such an MI value exceeds the new specification requirement, which is cell class 4 (<0.15 g/10min). Only one sample, Span 99_Tend

Table 5: Melt index data of six tested duct samples.

Bridge	Sample Description	MI (g/10 min)				
		Test 1	Test 2	Test 3	Test 4	Average
Nile Channel	Span 5_Tend 4_Gulf side_SEG 1	0.23	0.23	0.25	0.23	0.24
	Span 39_Tend 1_Gulf side_SEG 1	0.22	0.22	0.22	0.22	0.22
Channel 5	Span 1_Tend 1_Gulf side_SEG 1-5	0.20	0.18	0.18	0.18	0.19
Long Key	Span 99_Tend 4_Ocean side_SEG 1	0.20	0.20	0.18	0.20	0.20
	Span 99_Tend 4E_Ocean side_SEG 1	0.12	0.12	0.11	0.11	0.12
	Span 1_Tend 3_Ocean side_SEG 1-7	0.20	0.20	0.20	0.19	0.20

4E_Ocean side_SEG 1, met the new FDOT duct specification.

- Flexural modulus: The flexural test was performed according to ASTM D 790, Method 1, Procedure B. Five replicates were tested for each pipe sample. The average 2 percent modulus values are shown in Table 6. The flexural moduli of the six field samples are within the cell class (4), 80,000 to <110,000 psi.
-

Table 6: Two percent flexural modulus values.

Bridge	Sample	Average Depth (inch)	Average Width (inch)	2% Modulus (psi)
Nile Channel	Span5_Tend4_Gulf Seg 1	0.113	0.5	100593
	Span39_Tend1_Gulf_Seg1	0.112	0.5	95912
Channel 5	Span1_Tend1_Gulf_Seg1-5	0.112	0.5	99268
Long-Key	Span99_Tend4_Ocean_Seg1	0.110	0.5	107062
	Span99_Tend4E_Ocean_Seg1	0.111	0.5	108706
	Span1_Tend3_Gulf_Seg1-7	0.111	0.5	104415

- Tensile yield strength: The tensile yield strength test was performed according to ASTM D 638 Type IV. The average tensile properties are shown in Table 7. The yield stress of all duct samples conform to cell class (4) of ASTM D 3350, ranging from 3000 to < 3500 psi.

Table 7: Tensile properties of seven tested duct samples.

Bridge	Sample	Average Thickness (inches)	Yield Stress (psi)	Yield Elongation* (%)	Break Stress (psi)	Break Elongation* (%)
Nile Canal	Span5_Tend4_Gulf Seg 1	0.075	3170	15.6	3270	1011
	Span39_Tend1_Gulf_Seg1	0.077	2972	16.7	4422	1295
Channel 5	Span1_Tend1_Gulf_Seg1-5	0.076	3032	15.2	3378	1094
Long-Key	Span99_Tend4_Ocean_Seg1	0.075	2946	15.0	3110	976
	Span99_Tend4E_Ocean_Seg1	0.075	3128	14.8	3434	1055
	Span1_Tend3_Gulf_Seg1-7	0.077	2929	15.3	3364	1075

* Calculated based on cross head movement and 1.3 inch gauge length.

- NCLS test: The test was performed according to the latest FDOT specification. Five replicates were tested at applied tensile stresses of 800 psi (5.5 MPa). The notch depth was 20 percent of the thickness of the specimen. The test environment was 10 percent Igepal solution at 50°C. The failure time of each specimen was automatically recorded to the nearest 0.1 hour. The average failure time of the seven duct samples is shown in Table 8.

Table 8 – NCLS test data at 800 psi

Bridge	Sample	Failure Time (hr)
Niles Channel	Span5_Tend4_Gulf_ Seg 1	50.9
	Span39_Tend1_Gulf_Seg1	70.1
Channel 5	Span1_Tend1_Gulf_Seg1-5	12.6
Long-Key	Span99_Tend4_Ocean_Seg1	16.4
	Span99_Tend4E_Ocean_Seg1	243.3
	Span1_Tend3_Gulf_Seg1-7	12.4

The NCLS test data can be divided into three groups according to their material coding. For duct samples coded as PE 3406 (Channel 5-Span 1_Tend1, Long Key-Span 99_Tend 4, and Long Key-Span 1_Tend 3), failure times were between 12 and 16 hours. The two duct samples from the Nile Channel Bridge (Span5_Tend4_Gulf_ Seg 1, Span39_Tend1_Gulf_Seg1) exhibited an average failure time of 60 hours. On the other hand, all five samples passed the ESCR test cell class (3) requirement, which limits 20 percent to failure to within 192 hours. The duct coded PE 3408 (Span99_Tend4E_Ocean_Seg1) showed significantly longer failure times (hundreds of hours) than the other four duct samples.

It should be noted that the applied stress used in the NCLS test for these six duct samples was significantly higher than for tests on the SSK and Mid-Bay Bridges (Appendices D and A, respectively). The new specification requires 800 psi ligament applied stress which is approximately 25 percent of the yield stress of the materials. The previous NCLS tests were tested at 15 percent of the yield stress of the materials. Therefore, these

six duct samples have a significant higher stress crack resistance than ducts in the SSK and Mid-Bay Bridges.

- OIT test: The test was performed according to ASTM D3895 for the purpose of assessing the time required to oxidize the test specimen at an isothermal temperature of 200°C. Two replicates were tested for a majority of the samples. Test specimens were taken directly from duct samples. The average OIT values of six duct samples are shown in Table 9 and ranged from 12 to 18 minutes, which is much longer than those measured for ducts from the SSK and Mid-Bay Bridges.

Table 9: OIT data of seven duct samples.

Bridge	Sample Description	Pipe Std-OIT (min)			
		Test 1	Test 2	Test 3	Average
Nile Channel	Span 5_Tend 4_Gulf side_SEG 1	13.80	11.02	13.62	12.81
	Span 39_Tend 1_Gulf side_SEG 1	17.82	18.11	12.17	16.03
Channel 5	Span 1_Tend 1_Gulf side_SEG 1-5	13.47	15.57	20.47	16.50
Long Key	Span 99_Tend 4_Ocean side_SEG 1	18.76	13.20	12.72	14.89
	Span 99_Tend 4E_Ocean side_SEG 1	22.67	20.11	11.22	18.00
	Span 1_Tend 3_Ocean side_SEG 1-7	14.48	19.67	20.74	18.30

DISCUSSION OF MATERIAL PROPERTIES OF THE SIX FIELD DUCT SAMPLES FROM KEY'S BRIDGES

As indicated in Table 1, there are three different material specifications for the six duct samples retrieved from the three Key's bridges. Only the one duct sample from the Channel 5 Bridge indicated a series of cell classes according to ASTM D 3350. The other five duct samples from Nile Channel and Long Key Bridges were coded as either PE 3406 or PE 3408. According to ASTM D 2239, PE 3406, such duct has a lower hydrostatic design stress than PE 3408 duct. In other words, the PE 3406 ducts would have lower stress crack resistance than the PE 3408 ducts. This was confirmed by the NCLS test results. The failure times of PE 3408 duct samples were at least 15 times longer than those of the PE 3406 ones. Another noticeable difference in the material properties between these six duct samples is the MI values. The PE 3408 ducts exhibited lower MI values than the others, suggesting that a higher molecular weight polymer was used.

Regarding oxidation resistance, which is assessed by the OIT test, the six field samples have very similar values ranging from 12 to 18 minutes.

By comparison, field duct samples from the three Key's bridges showed a significantly greater stress crack resistance and oxidation resistance than those from the SSK and Mid-Bay Bridges; and, consistent with this, better field performance has been observed for the former than latter.

CONCLUSION

Material properties of six field duct samples from three Key's bridges were evaluated and compared to requirements of the latest FDOT specification. The test results indicated that the ducts coded as PE 3406 have slightly lower SCR than those with PE 3408. However, all six field duct samples exhibited a significantly higher SCR than those from SSK and MB Bridge.

APPENDIX D

EVALUATION OF THE HIGH DENSITY POLYETHYLENE DUCTS IN THE SUNSHINE SKYWAY BRIDGE

INTRODUCTION

This Appendix presents the test results of high-density polyethylene (HDPE) duct samples that were retrieved from supporting columns and superstructure spans of the Sunshine Skyway (SSK) Bridge. The properties of the HDPE ducts, particularly the stress cracking resistance (SCR), were evaluated. For samples that contained cracks, the cracking mechanism was investigated. The material properties were assessed using the ASTM D 3350 specification. In addition, the single point notched constant tensile load (SP-NCTL) test was utilized to determine the SCR while the oxidation induction time (OIT) test was used to assess the remaining antioxidants in the retrieved field samples.

TEST MATERIALS

Two groups of samples were evaluated in this study. One group was taken from supporting columns of the bridge and the other was from the superstructure spans.

Column Samples

Thirty-two samples were retrieved from different columns, as shown in Table 1. Half of these were retrieved from southbound columns and the others from northbound columns. Four of the 32 samples had a longitudinal crack. Two of the cracked ducts were taken from southbound and the other two from northbound columns. The thickness of each of the 27 ducts was measured to determine the precision of the manufacturing. Material properties were evaluated on 14 of the 32 samples.

Span Samples

Thirty-four span samples were retrieved from the superstructure. Table 2 shows the locations of these with respect to different sections of the bridge. The numbers listed in Table 2 were used for sample identification in data analyses. Three samples had a longitudinal crack, and they were all taken from the northbound north approach (NB-NA) span.

THICKNESS EVALUATION OF COLUMN SAMPLES

Of the 32 retrieved column duct samples, 27 were selected to assess the precision of the thickness. The test procedure and analysis were performed according to ASTM D 2122. Eight individual thickness measurements, equally spaced from about the circumference, were made for each retrieved field sample. The average wall thickness, S, and wall thickness range, E, were calculated. The wall thickness range is expressed as a percentage according to the equation:

Table 1: Identification of the Thirty-two Retrieved Column Duct Samples

Sample No.	Duct Identification	Feature	Type of Test	
			Thickness	Material Property
Southbound				
C-1	91-SB-SW-5	Duct #1	X	X
C-2	91-SB-NE-5	Duct #2	X	X
	91-SB-NW-5	Duct #2	X	
C-3	103-SB-NW-12	Duct #2, Cut	X	X
	103-SB-NE-11	Duct #2	X	
	103-SB-NW-11	Duct #2	X	
	103-SB-NE-5	Duct #2	X	
	103-SB-NW-5	Duct #2	X	
C-4	118-SB-SE-6	Duct #1, Vertical Crack		X
	118-SB-NW-12	Duct #2	X	
	118-SB-NE-12	Duct #2	X	
C-5	118-SB-NW-6	Duct #2	X	X
	118-SB-NE-6	Duct #2	X	
C-6	131-SB-NE-5	Duct #2		X
	131-SB-SW-5	Duct #1	X	
C-7	131-SB-SE-6	Duct #1, Vertical Crack	X	X
Northbound				
C-8	92-NB-NE-5	Duct #2		X
C-9	92-NB-SW-5	Duct #1		X
	95-NB-SW-5	Duct #1	X	
	95-NB-SE-5	Duct #1	X	
C-10	95-NB-SE-8	Duct #1	X	X
	95-NB-SW-8	Duct #1	X	
	117-NB-NW-7	Duct #2	X	
C-11	117-NB-SW-7	Duct #1	X	X
	117-NB-NW-13	Duct #2	X	
	117-NB-SW-13	Duct #1	X	
C-12	117-NB-NW-8	Duct #2, Vertical Crack	X	X
C-13	119-NB-NW-11	Duct #2	X	X
	119-NB-NE-11	Duct #2	X	
	119-NB-NW-5	Duct #2	X	
	119-NB-NE-5	Duct #2	X	
C-14	119-NB-SE-12	Duct #1, Spiral Crack		X

Note:
Duct #1 was designated for the continuous duct coded SW-SE
Duct #2 was designated for the continuous duct coded NW-NE

Table 2: Identification of the Thirty-four Retrieved Span Duct Samples

No.	Sample Identification	Duct Feature
Southbound-North Approach (SB-NA)		
S-1	134-SB T1-SEG7	No Crack
S-30	133-SB T2-SEG7-N	No Crack
S-2	126-SB T1-SEG7	No Crack
S-28	121-SB T2-SEG7-N	No Crack
S-29	121-SB T3-SEG7-N	No Crack
S-3	117-SB T1-SEG7	No Crack
S-27	117-SB T1-SEG6-N	No Crack
Southbound-South Approach (SB-SA)		
S-7	105-SB T1-SEG7	No Crack
S-8	96-SB T1-SEG7	No Crack
S-26	95-SB T2-SEG1-N	No Crack
S-9	88-SB T1-SEG7	No Crack
Northbound-North Approach (NB-NA)		
S-4	134-NB T1-SEG1	No Crack
S-5	126-NB T1-SEG1	No Crack
S-34	124-NB T3-SEG4-N	Cracked
S-33	119-NB T4-SEG1	Cracked
S-32	118-NB T3-SEG6-N	Cracked
S-6	117-NB T1-SEG1	No Crack
Northbound-South Approach (NB-SA)		
S-31	105-NB T6-SEG1-N	No Crack
S-10	105-NB T1-SEG1	No Crack
S-11	96-NB T1-SEG1	No Crack
S-12	88-NB T1-SEG1	No Crack
Main Stay		
S-13	116-T116-W325-SEG1	No Crack
S-14	115-T115-E-209-SEG19	No Crack
S-15	115-T116-W-408-SEG11	No Crack
S-16	113-T113-E-320-SEG17	No Crack
S-17	113-T113-E-405-SEG10	No Crack
S-18	112-STAY21-W-SEG21	No Crack
S-19	111-T111-W-302-SEG70	No Crack
S-20	110-STAY21-E-SEG21	No Crack
S-21	109-T109-W-320-SEG9	No Crack
S-22	187-T109-W-405-SEG18	No Crack
S-23	108-T108-W-208-SEG1	No Crack
S-24	107-T107-E-408-SEG10	No Crack
S-25	106-T106-E325-SEG5	No Crack

$$E = \frac{A - B}{A} \times 100 \qquad (1$$

where : A = maximum wall thickness at any cross section, and
B = minimum wall thickness at any cross section.

Table 3 shows the individual thicknesses, minimum and maximum thicknesses, average of the eight values, and the thickness range of the eight values. The minimum wall thickness was from 0.131 to 0.176 inch, and the maximum thickness values from 0.161 to 0.192 inches. The average wall thickness ranged from 0.153 to 0.180 inch, while the thickness range percentage varies from 3 to 32 percent.

Although the specification for the ducts was not available, the thickness tolerance should not exceed 0.020 inch for either inside or outside diameter controlled pipe. If the pipe was manufactured based on an inside diameter controlled specification, the maximum permitted wall thickness should be the defined minimum thickness value plus 0.02 inch. In this case, the nominal pipe diameter was 2.5 inches and the SIDR 15. According to ASTM D 2239, the minimum wall thickness should be 0.165 inch; thus, the maximum thickness should be limited to 0.185. The majority of the pipes failed to pass this dimension specification.

EVALUATION OF CRACKING MECHANISM

The cracking mechanism was investigated by examining the microstructure of the fracture surfaces using a scanning electron microscope (SEM). From the fracture morphology, the crack initiation sites and propagation direction can be identified, as well as the cracking mechanism.

The microstructure of the cracked samples was evaluated by taking representative SEM specimens at different locations along the crack. One cracked column sample and one cracked span sample were examined.

- Column Sample 131-SB-SE-6

  A sketch of the crack in this sample is shown in Figure 1. The length of the sample was approximately 34 inch long. The crack propagated longitudinally in a curved pattern. Two positions were marked as matching points. Three SEM specimens were taken from along the crack with their approximate locations being as indicated in Figure 1.

Table 3: Wall Thickness Information (unit in inch).

Sample	Duct Identification	Individual Thickness Value								Minimum Thickness	Maximum Thickness	Average Thickness	Thickness Range (%)
Southbound													
91-SB-NE-5	Duct #2	0.179	0.171	0.169	0.181	0.159	0.170	0.160	0.173	0.159	0.181	0.169	12%
91-SB-NW-5	Duct #2	0.180	0.189	0.169	0.180	0.192	0.177	0.169	0.184	0.169	0.192	0.180	12%
103-SB-NW-12	Duct #2	0.172	0.180	0.178	0.179	0.156	0.169	0.168	0.157	0.156	0.180	0.170	13%
103-SB-NE-11	Duct #2	0.187	0.176	0.170	0.168	0.170	0.173	0.176	0.184	0.168	0.187	0.176	10%
103-SB-NW-11	Duct #2	0.152	0.168	0.170	0.155	0.148	0.169	0.169	0.152	0.148	0.170	0.160	13%
103-SB-NE-5	Duct #2	0.180	0.172	0.163	0.161	0.160	0.160	0.174	0.172	0.160	0.180	0.168	11%
103-SB-NW-5	Duct #2	0.176	0.154	0.158	0.172	0.164	0.152	0.154	0.172	0.152	0.176	0.163	14%
118-SB-NW-12	Duct #2	0.161	0.161	0.172	0.150	0.172	0.168	0.164	0.166	0.150	0.172	0.164	13%
118-SB-NE-12	Duct #2	0.167	0.172	0.176	0.169	0.163	0.169	0.173	0.167	0.163	0.176	0.170	7%
118-SB-NW-6	Duct #2	0.174	0.189	0.178	0.170	0.177	0.184	0.191	0.168	0.168	0.191	0.179	12%
118-SB-NE-6	Duct #2	0.169	0.181	0.180	0.182	0.179	0.173	0.176	0.188	0.169	0.188	0.179	10%
131-SB-NE-5	Duct #2	0.174	0.188	0.150	0.174	0.175	0.165	0.151	0.162	0.150	0.188	0.167	20%
131-SB-SW-5	Duct #1	0.157	0.154	0.161	0.141	0.160	0.153	0.157	0.140	0.140	0.161	0.153	13%
131-SB-SE-6	Duct #1	0.156	0.151	0.183	0.168	0.168	0.172	0.179	0.169	0.151	0.183	0.168	17%
Northbound													
95-NB-SW-5	Duct #1	0.174	0.165	0.173	0.167	0.174	0.169	0.164	0.172	0.164	0.174	0.170	6%
95-NB-SE-5	Duct #1	0.172	0.167	0.150	0.174	0.163	0.170	0.158	0.158	0.150	0.174	0.164	14%
95-NB-SE-8	Duct #1	0.165	0.157	0.159	0.175	0.164	0.153	0.171	0.176	0.153	0.176	0.165	13%
95-NB-SW-8	Duct #1	0.183	0.171	0.168	0.177	0.170	0.171	0.161	0.177	0.161	0.183	0.172	12%
117-NB-NW-7	Duct #2	0.165	0.169	0.163	0.171	0.163	0.176	0.156	0.150	0.150	0.176	0.164	15%
117-NB-SW-7	Duct #1	0.176	0.178	0.181	0.182	0.178	0.182	0.178	0.177	0.176	0.182	0.179	3%
117-NB-NW-13	Duct #2	0.151	0.175	0.186	0.167	0.171	0.145	0.174	0.173	0.145	0.186	0.168	22%
117-NB-SW-13	Duct #1	0.174	0.153	0.179	0.175	0.178	0.158	0.148	0.180	0.148	0.180	0.168	18%
117-NB-NW-8	Duct #2	0.176	0.179	0.158	0.158	0.192	0.131	0.174	0.158	0.131	0.179	0.166	32%
119-NB-NW-11	Duct #2	0.175	0.182	0.178	0.172	0.173	0.170	0.176	0.170	0.170	0.182	0.175	7%
119-NB-NE-11	Duct #2	0.172	0.153	0.165	0.166	0.175	0.177	0.178	0.171	0.153	0.178	0.170	14%
119-NB-NW-5	Duct #2	0.168	0.171	0.165	0.168	0.170	0.165	0.170	0.169	0.165	0.171	0.168	4%
119-NB-NE-5	Duct #2	0.158	0.167	0.173	0.177	0.176	0.175	0.166	0.163	0.158	0.177	0.169	11%

A general view of the fracture surface of Specimen 1 is shown in Figure 2. Here, the hemisphere morphology reveals the crack initiation as having started from the inside surface of the duct and propagated through the thickness. The initiation seems to have been caused by a material defect on the inner surface of the duct, as shown in Figure 3.

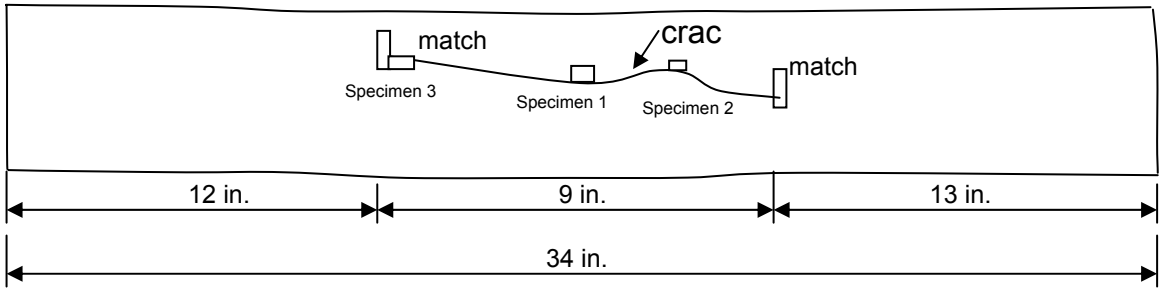

Figure 1: Sketch of column Sample 131-SB-SE-6.

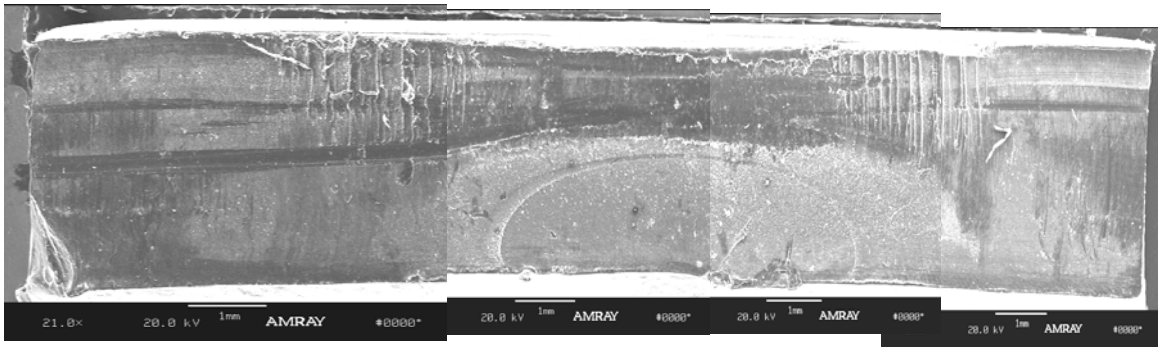

Figure 2: Fracture surface of Specimen 1 from Sample 131-SB-SE-6.

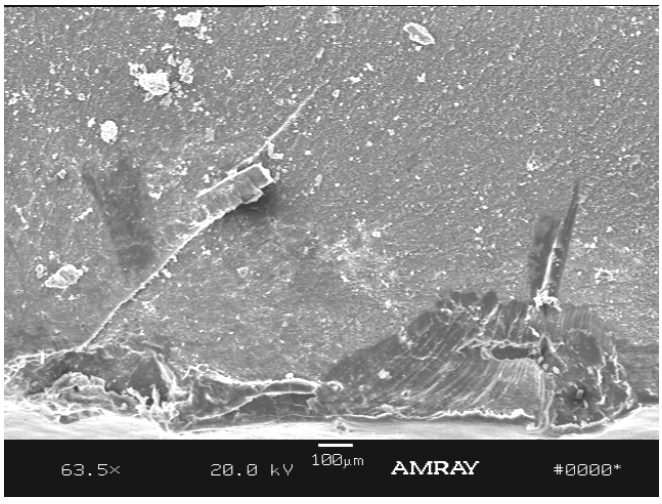

Figure 3: Close-up view at the crack initiation point in Figure 2.

The fracture surface of Specimen 1 was covered with a ort fibril structure, as can be seen in Figure 4. Such a morphology resulted from slow crack growth via breaking down of fibers in a craze.

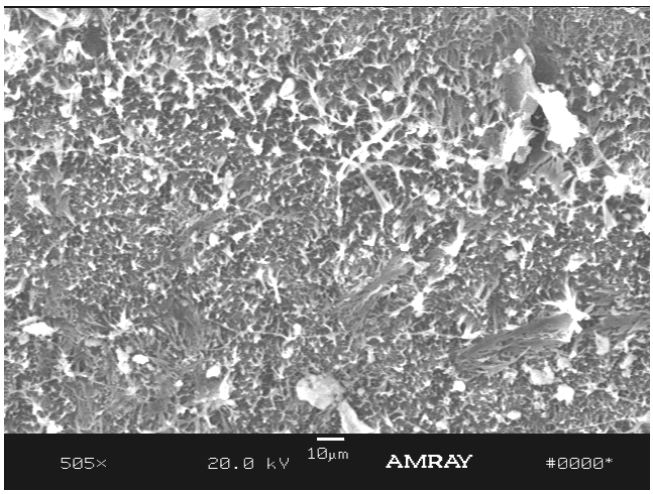

Figure 4: Fracture morphology on the surface of Specimen 1.

Specimen 2 was taken some distance away from the crack initiation. The general appearance of the facture surface is shown by Figure 5. The area marked "A" seems to be another crack initiation along this long crack. A close-up view of area "A" can be seen in Figure 6. The defect appears to be very similar to the one in Figure 3.

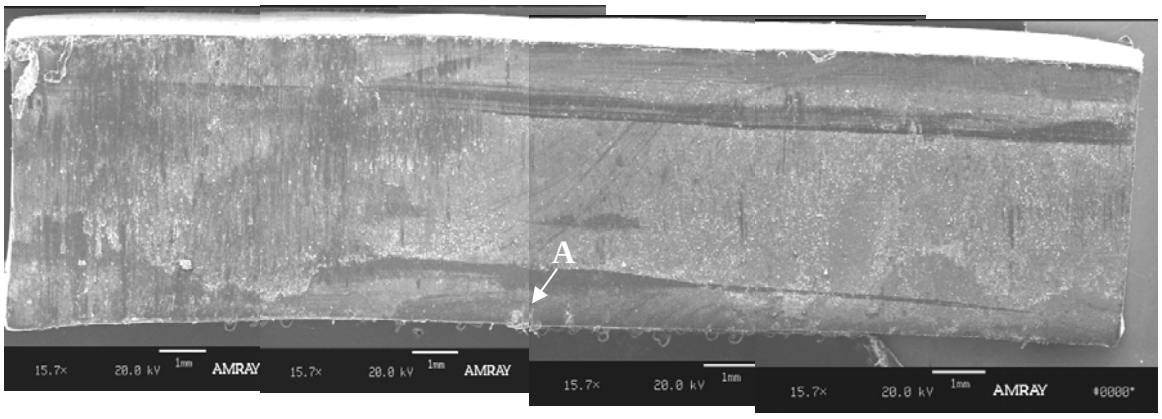

Figure 5: General view of fracture surface of Specimen 2 from Sample 131-SB-SE-6.

Specimen 3 was taken at the tip of the longitudinal crack. The general view of the fracture surface is revealed in Figure 7. The fracture surface of this specimen was covered with small fibril

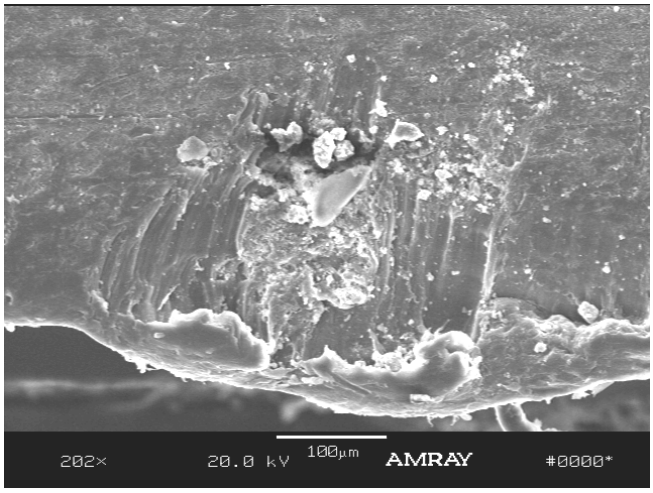

Figure 6: Close-up view at area "A" of Figure 5.

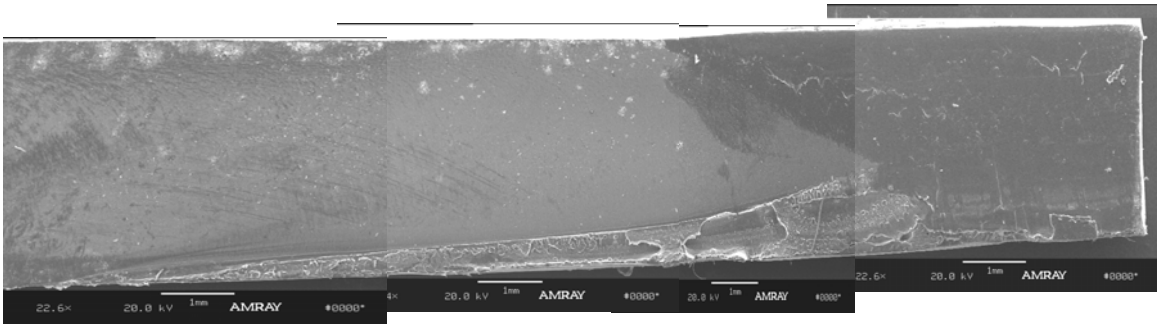

Figure 7: General view of the fracture surface of Specimen 3 from Sample 131-SB-SE-6.

structure, as shown in Figure 8.

- Span Sample 124NB-T3-SEG4-N

  This sample consisted of a section of a long longitudinal crack. Under close examination of the fracture surface, no obvious features that indicated crack initiation in this section were identified. Two SEM specimens were taken from along the crack at some distance away from each other.

  Figure 9 reveals the fracture surface of Specimen 1. Two unique morphologies were observed on the fracture surface. One is in area "A" on Figure 9. A close-up view of area "A" is shown in Figure 10. It seems that there was an impurity imbedded in the material. The second morphology is identified as area "B". A close-up view of this can be seen in Figure 11. A series of parallel fatigue lines was observed, suggesting that cyclic loading was involved in the crack growth.

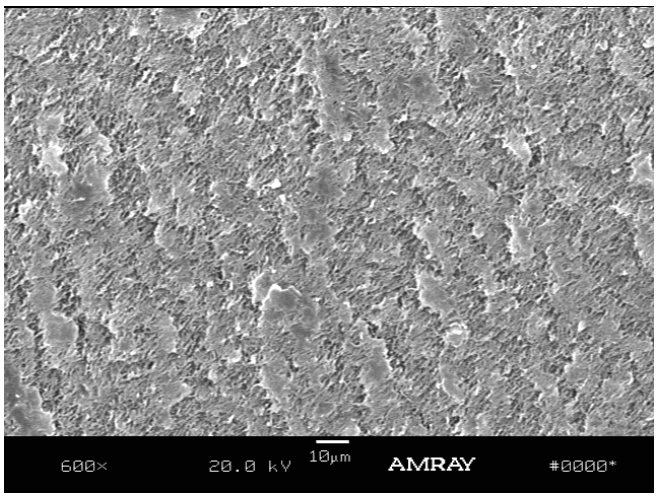

Figure 8: The close view of fracture morphology of Specimen 3.

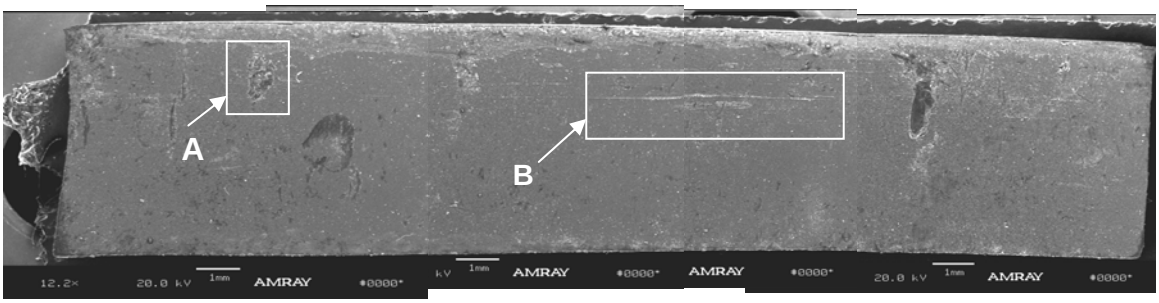

Figure 9: General view of the fracture surface of Specimen 1 from Span Sample 124-NB-T3-SEG4-N.

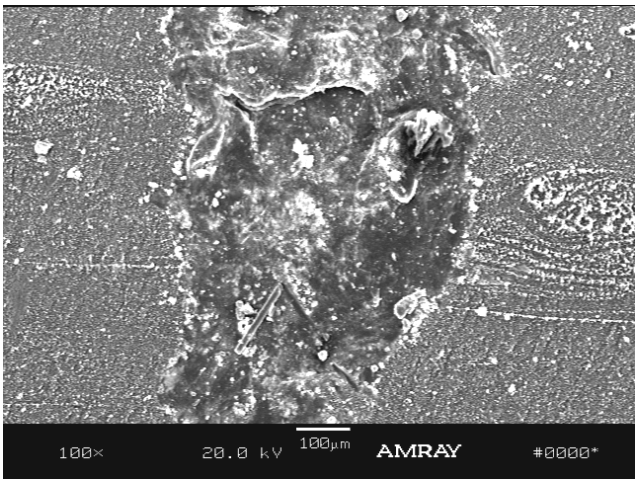

Figure 10: Close-up view of area “A” of Figure 9 revealing an impurity.

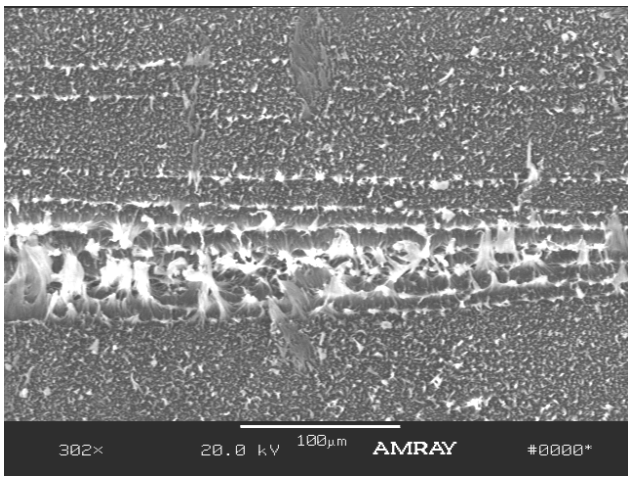

Figure 11: Close-up view of area "B" of Figure 9, revealing fatigue lines.

Figure 12 reveals the fracture surface of Specimen 2. Similar to Specimen 1, impurities and fatigue lines were also observed on this specimen, as shown in Figures 13 and 14, respectively. The fracture surfaces of both Specimens 1 and 2 were covered by small fibril structures, as shown in Figure 15. The cracking probably was caused by slow crack growth under periodical cycling loading.

Discussion of Cracking Mechanisms

The fracture morphology provided preliminary information regarding the cracking mechanism of the cracked column and span samples. The microstructure indicated that cracking started from the inner

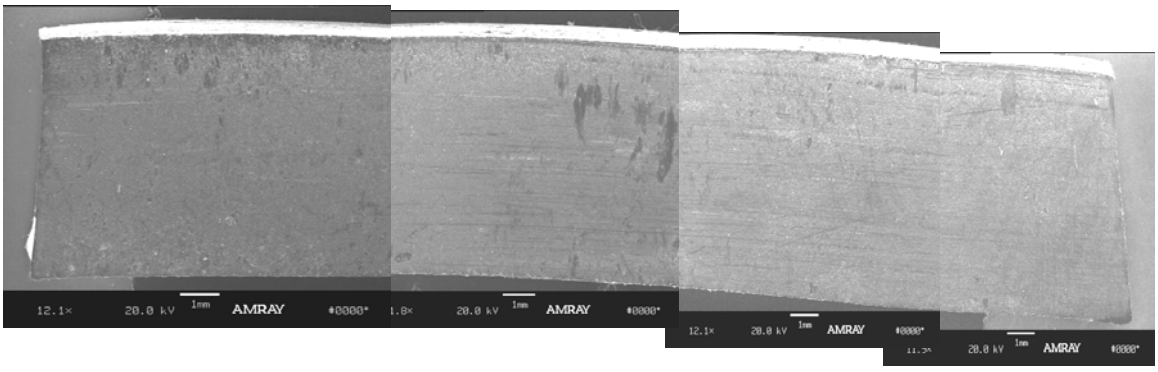

Figure 12: General view of the fracture surface of Specimen 2 from Span Sample 124-NB-T3-SEG4-N.

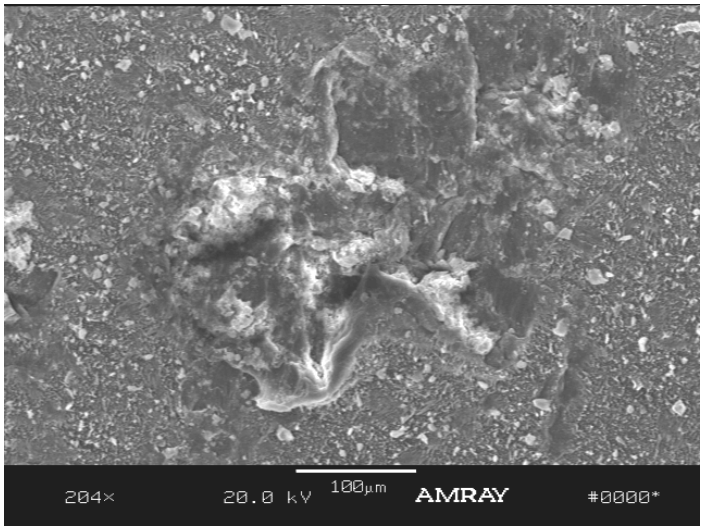

Figure 13: Impurity observed on fracture surface of Specimen 2.

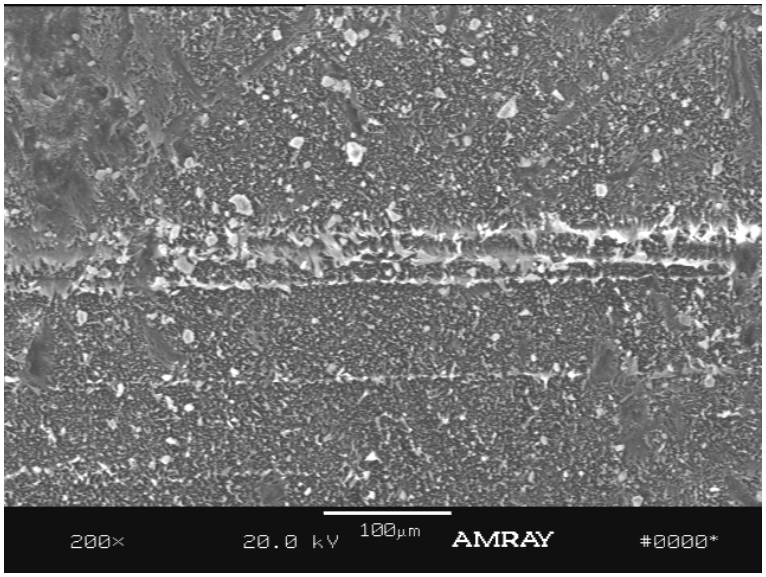

Figure 14: Fatigue lines on the fracture surface of Specimen 2.

surface of pipe wall and propagated through the wall thickness. The direction of the crack growth suggests that the inner duct surface was subjected to a tensile stress.

For column samples, crack initiations were found at defects or impurities located on the inner surface of the duct. However, the crack initiation of the span sample could not be identified. Fatigue lines provided a good indication regarding the crack growth direction. Furthermore, some impurities were

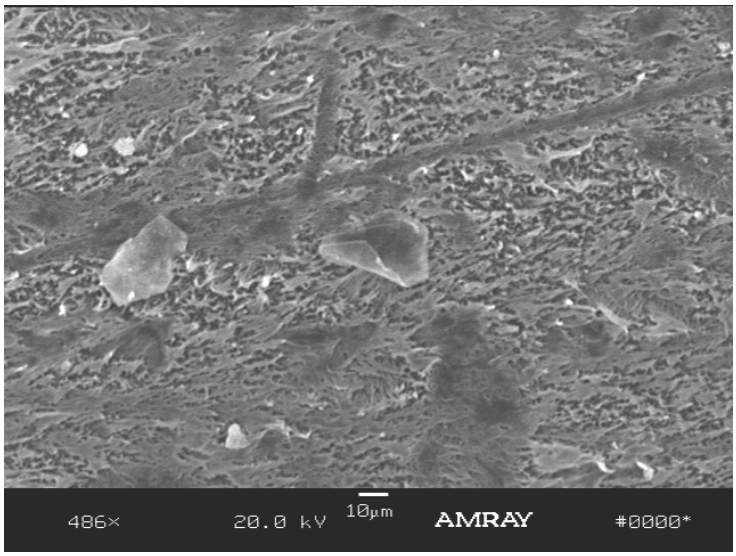

Figure 15: Small fiber structure covered the fracture surfaces of Specimens 1 and 2.

observed in the span sample; but they did not seem to act as the initiators of the crack. The cracking of both samples was governed by the slow crack growth mechanism.

MATERIAL PROPERTIES

Material properties of retrieved field ducts were evaluated largely based on test methods defined in ASTM D 3350. The SCR property was measured based upon the SP-NCTL test (ASTM D5397-Appendix) using the AASHTO M 294 specification. In addition, the oxidative inductive time (OIT) test was included to assess the amount of antioxidant remaining in the polymer.

As indicated in Table 1, 14 of the 32 retrieved column field samples were evaluated for their material properties. The four cracked ducts were included in the 14 samples. Nine field span samples (Sample numbers 26 to 34) were fully evaluated for their material properties. The other 25 samples were tested for melt index and stress crack resistance only.

According to Mr. Rodney Powers of FDOT, the specification for this bridge merely stated to use HDPE ducts. However, the specific material requirements for the HDPE ducts were not defined. For comparison purpose, the material specification of smooth PE ducts from AASHTO (2000) was used as reference in this study. The AASHTO specification requires that, "*Smooth plastic duct shall be made of*

polyethylene material and shall conform to the requirement of D 3350 with a cell classification PE 345433C". Table 4 shows the required properties and corresponding values according to ASTM D 3350.

Table 4: Specified Properties for HDPE Duct According to ASTM Specifications.

Property	Test Method	ASTM D 3350 Classification	Required Value
Density	ASTM D 1505	3	>0.940-0.955 (g/cc)
Melt index	ASTM D 1238	4	< 0.15 (g/10 min.)
Flexural Modulus	ASTM D 790	5	110,000 - <160,000 psi
Tensile yield strength	ASTM D 638 Type IV	4	3000 -<3500 psi
ESCR*	ASTM D 1693	3	F_{20} = 192 hr.
HDB**	ASTM D 2837	3	1250 psi
Carbon black	ASTM D 1603	C	> 2%
Additional Tests			
SP-NCTL+	AASHTO M294		> 24 hours
OIT	ASTM D3895		Not defined

* ESCR – environmental stress crack resistance
** HDB – hydrostatic design basis
\+ SP-NCTL – single point notched constant tensile load test
++ OIT – oxidative induction time

In this test program, material properties according to those listed in Table 4 were evaluated, but two of the specified tests were not included. One is the HDB test, which requires an uncracked pipe section; thus, the test was not applicable to retrieved field duct samples. The other is the ESCR test, ASTM D 1693, which is a qualitative test to evaluate stress crack resistance (SCR) of HDPE materials. The test cannot quantitatively distinguish SCR among different materials and is known to have poor precision. An alternative ESCR test, the SP-NCTL test according to ASTM 5397-appendix, was used in this study. The SP-NCTL test was recently adopted to replace the ASTM D 1693 test for corrugated HDPE non-pressured pipe in the AASHTO M294 specification. In addition, the OIT test was included to assess the amount of antioxidant remaining in the polymer. A short OIT value indicates low antioxidants. The result of this test can provide an indication on the level of antioxidant remaining in the duct samples.

Test Plaque Preparation.

All field duct samples were cleaned and cut into small pieces approximately one inch square in size. Compression molded plaques were prepared from these small pieces. The molding procedure followed

ASTM D4703 Method B (at a cooling rate of 15 ± 5 ^{o}C/min). Three plaques with thickness of approximately 0.075 inches and one with a thickness of approximately 0.125 inches were made for each duct sample. From these plaques, various test specimens were cut using appropriate dies and used for subsequent physical and mechanical testing and results were compared to values in the above indicated specification.

ASTM D3350 Specified Tests

The test procedure and results of each specified test are presented below:

- Density: The density test was performed according to ASTM D792 procedure B. The liquid used in the test was 1-Propanol with a density of 0.781 g/cc at 23^{o}C. The measurement was obtained using an analytical balance with an accuracy of 0.0001g. At least two replicates were evaluated for each sample. Note that the "true" resin density cannot directly be measured due to the added carbon black in the product; however, it can be calculated according to the equation,

$$\rho_{(resin)} = \rho_{(product)} - 0.0044C \qquad (1$$

where: C = % carbon black in the product.

Tables 5 and 6 show the measured product density, carbon black content, and the calculated resin density for column and span samples, respectively. The density values of column samples exhibit large variability with values ranging from 0.945 to 0.955 g/cc. Figure 16 shows the density values of 14 column samples as a bar chart plot. All four cracked ducts, samples 4, 7, 12 and 14, have densities equal or above 0.950 g/cc. Figure 17 shows a bar chart plot of density values of the nine span samples. These densities are generally higher than those of the column samples. Except for one sample, all density values are greater than 0.950 g/cc. All retrieved field samples from both column and superstructure of the bridge conformed to the required resin density range (0.940 – 0.955 g/cc) of cell class "3" in ASTM D3350.

- Carbon Black: The test to measure carbon black content was performed according to ASTM D 4812. Two replicates were evaluated for each sample. The test data are included in Tables 5 and 6 for column and span samples, respectively. Except for one column sample, the carbon black

content in both column and span samples was less than 2 percent, which is the minimum requirement as defined in the ASTM D3350. Furthermore, the range of carbon black content among different duct samples was very large, ranging from 0.3 to 2.1.

Table 5: Calculated Density of the Resin and Carbon Black of Column Samples.

No.	Sample Code	Product Density (g/cc)	Carbon Black (%)	Resin Density (g/cc)
Southbound				
C-1	91-SB-NE-5	0.949	0.50	0.947
C-2	91-SB-SW-5	0.958	0.90	0.954
C-3	103-SB-NW-12	0.956	0.30	0.955
C-4	118-SB-SE-6	0.956	1.00	0.952
C-5	118-SB-NW-6	0.954	1.60	0.947
C-6	131-SB-NE-5	0.960	1.90	0.952
C-7	131-SB-SE-6	0.961	2.10	0.952
Northbound				
C-8	92-NB-NE-5	0.958	0.40	0.956
C-9	92-NB-SW-5	0.955	0.30	0.954
C-10	95-NB-SE-8	0.947	0.20	0.946
C-11	117-NB-SW-7	0.952	1.70	0.945
C-12	117-NB-NW-8	0.956	1.00	0.952
C-13	119-NB-NW-11	0.948	0.60	0.945
C-14	119-NB-SE-12	0.954	0.80	0.950

Table 6: Calculated Density of the Resin and Carbon Black of Span Samples.

No.	Sample Code	Density (g/cc)	Carbon Black (%)	Resin Density (g/cc)
Southbound				
S-26	95SB T2-SEG1-N	0.953	0.50	0.950
S-27	117SB T1-SEG6-N	0.952	0.60	0.949
S-28	121SB T2-SEG7-N	0.961	1.20	0.956
S-29	121SB T3-SEG7-N	0.954	0.45	0.952
S-30	133SB T2-SEG7-N	0.955	0.60	0.952
Northbound				
S-31	105NB-T6-SEG1-N	0.957	0.65	0.954
S-32	118NB-T3-SEG1-N	0.961	1.45	0.954
S-33	119NB-T4-SEG1	0.959	1.30	0.953
S-34	124NB-T3-SEG4-N	0.955	0.70	0.952

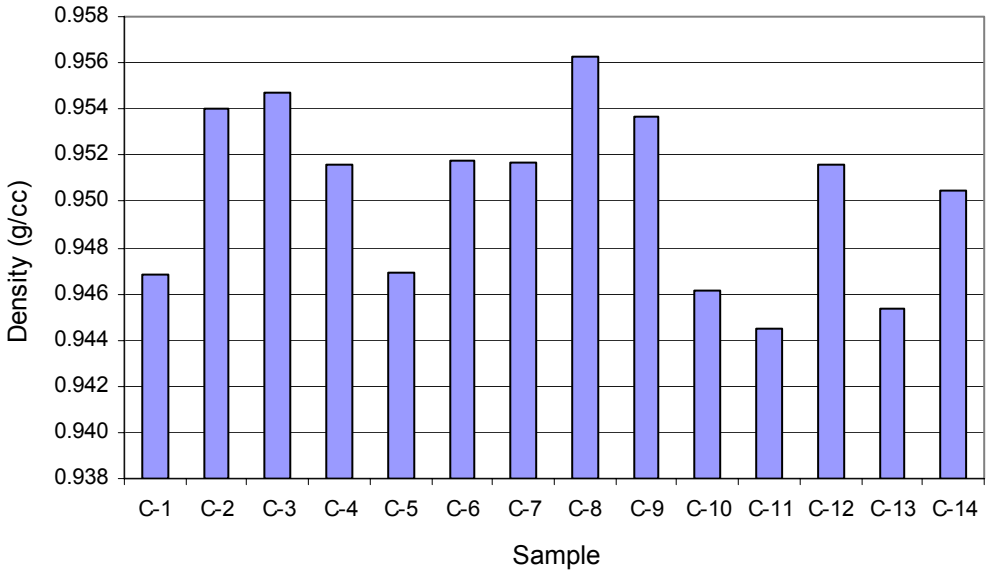

Figure 16: Density of fourteen column samples.

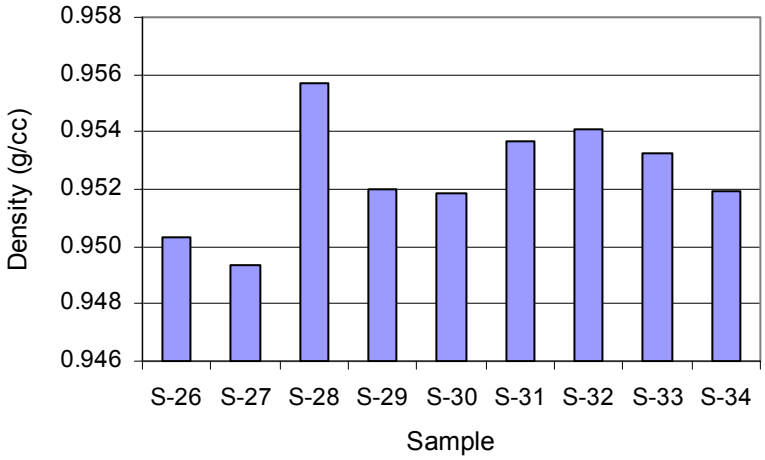

Figure 17: Density of nine field span samples.

Melt index: The melt index (MI) test was performed according to ASTM D1238 using a condition of 2.16 kg/190^{o}C. Two replicates were evaluated for each sample. The test results for 14 column samples are plotted in Figure 18, and the values are shown in Table 7. There is a large difference among the 14 field samples. The MI value ranges from 0.09 to 0.91g/10 min. Samples 4, 7 and 12, which exhibit a longitudinal crack, had much higher MI values than the others. Sample 14 exhibited spiral cracking and an average MI value.

The MI value of the 34 span samples are presented in Figure 19 and are listed in Table 8. The samples are divided into five sections according to their location in the bridge. The MI values vary significantly in each of the five sections, particularly the main stay (MS). In the NB-NA section, all six retrieved duct samples have MI values greater than 0.4 g/10 min. In both NB-SA and SB-NA sections, the MI values of the retrieved duct samples can be divided into two groups: one with values around 0.2 g/10 min and the other with values between 0.4 and 0.6 g/10 min. The ducts retrieved from the SB-SA section all have MI values less than 0.2 g/10 min. The greatest variation of MI is observed in the MS section, where values range from 0.1 to 1.1 g/10

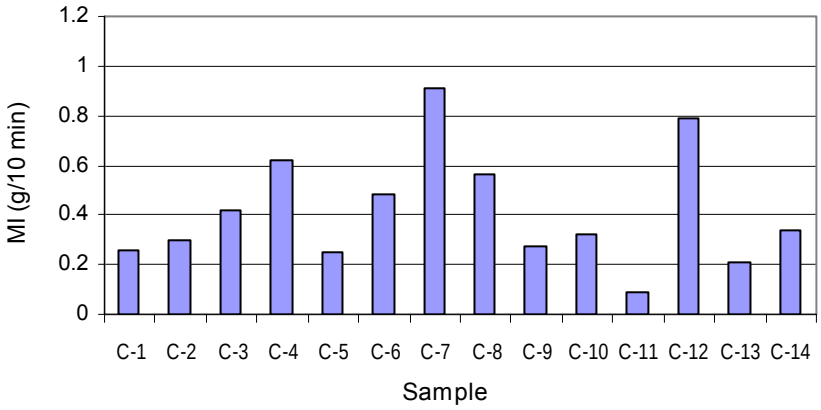

Figure 18: MI values of fourteen column samples.

Table 7: Melt Index Values of Column Samples.

No.	Sample Code	Average MI (g/10 min)
Southbound		
1	91-SB-NE-5	0.26
2	91-SB-SW-5	0.30
3	103-SB-NW-12	0.42
4	118-SB-SE-6	0.62
5	118-SB-NW-6	0.25
6	131-SB-NE-5	0.48
7	131-SB-SE-6	0.91
Northbound		
8	92-NB-NE-5	0.56
9	92-NB-SW-5	0.27
10	95-NB-SE-8	0.32
11	117-NB-SW-7	0.09
12	117-NB-NW-8	0.79
13	119-NB-NW-11	0.21
14	119-NB-SE-12	0.34

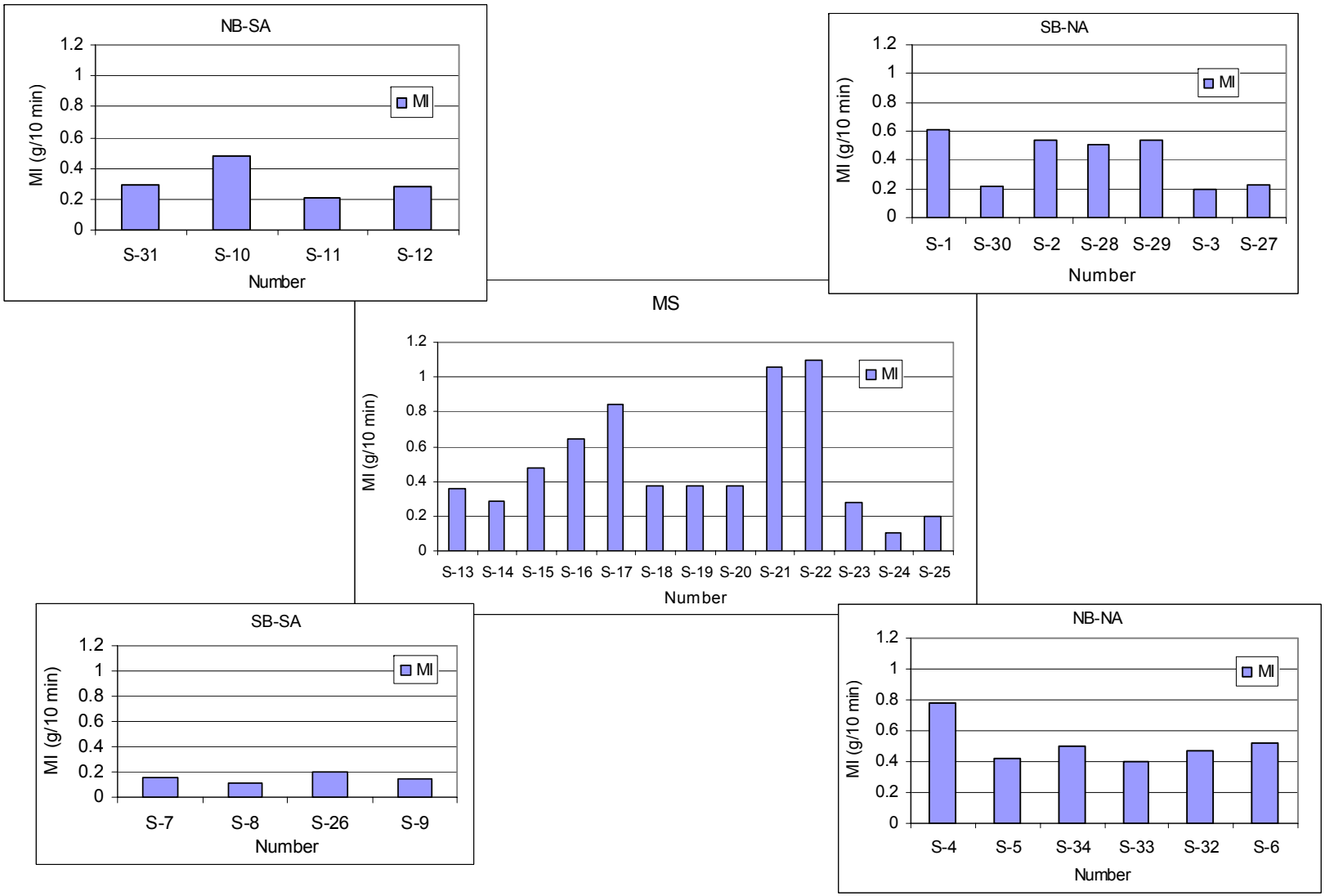

Figure 19: MI of thirty-four span samples.

Table 8: Melt Index Values of Span Samples.

No.	Sample Identification	MI (g/10 min)
Southbound-North Approach (SB-NA)		
S-1	134-SB T1-SEG7	0.61
S-30	133-SB T2-SEG7-N	0.22
S-2	126-SB T1-SEG7	0.54
S-28	121-SB T2-SEG7-N	0.51
S-29	121-SB T3-SEG7-N	0.54
S-3	117-SB T1-SEG7	0.20
S-27	117-SB T1-SEG6-N	0.23
Southbound-South Approach (SB-SA)		
S-7	105-SB T1-SEG7	0.15
S-8	96-SB T1-SEG7	0.11
S-26	95-SB T2-SEG1-N	0.20
S-9	88-SB T1-SEG7	0.16
Northbound-North Approach (NB-NA)		
S-4	134-NB T1-SEG1	0.78
S-5	126-NB T1-SEG1	0.42
S-34	124-NB T3-SEG4-N	0.50
S-33	119-NB T4-SEG1	0.40
S-32	118-NB T3-SEG6-N	0.47
S-6	117-NB T1-SEG1	0.52
Northbound-South Approach (NB-SA)		
S-31	105-NB T6-SEG1-N	0.29
S-10	105-NB T1-SEG1	0.28
S-11	96-NB T1-SEG1	0.21
S-12	88-NB T1-SEG1	0.48
Main Stay (MS)		
S-13	116-T116-W325-SEG1	0.36
S-14	115-T115-E-209-SEG19	0.29
S-15	115-T116-W-408-SEG11	0.48
S-16	113-T113-E-320-SEG17	0.64
S-17	113-T113-E-405-SEG10	0.84
S-18	112-STAY21-W-SEG21	0.37
S-19	111-T111-W-302-SEG70	0.37
S-20	110-STAY21-E-SEG21	0.37
S-21	109-T109-W-320-SEG9	1.10
S-22	187-T109-W-405-SEG18	1.10
S-23	108-T108-W-208-SEG1	0.28
S-24	107-T107-E-408-SEG10	0.10
S-25	106-T106-E325-SEG5	0.20

min. The highest MI values are for samples S-21, S-22, S-17 and S-16, which were taken from sections on either side of the central stay. All retrieved field samples from both the column and spans

of the bridge exhibited MI values well above the 0.15 g/10 min defined value based on cell classification of ASTM D3350.

- Tensile yield strength: The tensile yield strength test was performed according to ASTM D 638 Type IV. The values are shown in Tables 9 and 10 for column and span samples, respectively. All field samples conformed the cell class "4" of ASTM D 3350.

- Flexural modulus: The flexural test was performed according to ASTM D 790, Method 1, Procedure B. Five replicates were tested for each pipe sample. The 2 percent modulus values are shown in Tables 11 and 12 for column and span samples, respectively. All field samples exceeded the flexural modulus required range (110,000 to 160,000 psi) according to ASTM D 3350.

- SP-NCTL test: This test was performed according to the AASHTO M294 specification, which was developed based on the ASTM D 5397-Appendix. Five replicates were tested at applied tensile stresses that were equal to 15 percent of the yield strength of the material at room temperature. The notch depth was 20 percent of the thickness of the specimen. The failure time of each specimen was

Table 9: Tensile Properties of Column Samples.

No.	Sample	Average Thickness (inches)	Yield Stress (psi)	Yield Elongation* (%)	Break Stress (psi)	Break Elongation (in)	Break Elongation* (%)
Southbound							
C-1	91-SB-NE-5	0.077	4192	13.6	838	3.0	263
C-2	91SB-SW-5	0.071	4312	13.3	3079	0.2	18
C-3	103SB-NW-12	0.074	4047	13.8	1256	5.0	358
C-4	118-SB-SE-6	0.074	4317	13.0	1787	5.0	357
C-5	118-SB-NW-6	0.075	3981	14.1	1242.7	5.6	429
C-6	131SB-NE-5	0.074	3990	12.9	1355	2.0	136
C-7	131-SB-SE-6	0.077	4317	13.3	2612	1.0	103
Northbound							
C-8	92NB-SW-5	0.073	4257	12.9	738	5.0	376
C-9	92NB-NE-5	0.072	4519	12.5	1863	2.0	122
C-10	95-NB-SE-8	0.076	3858	14.3	1224	8.0	608
C-11	117-NB-SW-7	0.078	3654	15.3	2540	9.0	691
C-12	117-NB-NW-8	0.069	4356	12.6	2321	7.0	542
C-13	119-NB-NW-11	0.077	3932	14.4	1109	4.0	290
C-14	119-NB-SE-12	0.076	4294	13.1	1824	5.0	371

* the value is calculated based on cross head movement and 1.3 inch gauge length

Table 10: Tensile Properties of Span Samples.

No.	Sample	Average Thickness (inches)	Yield Stress (psi)	Yield Elongation* (%)	Break Stress (psi)	Break Elongation (in)	Break Elongation* (%)
Southbound							
S-26	95SB-T2-SEG1-N	0.075	3644	14.8	3240	16	1251
S-27	117SB-T-SEG6-N	0.073	3752	14	2234	9	729
S-28	121SB-T2-SEG7-N	0.072	3898	13.5	1810	2	137
S-29	121SB-T3-SEG7-N	0.073	3814	13.9	962	8	584
S-30	133SB-T2-SEG7-N	0.074	3786	14.7	2064	10	752
Northbound							
S-31	105NB-T6-SEG1-N	0.074	3896	14.2	1754	9	659
S-32	118NB-T3-SEG6-N	0.076	3858	14.0	1709	7	568
S-33	119NB-T4-SEG1	0.073	3947	13.2	1011	7	562
S-34	124NB-T3-SEG4-N	0.073	3869	14.1	1358	9.7	841

Table 11: Flexural Modulus of Column Samples.

No.	Sample	Average 2% Flexural Modulus (psi)
Southbound		
C-1	91-SB-NE-5	141340
C-2	91SB-SW-5	na
C-3	103SB-NW-12	142540
C-4	118-SB-SE-6	154380
C-5	118-SB-NW-6	138060
C-6	131SB-NE-5	na
C-7	131-SB-SE-6	141940
Northbound		
C-8	92NB-SW-5	na
C-9	92NB-NE-5	na
C-10	95-NB-SE-8	134380
C-11	117-NB-SW-7	121880
C-12	117-NB-NW-8	159160
C-13	119-NB-NW-11	134080
C-14	119-NB-SE-12	151280

na = not available due to insufficient material

automatically recorded to the nearest 0.1 hour. All 14 column samples were tested, and the average failure time values are shown in Table 13 and Figure 20. For the 34 span samples, 19 were tested; and the results from this are shown in Table 14. Figure 21 shows the SP-NCTL test results together with MI values as a comparison. The data show a large variation in the stress crack resistance

between retrieved field samples.

Table 12: Flexural Modulus of Span Samples.

No.	Sample	Average 2% Flexural Modulus (psi)
Southbound		
S-26	95SB-T2-SEG1-N	129480
S-27	117SB-T-SEG6-N	123900
S-28	121SB-T2-SEG7-N	147240
S-29	121SB-T3-SEG7-N	142540
S-30	133SB-T2-SEG7-N	122500
Northbound		
S-31	105NB-T6-SEG1-N	130640
S-32	118NB-T3-SEG6-N	125280
S-33	119NB-T4-SEG1	134360
S-34	124NB-T3-SEG4-N	130000

Table 13: SP-NCTL Test Results of Column Samples.

No.	Sample	Applied Stress (psi)	Average Failure Time (hr)
Southbound			
C-1	91-SB-NE-5	629	6.6
C-2	91-SB-SW-5	644	2.0
C-3	103-SB-NW-12	608	3.9
C-4	118-SB-SE-6	648	2.5
C-5	118-SB-NW-6	597	15.1
C-6	131-SB-NE-5	600	4.7
C-7	131-SB-SE-6	648	2.0
Northbound			
C-8	92-NB-NE-5	678	3.0
C-9	92-NB-SW-5	639	5.9
C-10	95-NB-SE-8	579	5.3
C-11	117-NB-SW-7	548	33.6
C-12	117-NB-NW-8	653	2.0
C-13	119-NB-NW-11	590	7.9
C-14	119-NB-SE-12	644	3.3

- OIT test: This test was performed according to ASTM D3895 and is based upon the time required to oxidize a test specimen at an isothermal temperature of 200^{o}C. Two replicates were tested for the majority of the samples. Test specimens were taken directly from duct samples. The average OIT values of column and span samples are shown in Tables 15 and 16, respectively. The

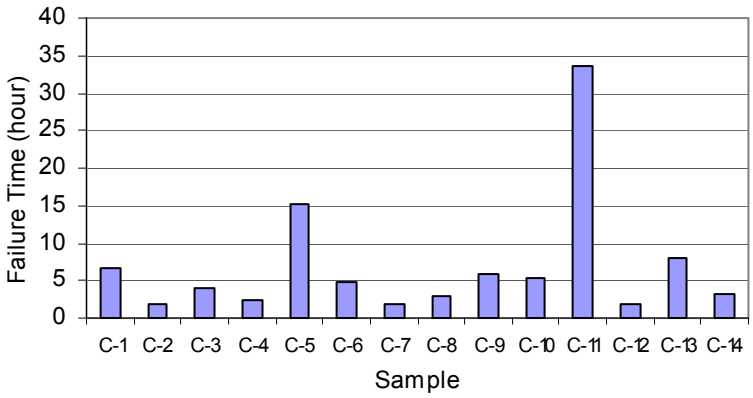

Figure 20: Failure time of fourteen column samples.

Table 14: SP-NCTL test Results of Span Samples.

No.	Sample Identification	Applied Stress (psi)	Failure Time (hr)
Southbound-North Approach (SB-NA)			
S-30	133-SB T2-SEG7-N	568	3.4
S-2	126-SB T1-SEG7	675	3.5
S-28	121-SB T2-SEG7-N	579	2.6
S-29	121-SB T3-SEG7-N	572	4.5
S-27	117-SB T1-SEG6-N	563	8.6
Southbound-South Approach (SB-SA)			
S-8	96-SB T1-SEG7	685	7.5
S-26	95-SB T2-SEG1-N	547	7.7
S-9	88-SB T1-SEG7	675	8.0
Northbound-North Approach (NB-NA)			
S-5	126-NB T1-SEG1	664	4.0
S-34	124-NB T3-SEG4-N	580	3.6
S-33	119-NB T4-SEG1	592	6.7
S-32	118-NB T3-SEG6-N	579	3.1
Northbound-South Approach (NB-SA)			
S-31	105-NB T6-SEG1-N	584	9.3
S-10	105-NB T1-SEG1	676	5.7
S-12	88-NB T1-SEG1	710	3.0
Main Stay (MS)			
S-16	113-T113-E-320-SEG17	662	3.6
S-17	113-T113-E-405-SEG10	657	2.8
S-19	111-T111-W-302-SEG70	669	11.5
S-21	109-T109-W-320-SEG9	667	3.1

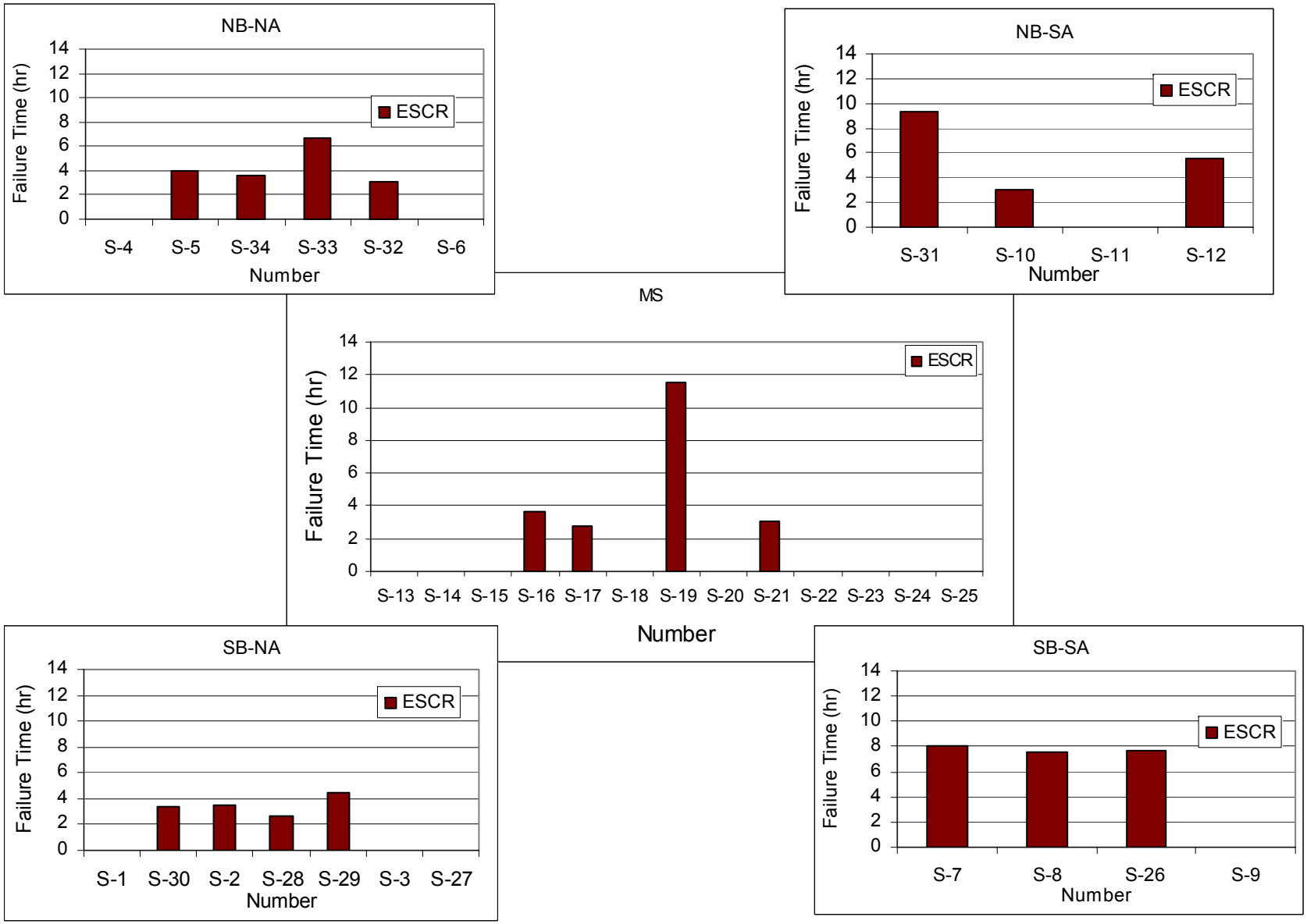

Figure 21: Failure time of eighteen span samples.

Table 15: OIT Values of Column Samples.

No.	Sample Code	Average OIT (min)
Southbound		
C-1	91-SB-NE-5	5.0
C-2	91-SB-SW-5	4.4
C-3	103-SB-NW-12	2.7
C-4	118-SB-SE-6	3.2
C-5	118-SB-NW-6	4.6
C-6	131-SB-NE-5	4.4
C-7	131-SB-SE-6	2.9
Northbound		
C-8	92-NB-NE-5	4.3
C-9	92-NB-SW-5	6.5
C-10	95-NB-SE-8	3.9
C-11	117-NB-SW-7	6.8
C-12	117-NB-NW-8	2.3
C-13	119-NB-NW-11	8.1
C-14	119-NB-SE-12	5.9

Table 16: OIT Values of Span Samples.

No.	Sample Code	Average OIT (min)
Southbound		
S-26	95SB-T2-SEG1-N	6.5
S-27	117SB-T1-SEG6-N	8.4
S-28	121SB-T2-SEG7-N	2.4
S-29	121SB-T3-SEG7-N	2.0
S-30	133SB-T2-SEG7-N	5.8
Northbound		
S-31	105NB-T6-SEG1-N	1.9
S-32	118NB-T3-SEG6-N	2.5
S-33	119NB-T4-SEG1	2.4
S-34	124NB-T3-SEG4-N	2.8

corresponding chart plots are shown in Figures 22 and 23 for column and span samples, respectively. The OIT values of all field samples were less than 10 minutes. Many of the span samples exhibited OIT value of approximately 2 minutes.

Discussion of Material Properties

It is well known that the SCR of HDPE is related to the molecular weight and crystallinity of the material as well as other factors such as polymerization techniques and type of catalysts

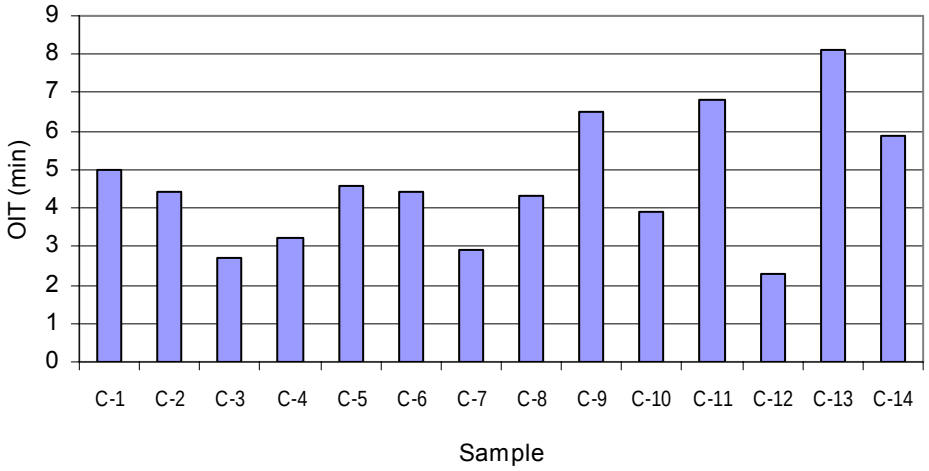

Figure 22: OIT values of column samples.

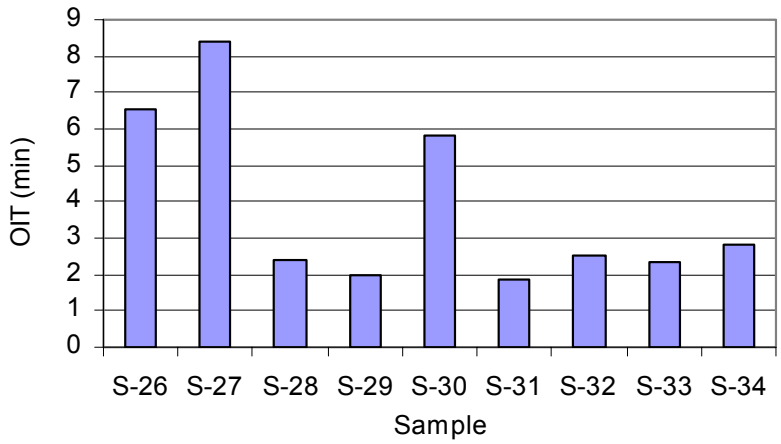

Figure 23: OIT values of span samples.

and co-monomers. In this study, the molecular weight of the polymer was assessed using the MI test, the crystallinity was reflected by the density, and SCR was measured by the failure time in the SP-NCTL test. The cracked duct samples exhibited higher MI and density values than non-cracked ones. (A high MI indicates a low molecular weight, while high density signifies high crystallinity.) Both high MI and density have a negative impact on the SCR of the material. However, the MI test has a greater accuracy than the density test.

Figure 24 shows a graph plotting MI value against failure time of the SP-NCTL test for all tested field samples, except for one case where failure time was over 30 hours. The data can be divided into two groups according to different MI ranges, as follows:

- MI value greater than 0.4 g/10 min with failure time less than 5 hours and
- MI value less than 0.4 g/10 min with failure time ranging from 2 to 34 hours.

Clearly, samples with MI values greater than 0.4 g/10 min are highly susceptible to stress cracking. Six out of 14 column samples and 15 out of 34 span samples had MI values greater than 0.4 g/10 min. For samples with MI values less than 0.4 g/10 min, the majority had failure times longer than 5 hours.

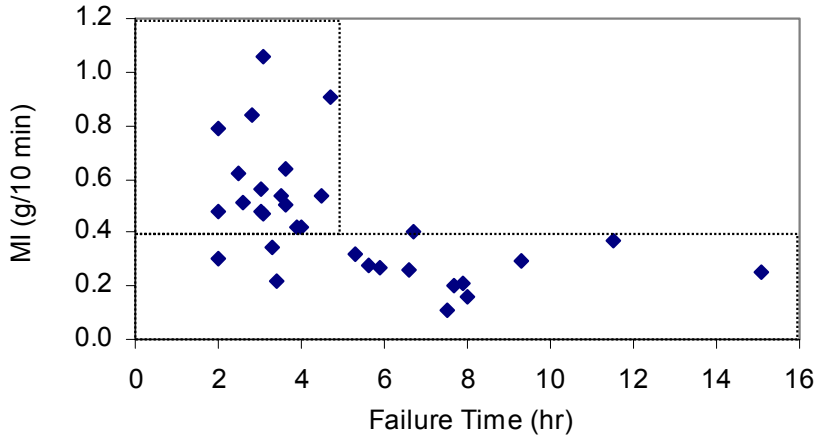

Figure 24: Failure Time versus MI of all evaluated field samples.

In order to identify the cracking potential of the ducts in different sections of the bridge, the MI and SP-NCTL failure times were placed side-by-side for each section, as shown in Figure 25 (a) to (e). Ducts in the SB-SA section had the lowest MI values and consistent failure times of 8 hours. In addition, ducts in the center stay (S-18, S-19 and S-20) exhibited the highest SCR property, while ducts with the worst SCR were located on both sides of the center stay.

Figure 26 shows a graph plotting density against failure time. It seems that the correlation between density and failure time is very poor. Nevertheless, samples with high density values tended to have short failure times. Samples with density less than 0.948 g/cc had failure times greater than 5 hours.

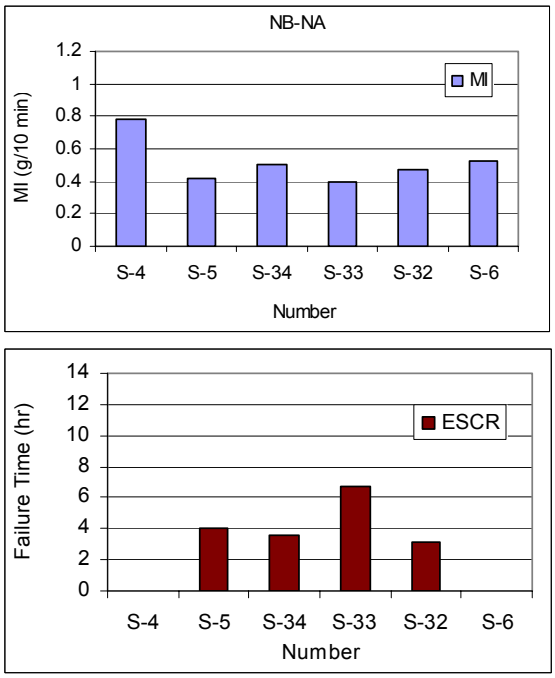
NB-NA
MI (g/10 min)
1.2
1
0.8
0.6
0.4
0.2
0
MI
S-4
S-5
S-34
S-33
S-32
S-6
Number
Failure Time (hr)
14
12
10
8
6
4
2
0
ESCR
S-4
S-5
S-34
S-33
S-32
S-6
Number

(a)

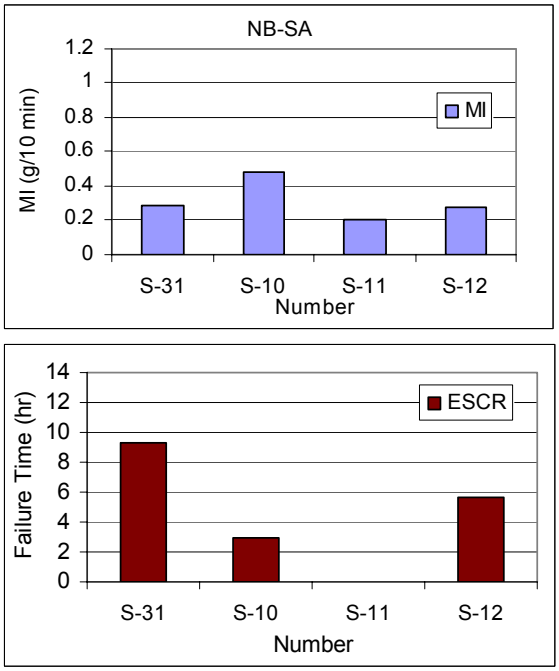
NB-SA
MI (g/10 min)
1.2
1
0.8
0.6
0.4
0.2
0
MI
S-31
S-10
S-11
S-12
Number
Failure Time (hr)
14
12
10
8
6
4
2
0
ESCR
S-31
S-10
S-11
S-12
Number

(b)

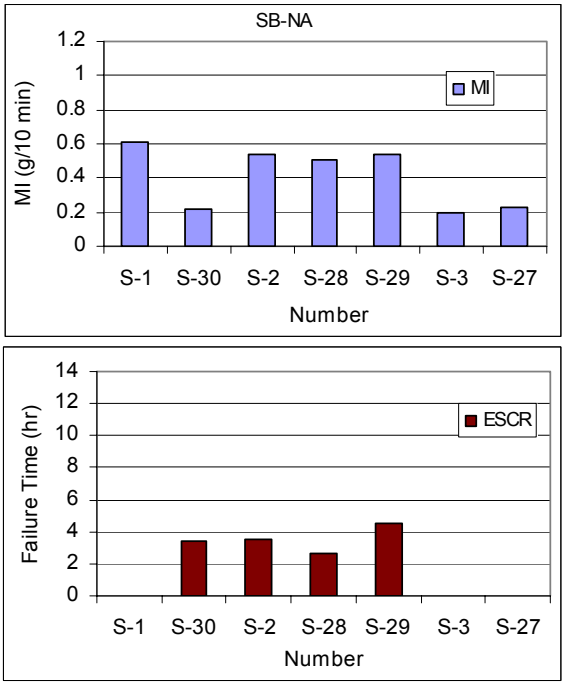
SB-NA
MI (g/10 min)
1.2
1
0.8
0.6
0.4
0.2
0
MI
S-1
S-30
S-2
S-28
S-29
S-3
S-27
Number
Failure Time (hr)
14
12
10
8
6
4
2
0
ESCR
S-1
S-30
S-2
S-28
S-29
S-3
S-27
Number

(c)

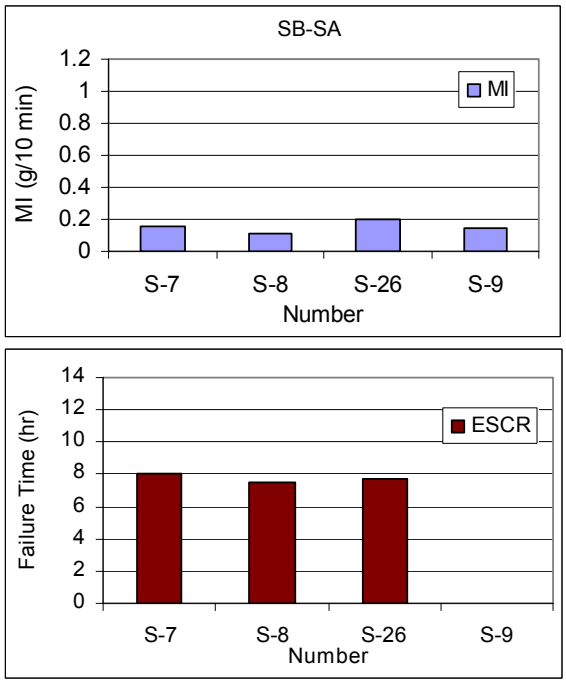
SB-SA
MI (g/10 min)
1.2
1
0.8
0.6
0.4
0.2
0
MI
S-7
S-8
S-26
S-9
Number
Failure Time (hr)
14
12
10
8
6
4
2
0
ESCR
S-7
S-8
S-26
S-9
Number

(d)

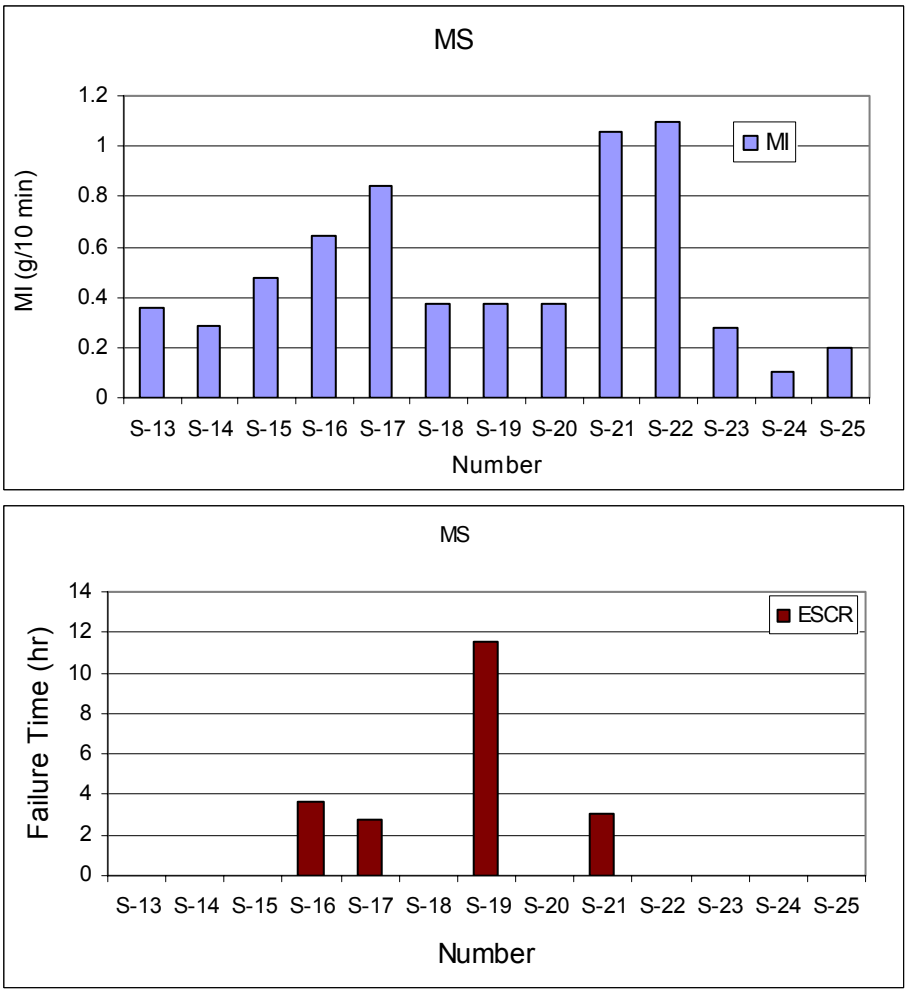

(e)

Figure 25: Comparison of MI and failure time of span samples.

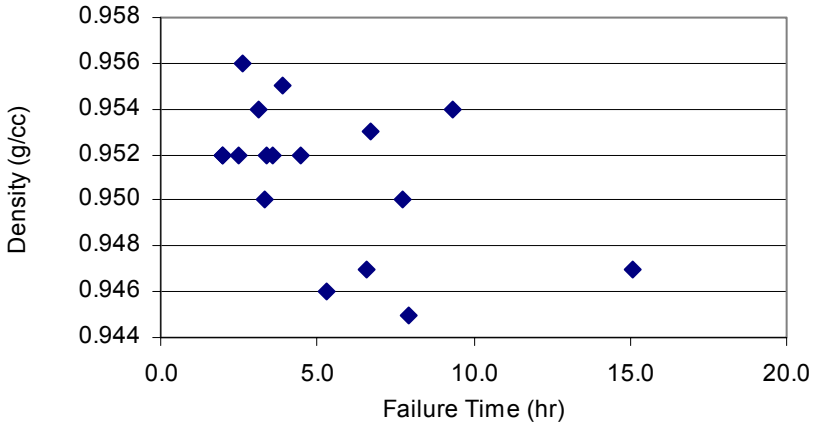

Figure 26: Density versus failure time of all evaluated field samples.

In summary, molecular weight (MI) and crystallinity (density) can have an effect on the SCR, but they cannot confidently predict the SCR of the material. Samples with low MI and density, in general, exhibited higher SCR, as reflected by the long failure time in the SP-NCTL test. Between MI and density properties, the MI correlated to SCR slightly better than density.

CONCLUSIONS

Duct samples were retrieved from both the column and superstructure of the SSK Bridge. Fourteen samples were taken from various columns of which four contained a longitudinal crack. From the superstructure, 34 samples were removed; and three of these had longitudinal cracks. The cracking mechanisms were investigated on two samples, one from the column (131-SB-SE-6) and one from the superstructure (Span 124NB-T3-SEG4-N). The fracture morphology indicated that slow crack growth was the governing mechanism. The crack initiations of column samples were caused by defects at the inner surface of the duct. For the span sample, the crack initiation could not be identified on the section of the cracked duct evaluated. However, impurities were observed in the examined sample. In addition, fatigue lines were observed on the fracture surface indicating that a cyclic loading was involved in the crack growth.

The material properties were evaluated according to the AASHTO specification based on ASTM D 3350 material specification. Two of the specified tests were not performed due to sample configuration and poor precision of the test. However, the SP-NCTL and OIT tests were added to the material evaluation. In Table 17, values from the different tests are compared with the corresponding specified values that are prescribed by the AASHTO specification. A majority of the field samples failed to conform to the requisite melt index and carbon black requirements. Except for two column samples, all failure times were less than 10 hours in the SP-NCTL test.

Table 17: Comparison of Test Results with Specified Values.

Property	ASTM D 3350 Classification	Required Value	Test Results
Density (g/cc)	3	>0.940-0.955	0.945 – 0.956
Melt Index (g/10 min)	4	< 0.15	0.09 – 0.91
Flexural Modulus (psi)	5	110,000 - < 160,000	124,000 – 159,000
Tensile Strength (psi)	4	3000 -<3500	3600 - 4500
Carbon black (%)	C	> 2	0.20 – 1.7
Additional Tests			
SP-NCTL (hour)		> 24	2.0 – 33.6
OIT (min)		Not defined	1.9 – 8.4

Regarding the long-term stability of the duct, the OIT test was used to assess the amount of antioxidant remaining in the ducts. All field samples had OIT values less than 10 minutes. The four span samples taken from the northbound span had OIT value less than 3 minutes. Although the OIT values were very low, some antioxidants still remained in the duct. For the SSK Bridge, it is important to monitor the depletion of antioxidants with time, particularly for ducts along the northbound of the spans.

Based on test data of fourteen duct samples that were taken from different columns of the SSK Bridge, the quality of the ducts varied significantly. The wall thickness variability was outside the specification requirement. The MI and density test data suggest that these ducts were not manufactured from the same lot of resin. The large difference in the MI values, from 0.09 to 0.9 g/cc, may even imply that these ducts were fabricated by different extrusion processes.

The test results also indicate large variability in the properties of the 34 retrieved span samples. The greatest variability occurred in the main stay section of the bridge. In the four approaching sections, ducts taken from SB-SA have the most uniform material properties. In addition, there seems to be two groups of resins, one with MI around 0.25 g/10 min and the other around 0.48 g/10 min.

By comparing failure time in the SP-NCTL tests to density and MI, it was concluded that the relatively low molecular weight (high MI) and high crystallinity (high density) of the resins were contributing factors to the cracking.

APPENDIX E

DUCT COEFFICIENT OF THERMAL EXPANSION

The coefficient of thermal expansion of a material is given by the expression,

$$\alpha = \frac{\varepsilon}{\Delta T}, \qquad (1$$

where,

α is the coefficient of thermal expansion [1/˚C],

ε is strain, and

ΔT is the temperature span over which ε is measured [˚C].

The experiment consisted of measuring changes in strain on a specimen of the selected material due to a change in temperature. To accomplish this, a strain gage and a thermocouple were attached to specimens of dimensions 25mm x 25mm x 6mm. Figure 1 illustrates the experimental arrangement.

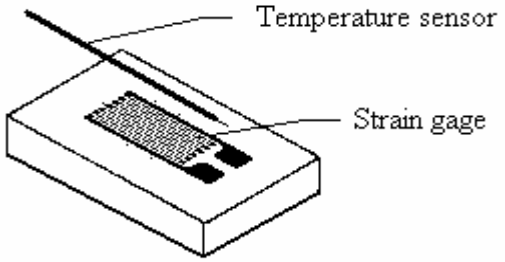

Figure 1. Schematic illustration of a specimen for determination of thermal expansion coefficient.

The test was performed on three materials, a grout sample from the Sunshine Skyway Bridge, a duct sample from the Mid Bay Bridge, and a sample of new HDPE 3408 pipe. The tests measured strain as temperature was varied between -39 and 45 ˚C.

Plots of strain gage output versus temperature are presented in Figure 2. The coefficient of thermal expansion for each material was calculated on the basis of a linear approximation of each curve (heating and cooling). Table 1 presents the coefficients of thermal expansion so determined.

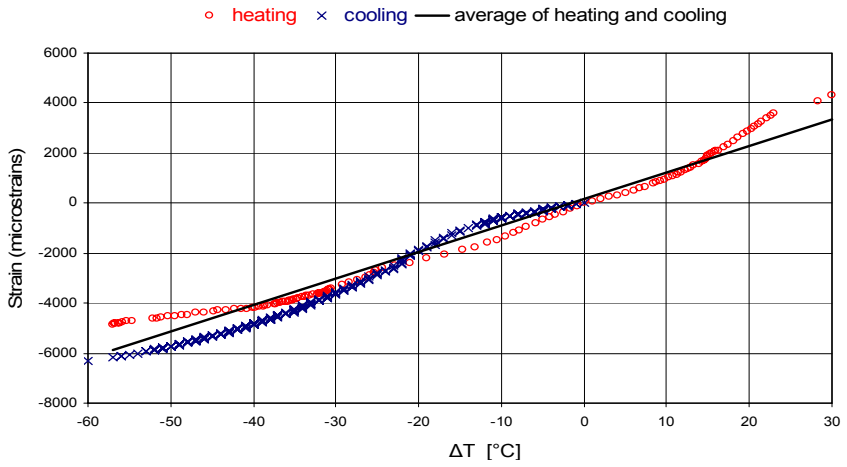

(a)

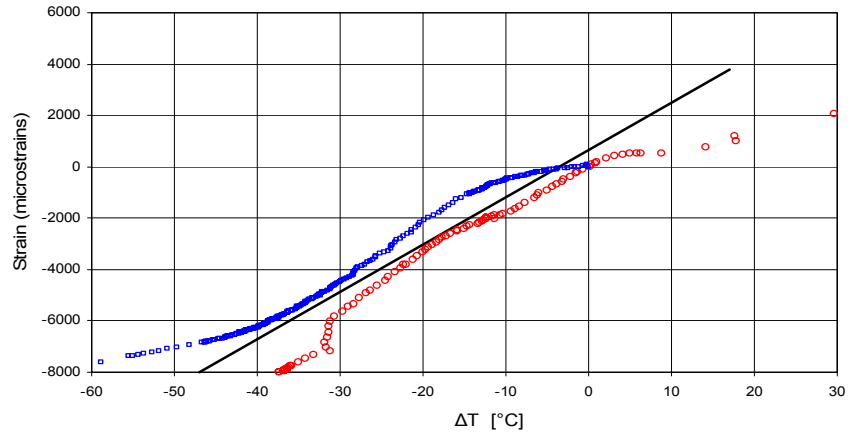

(b)

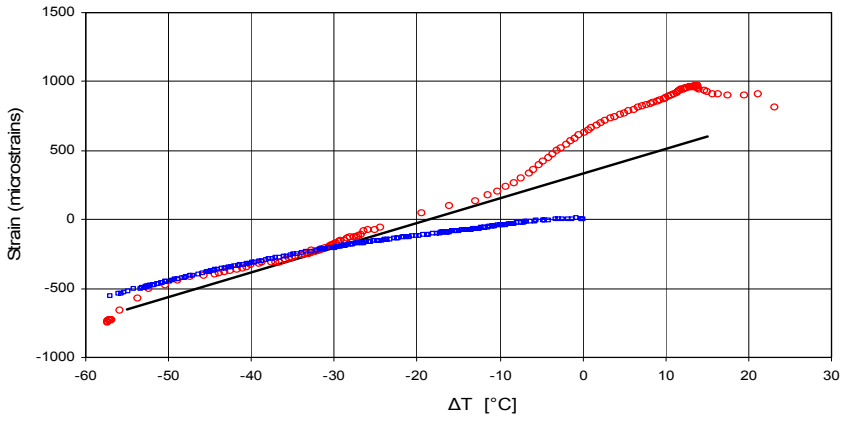

(c)

Figure 2: Plots of strain gage readings versus temperature for a) HDPE 3408, b) duct sample from the Mid Bay Bridge, and c) grout sample from a Sunshine Skyway Bridge column.

Table 1: Coefficients of thermal expansion.

Material	Source	Coefficient of Thermal Expansion, με/oC		
		Cooling	Heating	Average
PE 3408	New	127	106	117
HDPE	Mid Bay Bridge	172	183	178
Grout	Sunshine Skyway Bridge	10	22	16

APPENDIX F

DUCT RESIDUAL STRESS MEASUREMENTS

Two methods for measuring the residual stress in the duct were employed. The first (Method 1) was to attach a circumferentially oriented strain gage on the outer surface of a duct sample and measure the strain upon splitting of the pipe. The second (Method 2) was to calculate the stress from the change in outside diameter that occurred subsequent to splitting, according to the equation presented in the standard ASTM E 1928-99 [13],

$$\sigma = \frac{Mc}{I} = \pm \frac{Et}{1-\mu^2} \frac{\left(D_1 - D_0\right)}{D_1 D_0}, \qquad 1)$$

where,

M is the residual moment in the duct,

c is the distance from the neutral axis to the point of maximum strain,

I is the moment of inertia of the cross section of the specimen,

E is the Flexural Modulus,

t is the specimen thickness,

μ is Poisson's ratio,

D_o is the mean outside diameter before splitting, and

D_1 is the mean outside diameter after splitting.

Due to the lack of complete sections of pipe from the bridges, the experiment was only performed on PE 3408 specimens. The specimens were sections of 0.25 m long HDPE PE3408 pipe of SDR 17, 21, and 26. Also, specimen B2 from the tendon simulation experiment was tested at the time it was autopsied. Figure 1 illustrates the specimens and the test method. The results are presented in Table 1.

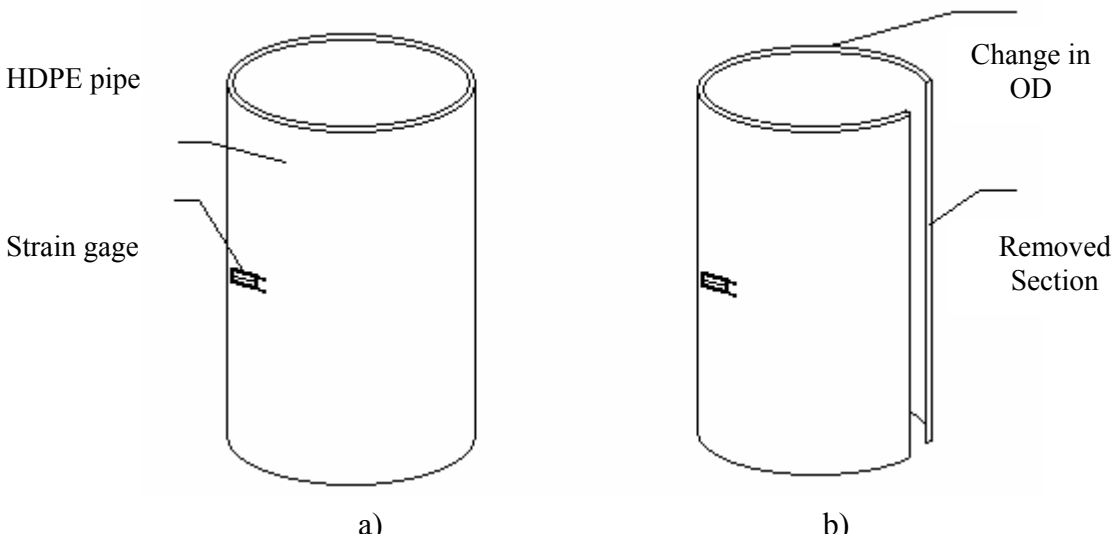

Figure 1: Residual stress measurement: a) Original pipe section and b) strip of pipe is removed and strain changes in OD are recorded.

Table 1: Results from residual stress measurement.

Material	Strain Change, micro-units	Stress, MPa	
		Method 1	Method 2
PE-3408 SDR 17	5249	4.92	6.89
PE-3408 SDR 26	3540	3.32	5.42
PE-3408 SDR 22	3530	3.31	5.89
Specimen B2	5510	5.19	8.23